



AWESOME

WATER-ECOSYSTEM-FOOD

CLIMATE SCENARIOS

July 2021



This project is part of the PRIMA Programme supported by the European Union, having received funding from it under grant agreement No 1942



Project Number: 1942
Project Title: AWESOME
Partners: POLIMI (Project Coordinator), AUEB, YVC, UH, ZG, RWTH, FEEM

Work-Package: WP2
Deliverable #: D2.2
Deliverable Type: Document
Contractual Date of Delivery: 31 July 2021
Actual Date of Delivery: 28 July 2021
Title of Document: Climate Scenarios
Author(s): Andrea Castelletti, Matteo Giuliani, Elena Matta

Content of this report: Report about the climate scenarios developed for the AWESOME project, including the analysis of downscaled climate change projections until 2100 according to different forcing scenarios and across the spatial scales requested by the AWESOME models.

Availability: This report is public.

| Document revisions | | |
|---------------------------|---------------------------------------|---------------|
| <i>Author</i> | <i>Revision content</i> | <i>Date</i> |
| Elena Matta | D2.2_v01 – First draft of the report | June 23, 2021 |
| Matteo Giuliani | Internal revision | June 29, 2021 |
| Elena Matta | D2.2_v02 – Second draft of the report | June 30, 2021 |
| Ricarda Lothmann | Internal revision | July 6, 2021 |
| Davide Danilo Chiarelli | Internal revision | July 8, 2021 |
| Elena Matta | D2.2_v03 – Third draft of the report | July 11, 2021 |
| Andrea Castelletti | Final revision | July 16, 2021 |
| Elena Matta | D2.2_F – Final draft of the report | July 28, 2021 |

Table of Content

| | |
|--|----|
| Table of Content | 3 |
| LIST OF ACRONYMS | 5 |
| EXECUTIVE SUMMARY | 6 |
| 1. INTRODUCTION | 7 |
| 2. CLIMATE CHANGE ASSESSMENT | 9 |
| 2.1 CLIMATE CHANGE IN AFRICA | 9 |
| 2.1.1 Egypt | 10 |
| 2.2 METHODOLOGY | 11 |
| 2.2.1 Representative Concentration Pathways | 11 |
| 2.2.2 General circulation models and dynamic downscaling | 13 |
| 2.2.3 Bias correction | 14 |
| 2.2.4 Climate uncertainty | 15 |
| 3. CLIMATE DATA | 17 |
| 3.1 SPATIAL DOMAIN | 17 |
| 3.2 GLOBAL DATASETS | 18 |
| 3.3 CLIMATE DATA COLLECTION AND PROCESSING | 19 |
| 4. CLIMATE ANALYSIS | 21 |
| 4.1 TREND ANALYSIS | 21 |
| 4.1.1 Main Nile sub-basin | 21 |
| 4.1.2 Blue Nile sub-basin | 26 |
| 4.1.3 White Nile sub-basin | 30 |
| 4.2 CLIMATE INDICATORS | 34 |
| 4.2.1 Main Nile sub-basin | 35 |
| 4.2.2 Blue Nile sub-basin | 38 |
| 4.2.3 White Nile sub-basin | 42 |
| 4.3 A CLOSER LOOK AT EGYPT | 46 |
| 4.3.1 Comparing different futures | 53 |

| | |
|------------------------|---|
| D2.2 CLIMATE SCENARIOS | 3 |
|------------------------|---|

| | |
|---|----|
| 5. FINAL REMARKS | 56 |
| REFERENCES | 57 |
| ANNEX I | 59 |
| I. MASH PLOTS OF THE OTHER NILE SUB-BASINS | 59 |
| Tekeze-Atbara sub-basin | 59 |
| Baro Akobbo Sobat sub-basin | 60 |
| Bahr El Jebel sub-basin | 61 |
| Bahr El Ghazal sub-basin | 62 |
| Victoria Nile sub-basin | 63 |
| Lake Victoria sub-basin | 64 |
| Lake Albert sub-basin | 65 |
| ANNEX II | 67 |
| II. CLIMATE INDICATORS OF THE OTHER NILE SUB-BASINS | 67 |
| Tekeze-Atbara sub-basin | 68 |
| Baro Akobbo Sobat sub-basin | 69 |
| Bahr El Jebel sub-basin | 70 |
| Bahr El Ghazal sub-basin | 71 |
| Victoria Nile sub-basin | 72 |
| Lake Victoria sub-basin | 73 |
| Lake Albert sub-basin | 74 |
| ANNEX III | 75 |
| III. Egypt | 75 |

LIST OF ACRONYMS

Abbreviations

| | |
|---------|--|
| AFR: | Africa |
| CS: | Case Study |
| CCI: | Climate Change Indicators |
| CGE: | Computable General Equilibrium |
| CHIRPS: | Climate Hazards Group InfraRed Precipitation with Station data |
| CHIRTS: | Climate Hazards Centre Infrared Temperature with Stations |
| CORDEX: | Coordinated Regional Downscaling Experiment |
| CP: | Control Period |
| ETCCDI: | Expert Team on Climate Change Detection and Indices |
| GCM: | General Circulation Model |
| IAM: | Integrated Assessment Models |
| ICHEC: | Irish Centre for High-End Computing |
| IPCC: | Intergovernmental Panel on Climate Change |
| MASH: | Moving Average over Shifting Horizon |
| NRB: | Nile River Basin |
| POLIMI: | Politecnico di Milano |
| RF: | Radiative Forcing |
| RR: | Rainfall |
| RCM: | Regional Climate Model |
| RCP: | Representative Concentration Pathway |
| SMHI: | Swedish Meteorological and Hydrological Institute |
| TN: | Minimum Temperature |
| TX: | Maximum temperature |
| WP: | Work Package |

EXECUTIVE SUMMARY

The Deliverable D2.2 Climate Scenarios reports about the climate scenarios developed for the AWESOME project, including the analysis of downscaled climate change projections across the different spatial scales requested by the AWESOME models. In particular, the scenarios rely on the IPCC fifth assessment report projections and explore different concentration pathways: RCP 2.6 (low impact scenario), 4.5 (baseline scenario), and 8.5 (high impact scenario). The spatial domain considered is the Nile River Basin, with an additional part covering Egypt since it is the location of the AWESOME demo-sites experiments. CORDEX-Africa provides the regional climate data for the study, while the CHIRTS and CHIRPS global datasets at 0.05° resolution over Africa are used to bias-adjust the climate variables over the Nile. The climate analysis conducted shows that temperatures will relevantly rise in all scenarios analysed. Precipitation presents a more complex behaviour, having a higher spatial and temporal variability, but also considering the wide extension of the Nile River Basin and its distinct climatic, topographical, and hydrological characteristics.

1. INTRODUCTION

This report describes the climate scenarios and data generated for the AWESOME project within task T2.2 *Climate Scenarios* of Work Package 2 (WP2). WP2 focuses on the generation of plausible future scenarios for simulating water, food, energy demands and projected climatic conditions, including ecosystem services assessment and the analysis of related international policies. The output of WP2 will serve to evaluate the impacts of these projections on the Water Energy Food Ecosystems (WEFE) Nexus at both the macro and meso levels in WP3 and WP4, respectively, as illustrated in Figure 1.

In particular, task T2.2 aims at collecting historical climate data and generating projections of climate variables for the analysis of climate change impacts relevant to achieve the AWESOME goals. T2.2 relies on the climate scenarios published in the Intergovernmental Panel on Climate Change (IPCC) Fifth Assessment Report¹, which are based on the Representative greenhouse gases Concentration Pathways (RCPs). The regional climate data for the different RCPs are retrieved from the most recent results of the Coordinated Regional Downscaling Experiment (CORDEX) available for Africa at a resolution of 44° (CORDEX-AFR44), while suitable global datasets at higher resolution are used as observational data for their bias correction. Among the different modelling ensembles of CORDEX-AFR44, the ICHEC EC-EARTH General Circulation Model (GCM) and SMHI RCA4 Regional Climate Model (RCM) are chosen, exploring RCP 2.6, 4.5 and 8.5 until the end of the century (2006-2100), and considering 1981-2005 as control period (CP).

The document starts by briefly describing climate change in Africa and Egypt (location of the AWESOME demo-sites) and the methodology lying behind this work (section 2), then it continues presenting the spatial domain considered for the study, the climate observation and CORDEX data used (section 3). Section 4 is dedicated to climate analysis and postprocessing, by exploring climate trends and the most relevant indices for the study area. Finally, section 5 gives some final remarks. The document ends with the references and the two annexes (Annex I, II), where additional results are reported.

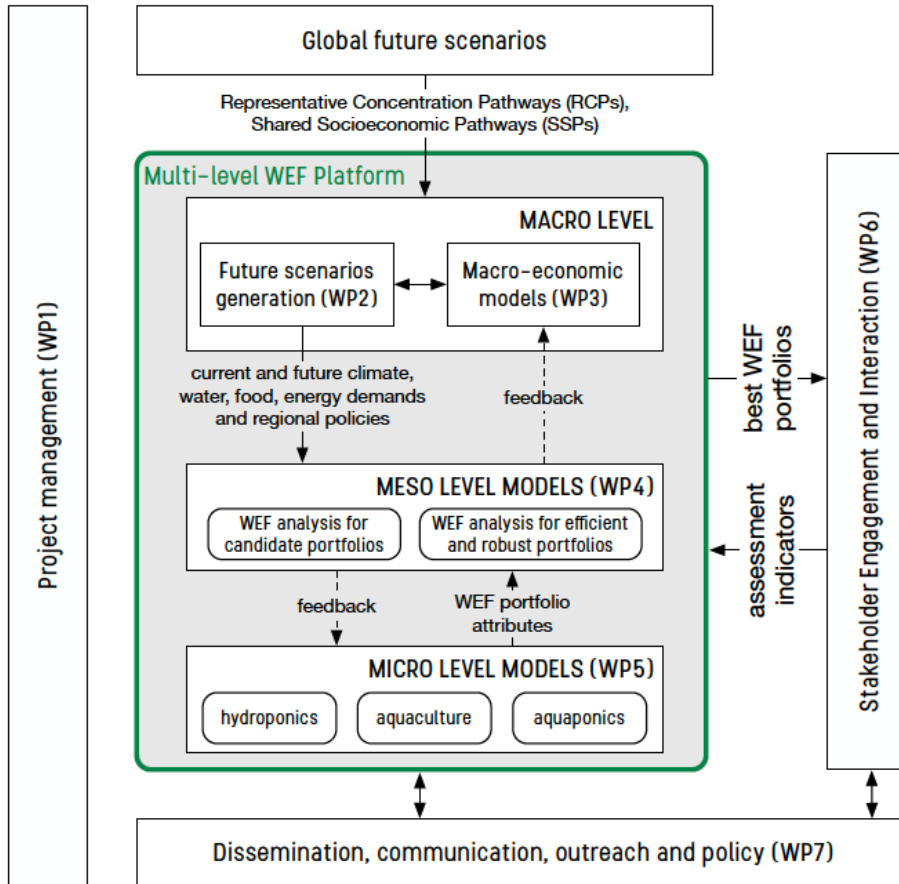


Figure 1 – AWESOME project structure

2. CLIMATE CHANGE ASSESSMENT

2.1 CLIMATE CHANGE IN AFRICA

Climate scenarios are plausible representations of future climate conditions (temperature, precipitation and other climatological phenomena)² and are fundamental tools to assess climate change and tackle the global challenges of climate mitigation and adaptation measures.

In Africa, climate characterization is very uncertain, mainly due to the low density of meteorological stations and thus low measurement availability³. Also, uncertainty in surface climate observations over the African region is particularly evident for the projections of precipitation, as regional climate models give reliable simulations of rainfall, but with noteworthy biases over different subregions⁴. Plenty of literature⁵⁻⁷ can be found on climate research in Africa, often related to the impacts on large dams' operations and water resources management along the NRB.

Climate change is projected to increase the interannual variability of rainfall, which can cause devastating droughts and floods⁸. Regions of Africa, particularly the eastern part, are found to be highly vulnerable to changes in climate and climate extremes, and more extreme events such as frequent droughts, floods, and heavy rainstorms are projected in the future⁸. Several studies highlighted that the variability in rainfall especially in East Africa is linked to large-scale climate variability, including the El Niño Southern Oscillation (ENSO)⁹. Also, changes in sea surface temperature affect the rainfall amount (e.g., decrease during the rainy season) by changing wind patterns and moisture fluxes¹⁰.

The IPCC fifth assessment report states that - under the assumptions of the RCPs (s. section 2.2) - end-of-century mean global surface temperatures relative to 1986–2005 are likely to increase by between 0.3 °C -1.7 °C following RCP 2.6, 1.1 °C - 2.6 °C following RCP 4.5, and 2.6 °C - 4.8 °C following RCP 8.5. This is worsened in Africa by the fact that regional climate response to these targets is likely to be faster there than the global warming average. Of particular concern in Africa are heatwaves and their duration, as well as rainfall extremes because of the devastating impact they have across natural and socioeconomic systems^{11,12}. E.g., simulating temperature extremes in Africa, it is observed that the most severe effects of global warming will be related to the frequency and severity of extreme events¹³.

Analyses¹⁴ on the drought risk in Africa show that northern African countries might experience an aggravating drought hazard, but the drought risk ratio is found to be highest in central African countries because of vulnerability and population rise in that region. It is pointed out how climate change adaptation shall be soon implemented, to mitigate anticipated drought hazard and risk. E.g., controlling population growth is found to be an effective countermeasure, as it improves socioeconomic vulnerability and reduces potential exposure to drought^{7,14}. It is evident that much

work is needed to enhance our understanding of African regional responses of climate and climate related impacts to the ongoing rapid climate change.

2.1.1 Egypt

Egypt lies in the north-eastern part of the African continent and has a total area of about 1 million km². Most of the country area is desert land, while most of the cultivated area is located close to the Nile River banks and in the Delta. It is thus an arid region with a hot and dry summer lasting from May to October, and a mild winter from November to April. Summer temperatures are high, reaching 38 °C to 43 °C with extremes of 49 °C in the southern and western deserts. The northern areas on the Mediterranean coast are cooler, with 32 °C as a maximum. Rainfall is irregular, unpredictable and very low with an annual mean of 51 mm¹⁵. Also, it presents high spatial variability, as in general higher precipitation (still low) occurs in the northern territories along the northern coast, in the Delta, in the mountain along the Suez gulf, and the Sinai Peninsula. The southern part of Egypt is almost completely dry over the year. Figure 2 shows two snapshots of the spatially distributed precipitation on the two wettest days in the period 1981-2005, respectively on the 11th of March 1984 and the 1st of May 1997. The daily rainfall values are represented in a coloured scale progressively ranging from dark blue to green to yellow, as precipitation decreases from the highest values (up to 60 mm/d) to the lowest (null). The white area indicates the Qattara depression in the north-western desert.

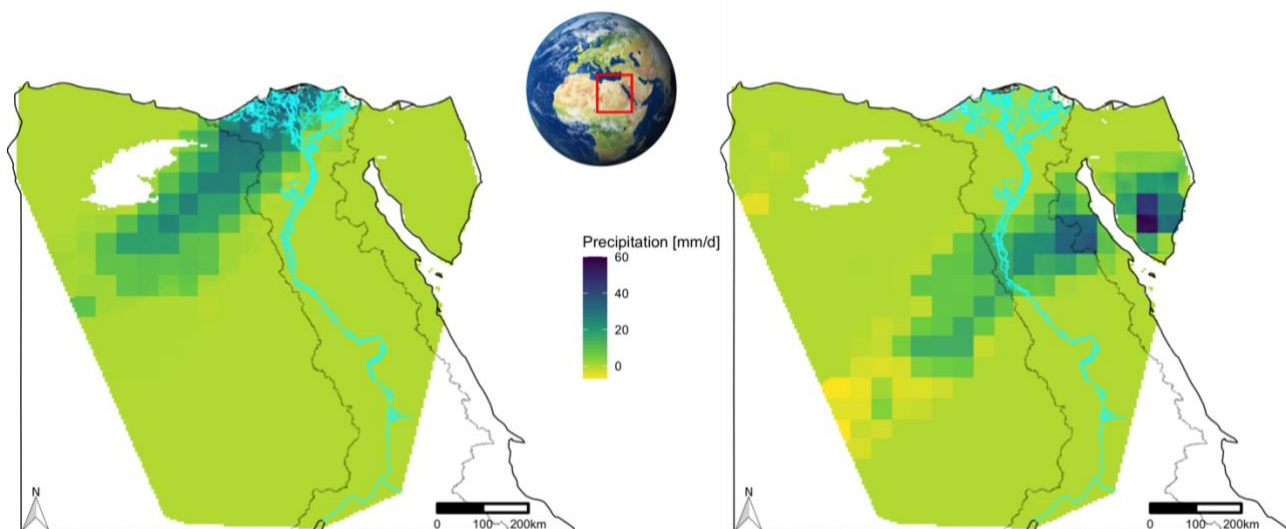


Figure 2 – Snapshots of the spatially distributed precipitation [mm/d] in Egypt on the two wettest days in the period 1981-2005 (at the high spatial resolution of 0.05°, approx. 5 km): 11th of March 1984 (left) and 1st of May 1997 (right). The white area indicates the Qattara depression in the north-western desert. The river stretch and the main canals of the Main Nile are represented in cyan, while the boundary of its hydrological sub-basin in black (thin).

Egypt is almost entirely dependent on the water of the NRB, which supplies an annual water volume of approximately 55.5 Gm³, accounting for 93% of the country’s conventional water resources¹⁶. Climate change might have direct impacts on water quantity in Egypt, leading to risks of sea level rise and to indirect effects on Mediterranean saltwater intrusion to groundwater, which exposes agriculture to high vulnerability. Previous studies report that air temperature in Cairo is predicted to increase by 4 °C and around 3.1 °C - 4.7 °C in the rest of Egypt by the year 2050 for high emission scenarios. Rainfall projections are highly uncertain, while evapotranspiration will increase due to the temperature rise^{17,18}. Further details on future projections in the NRB and Egypt are given in section 4.

2.2 METHODOLOGY

The methodology for the generation of local climate projections can be schematized as in Figure 3. The scheme represents how local scale climate scenarios are downscaled from global ones through different steps. First, the General Circulation Models (GCM) are generated by simulating three different Representative Concentration Pathways (RCP 2.6, RCP 4.5, RCP 8.5) for different combinations of climate models, where the RCPs represent different assumptions of climate-altering gas concentration following various emission policies. Consequently, GCM are dynamically downscaled to Regional Climate Models (RCM), which are in turn bias adjusted to obtain climate projections at the local scale. The fundamental components of this process and the different working steps are reported in the following subsections.

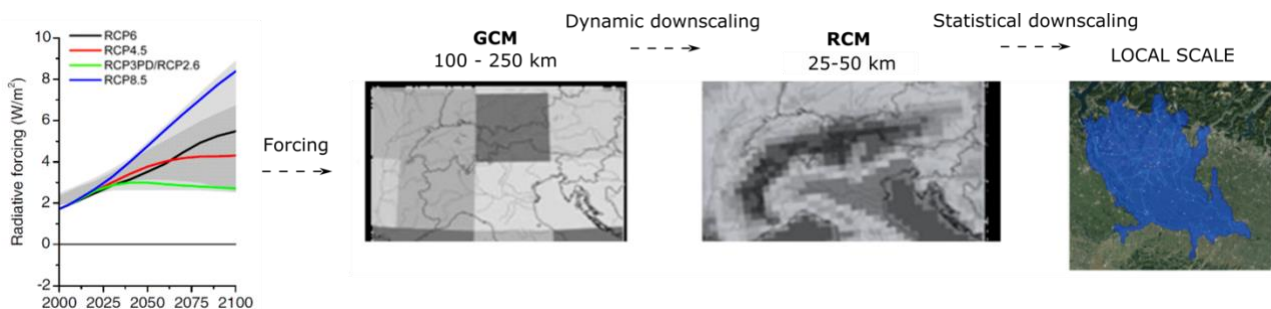


Figure 3 – Scheme of the methodology

2.2.1 Representative Concentration Pathways

The IPCC is the United Nations body for assessing the science related to climate change and has the main objective to provide governments at all levels with scientific information that they can use to develop climate policies. The IPCC fifth assessment report is the most recent and comprehensive

document available as well as the common reference for the current climate related studies, while the IPCC sixth assessment report is in preparation and will be completed by May 2022.

RCPs are a set of global datasets produced by the IPCC representing the trajectories of radiative forcing (RF) in the years between 1850 and 2100 following different scenarios of demographic development, greenhouse gas emissions and land and energy use. The RF [Wm^{-2}] measures the imbalance in the Earth's energy budget caused by a perturbation of the climate system, for example, changes in atmospheric composition driven by human activities¹⁹. In fact, RF is the difference between the solar energy absorbed by the Earth and that radiated into space and is considered proportional to the global warming potential. In total, four RCPs were generated, each of which takes its name from the RF value calculated in the year 2100: RCP 2.6, RCP 4.5, RCP 6 and RCP 8.5, among which RCP 6 is rarely considered in the literature. The main characteristics of the RCPs (from the point of view of energy and soil use and greenhouse gas emissions) are shown in Table 1.

Table 1 – Description of the radiative forcing concentration pathways

| RCP name | Radiative forcing | CO ₂ eq concentration [ppm] | Increase in temperature [°C] | Pathway |
|----------|--|--|------------------------------|---------------------------------|
| RCP 2.6 | Peak at 3 W/m ² before 2100 and decline | Peak at 490 before 2100 and then decline | 1.5 | Peak and decline |
| RCP 4.5 | Stabilization around 6 W/m ² after 2100 | Stabilization around 650 after 2100 | 2.4 | Stabilization without overshoot |
| RCP 6.0 | Stabilization around 6 W/m ² after 2100 | Stabilization around 850 after 2100 | 3 | Stabilization without overshoot |
| RCP 8.5 | > 8,5 W/m ² | Stabilization around 1,370 after 2100 | 4.9 | Rising |

These pathways (Figure 4) are linked to social, technological, and economic variables, as described in the following:

- RCP 2.6 responds to a situation where a global ecologic transition is implemented through a high increase of renewable energy and biofuels production coupled with the installation of carbon capture and storage systems in plants using fossil fuels, stabilization of the population and the land use, drastic reduction of high emission intensified agriculture.
- RCP 4.5 presents a lower reduction of emissions from the energy and agricultural sector with respect to RCP 2.6. It corresponds to a business-as-usual scenario, where the population

peaks in 2050 and declines afterwards. Rapid changes in the economic structure and the increase of cooperation help to improve equity, and sustainability.

- RCP 6 foresees a population increase after 2050, and a slow economic and technological growth, the focus is on local solutions towards sustainability.
- RCP 8.5 forecasts an important population and economic growth, which causes an increase in the demand for energy production from fossil fuels, and in land use change.

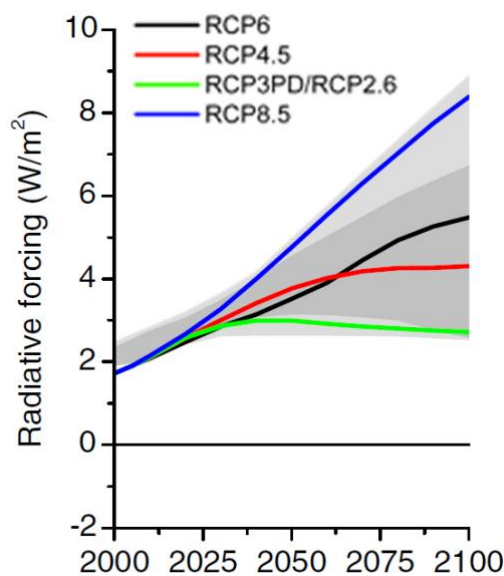


Figure 4 – Radiative forcing (W/m²) in the Representative Concentration Pathways (RCPs) until 2100¹.

2.2.2 General circulation models and dynamic downscaling

General circulation models (GCM) are currently the most advanced tools for simulating the response of the climate system to the increase of greenhouse gas emissions. Their implementation includes the characterization of the physical processes that occur in the atmosphere, oceans, cryosphere and on the Earth's surface. In GCM, the planet is discretized using a three-dimensional grid with horizontal resolution between 100 and 250 km, and with variable GCM can provide reliable projections of how the climate of the Earth may change in the future, forced by the RCPs described above. However, the typical resolution for a GCM is too coarse to assess the impacts of a changing climate and the adaptation strategies required to deal with them, occurring on more regional and national scales. For this reason, downscaling is a necessary step to derive the information at higher resolution needed by the impact models⁽²⁰⁾.

The dynamic downscaling (DD) technique is thus applied to increase this resolution of the smallest scale circulation model available. DD consists in nesting an RCM into a GCM, thus operating at a higher resolution (50 - 25 km), as shown in Figure 5. The boundary conditions for the simulation are provided by the GCM, while the RCM add regional forcing (e.g., orography, land use) and provide more accurate projections at the regional scale in comparison to the GCM.

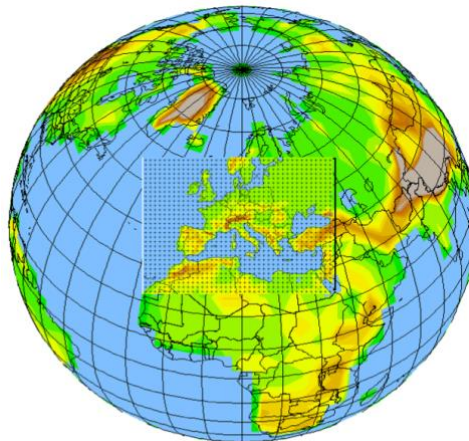


Figure 5 – Three-dimensional gridded representation of the Earth, where the course cell resolution corresponds to the GCM and the higher resolution to the RCMs

2.2.3 Bias correction

The bias correction on RCM data is performed to obtain climatic scenarios at the same resolution as the observation data over the historical period considered, as previously schematized in Figure 3. This procedure is usually implemented in climate-related research when the spatial resolution obtained through the dynamic downscaling is not sufficient to evaluate the impacts at the desired scale of the specific study (local). The bias correction aims to find a statistical relationship between a large-scale independent variable X , produced by an RCM and a local scale dependent variable Y , that is:

$$Y = f(X) \quad (1)$$

where Y is the variable used for local impact studies.

X and Y are usually represented by the same variable (e.g., precipitation), and the downscaling process leads to a correction of the bias due to the different observation scales, orography, and conformation of the territory.

From a methodological point of view, the bias correction consists of two distinct phases:

1. Calibration: the relationship shown in (1) is estimated starting from historical observations and RCM outputs over a stationary, historical period (with no climate trend).
2. Projection: the estimated relationship is applied to climate projections.

In the literature, there are several techniques to implement this bias correction, among which the quantile-quantile mapping method represents one of the more flexible and more accurate ones²⁰. Figure 6 shows a schematic representation of this approach, which consists in correcting the shape of the probability distribution (extremes included) of the projections by adapting the distribution of the variable X to the probability distribution of Y.

For this study, the quantile-quantile mapping method with a moving temporal window is used to account for intra-annual variations in the form of the probability distribution of the variable under consideration.

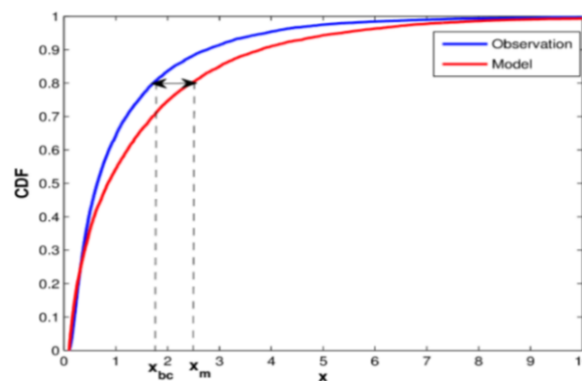


Figure 6 – Schematic representation of the quantile-quantile mapping method

2.2.4 Climate uncertainty

As can be read in more detail in ²¹, the methodology reported in this document follows a ‘top-down’ approach (also known as ‘scenario led’), running from global scenarios to local ones to then feed the impacts models (e.g., to estimate future streamflow or crop yields), before finally invoking adaptation measures to maximize any benefits or to anticipate risks. The term ‘top down’ is used because the information is cascaded from one step to the next one, with the number of permutations of emission scenario, climate model, downscaling method, and so on, proliferating at each stage, as shown in Figure 7. The cascade of uncertainty proceeds from different socio-economic and demographic pathways, their translation into radiative forcing, expressed climate outcomes in global and regional models, translation into local impacts on human and natural systems, and implied adaptation responses. The increasing number of triangles at each level symbolizes the growing number of permutations and hence expanding envelope of uncertainty.

Although this is the most widely represented approach within the scientific evidence reviewed by the IPCC, there are very few tangible examples of anticipatory or planned adaptation decisions arising from this route. Most of the research studies stop at the impact assessment stage.

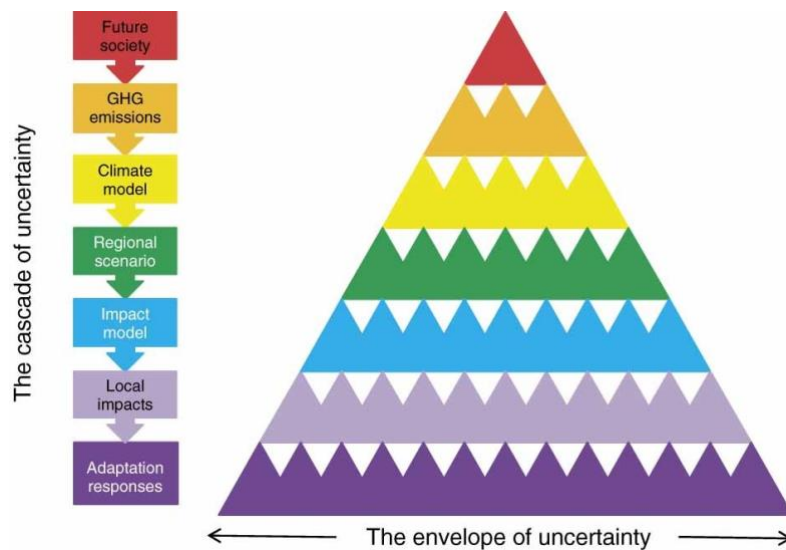


Figure 7 – The cascade and envelope of climate uncertainty following a top-down approach described by ²¹

3. CLIMATE DATA

This section describes the climate data used to produce the downscaled climate projections of the AWESOME project: observation data from global datasets, CORDEX regional data, variables analysed along with temporal and spatial scales are reported.

3.1 SPATIAL DOMAIN

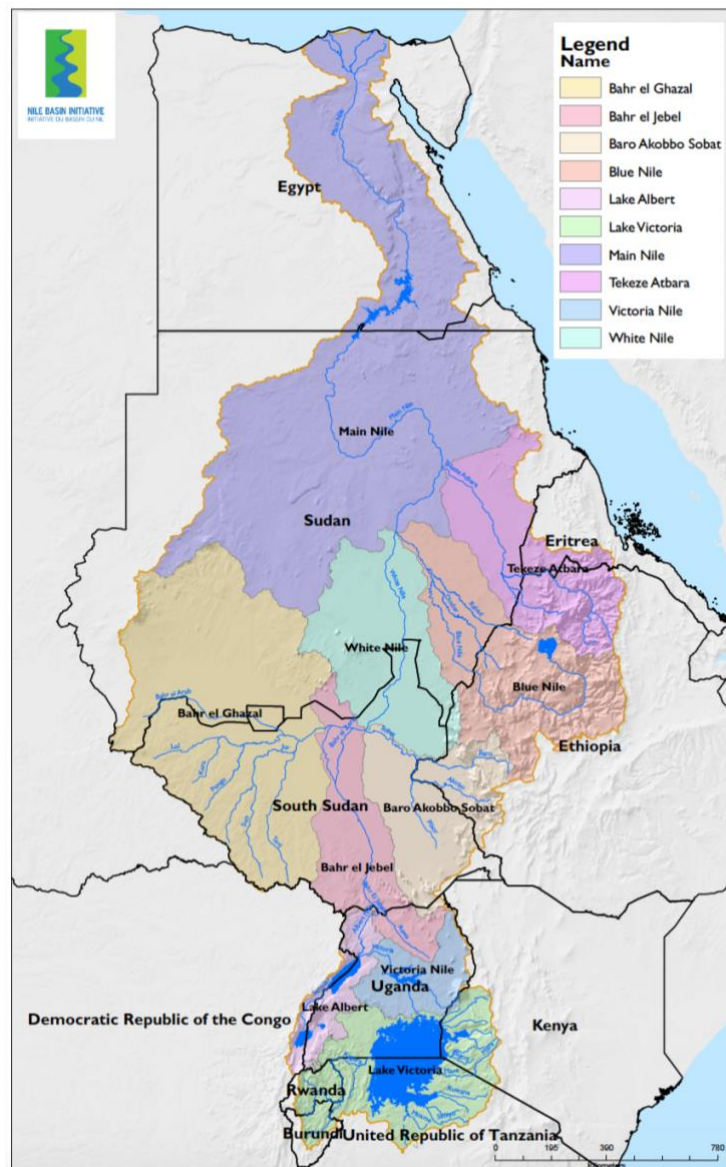


Figure 8 – Graphical representation of the main Nile hydrological sub-basins²²

The AWESOME project is running across three main spatial scales: the macro level is covering the South Mediterranean region and north-eastern Africa, the meso level is at the NRB, and the micro level focuses on Egypt, where the demo-sites of soilless agriculture are being built and tested. The GCM and RCM climate data available by the different climate communities (e.g., CORDEX) are perfectly suitable for the AWESOME modelling assessments. Therefore, the spatial domain chosen to downscale climate data is the hydrological NRB, with an additional focus on Egypt.

The Nile is the primary water resource of Egypt and Sudan and is a transboundary river, including portions of 11 countries, Burundi, Democratic Republic of Congo, Egypt, Eritrea, Ethiopia, Kenya, Rwanda, South Sudan, Sudan, Tanzania, and Uganda²³. The main tributaries to this river are the Blue Nile and the White Nile, which merge in Khartoum, Sudan. The Blue Nile has its origin at the Lake Tana in Ethiopia, whereas the White Nile is born at the Lake Victoria situated between Uganda, Kenya and Tanzania but is called Victoria Nile until it passes through the Sudd wetlands in Sudan. Being about 6,650 km long, the Nile has many sub-basins in different physiographic regions: highlands, open water surfaces, wetlands, flat lands, and deserts. It enters the arid climate in Sudan and Egypt.

With the goal of detecting the climate variability in such a wide area, but also for better handling the high computational effort required by the RCM bias adjustment with 0.05° high resolution observation data, the projections are run dividing the NRB into ten main hydrological sub-basins, i.e., Main Nile, Tekeze Atbara, Blue Nile, White Nile, Baro Akobo Sobat, Bahr El Jebel, Bahr El Ghazal, Lake Albert, Victoria Nile, and Lake Victoria (Figure 8).

3.2 GLOBAL DATASETS

Analyses of climate variability and trends require long-term and temporally consistent historical records, which are often unavailable or inadequate over many parts of the world due to sparse or non-existent station networks, or to limited data accessibility²⁴. Global datasets derived from global atmospheric reanalysis, satellite products and station data have been increasingly used as complements or in place of ground-based observations to conduct climate research and thus bias correcting global climate data.

There are several datasets freely available on the web and recommended for Africa, some of them are briefly reported in the following:

- ERA5²⁵ are the most recent Copernicus reanalysis data, available in hourly and monthly frequency at 0.33° resolution, from 1950 to date.
- CRU²⁶ are global monthly data at 0.05 resolution, from 1901 to 2019.

- HydroGFD3.0²⁷ are recently published SMHI bias adjusted reanalysis daily data at 0.25° resolution, from 1980 to date.
- CHIRPS²⁸ and CHIRTS²⁹ are combined satellite imagery with in-situ station data produced by the Climate Hazard Centre (CHC) of UC Santa Barbara, available in daily and monthly frequency at 0.05° resolution, from 1981 to date for precipitation data, while from 1983 to 2016 for temperature data.

ERA5 data are proved to have robust performance with respect to spatial covariance and daily anomalies but underestimate temperatures in Africa, especially concerning the extremes. Similar behaviour was observed from CRU data, which effectively capture temperatures on continental and global scales, but miss important extreme events in continents with lower station data availability^{29,30}. On the contrary, CHC products are explicitly designed for monitoring agricultural drought and global environmental change over land, as well as to support the monitoring of temperature extremes, specifically for countries like Africa, which are poorly instrumented. Therefore, CHIRPS was used to retrieve daily mean precipitation observations, while CHIRTS for daily maximum and minimum temperatures. More detail on the CHC datasets can be found at the following link, which is also a reference for the previous statements: <https://www.chc.ucsb.edu/data>.

3.3 CLIMATE DATA COLLECTION AND PROCESSING

The CORDEX³¹ program runs under the mandate of the World Climate Research Project (WCRP) Working Group on Regional Climate (WGRC) and complements the WCRP Working Group on Coupled Modelling (WGCM), which oversees the Coupled Model Intercomparison Project (CMIP) data development. CORDEX is steered by a Science Advisory Team reporting to the WGRC and seeks to develop regional climate projections for all terrestrial regions through RCM and bias correction. The CORDEX framework evaluates regional climate model performance through a set of experiments aiming at producing regional climate projections for all regions of the world driven by GCM forced by different RCP. The most recent experiments available at the regional scale comprise the fifth phase of the Coupled Model Intercomparison Project (CMIP5).

The climate data used in this study were provided by the CORDEX-Africa initiative, developed to analyse downscaled regional climate data over the CORDEX-African domain. The RCM considered in this study is the RCA4 (Rossby Centre Regional Atmospheric model), developed by the Swedish Meteorological and Hydrological Institute (SMHI), driven by the EC-EARTH global model (GCM) scenarios co-developed by the Irish Centre for High-End Computing (ICHEC). The selection of these combinations of models is motivated by the incompleteness of the CORDEX-Africa RCM-GCM

matrix: as noted in previous studies^{4,32}, only one RCM (RCA4) downscaled all the GCMs, and only one GCM (EC-EARTH) has been downscaled by all RCMs. In addition, CORDEX Africa does not provide multiple downscaled realizations for the same GCM-RCM model combination thus constraining the possibility of exploring internal model variability. However, ³² showed that their results based on the “one simulation one vote” approach are often robust regardless of the choice of the specific RCMs or GCMs. The RCPs considered are RCP 2.6, 4.5 and 8.5, to investigate low impact, business-as-usual and high impact scenarios, as described in higher detail in section 2.2. The variables chosen for the analysis and downloaded from CORDEX are the mean precipitation (pav) and the mean, maximum and minimum air surface temperature (tas, tasmax, tasmin, respectively). The temporal period considered for the climate analysis is a control period (CP) from 1981 to 2005 (as the observations period) and a projection period from 2006 to 2100 (following the above-mentioned RCPs).

The main steps followed to pre-process the climate data are summarized hereafter:

1. Find and edit the boundaries of the NRB and its main sub-basins
2. Collect gridded observation data from global datasets (CHIRPS, CHIRTS) and download CORDEX-AFR44 data
3. Cut observation data and CORDEX-AFR44 data with the NRB boundary, as well as its ten main sub-basins
4. Cut observation data and CORDEX-AFR44 data to match the CP in preparation for the bias correction
5. Compute mean temperature of observation data from CHIRTS (only available as maximum and minimum temperature) in preparation for the downscaling
6. Analyse the pre-processed climate data (1-5) following two different paths, applying the downscaling of the regional climate data cell by cell for each sub-basin (*gridded*) and computing the mean trajectories for each sub-basin before the downscaling (*mean*)

The computational toolbox used in this study to pre-process and downscale climate data is freely accessible on GitHub at the following link: <https://tinyurl.com/fuyyz5ac>.

4. CLIMATE ANALYSIS

The analysis of the downscaled climate data is done for all data (*mean* and *gridded*) as explained in section 3. In this part, the relevant plots and outcomes of the *mean* data are reported, along with some highlights from the *gridded* data when a higher resolution in the analysis is needed to provide more information (e.g., for Egypt). Each sub-section is dedicated to a different climate analysis, with a focus on the Main Nile, the Blue Nile, and the White Nile sub-basins, as the more relevant ones for the hydrology of the Nile, and thus for AWESOME models. The plots and indices generated for the resting seven Nile sub-basins are reported in Annex I and II. A closer look at Egypt’s climate projections is also given at the end of the section, along with an integration in Annex III.

4.1 TREND ANALYSIS

To investigate how precipitations and temperatures undergo the effects of climate change over time and for the different sub-basins, the MASH method is applied (detailed information here³³). The MASH is a tool used in the literature which allows to simultaneously investigate the seasonality in the data and filter out the effects of interannual variability. The MASH is applied in Exploratory Data Analysis for the detection of temporal trends in hydrological variables (e.g., ³⁴). In this analysis, the MASH plots are obtained by collecting the trajectories of the moving average over 20 consecutive days computed on a shifting horizon of 30 consecutive years. The figures are generated from the RCA4 model for the RCP 2.6, 4.5 and 8.5 emission scenarios, where each line of the plot represents the moving average indicated by shaded colours as time runs from 2006 (blue) to 2050 (green) until the end of the century (yellow). The shaded black line identifies the mean of the trajectories of the CP, thus the simulation over the control period 1981-2005, bias-adjusted applying the Quantile-Quantile mapping method and averaged over 20 consecutive days for each year (no climate trend given to the hypothesis of stationarity, s. section 2.2).

4.1.1 Main Nile sub-basin

Figures 9, 10 and 11 show the MASH plots of the mean precipitation over the Main Nile sub-basin, respectively for RCP 2.6, 4.5, 8.5. In the Main Nile, precipitation is almost null the entire year and, when present, its values are around 1 mm/d. In the CP (black shaded line), two peaks of a maximum 0,62 mm/day are reached during the year, one around May and the second around August, while the rest of the year is almost dry. In future projections, rainfall occurs in the same two periods, but following different behaviours. RCP 2.6 shows the highest peak of approx. 0.6 mm/d in late summer (delayed) and another one of approx. 0.2 mm/d in May, both in the years before the mid of the

century (blue), while a clear decrease towards the end of it (green to yellow). In RCP 4.5, the first peak is lower than in RCP 2.6 (down to 0.13 mm/d) while the second is higher, up to approx. 0.7 mm/d, both reached around the mid of the century. The peaks are shifted (anticipated to the end of April and delayed to the end of August- September, respectively) as they are progressively approaching 2100. In the worst scenario RCP 8.5, the range of precipitation seems slightly lower compared to the other two scenarios, with the two peaks respectively of 1.2 mm/d in April-May and lower than 0.6 mm/d in late August, both delayed in time. All RCPs show some rainfall also in October towards the end of the century. In general, very low precipitation and high interannual variability are expected.

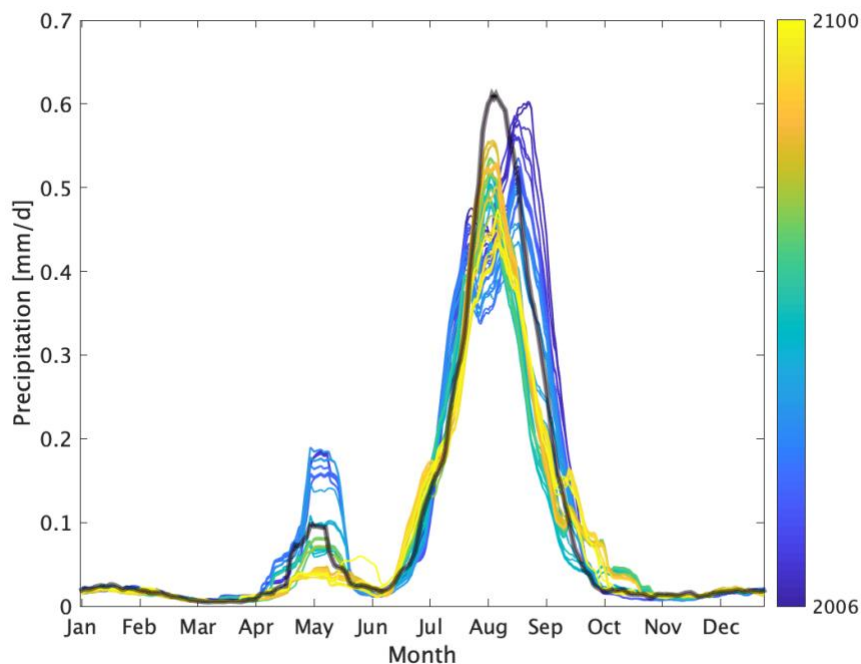


Figure 9 – MASH plot for precipitation in the Main Nile sub-basin for RCP 2.6. The black shaded line represents the mean over the CP (bias-adjusted).

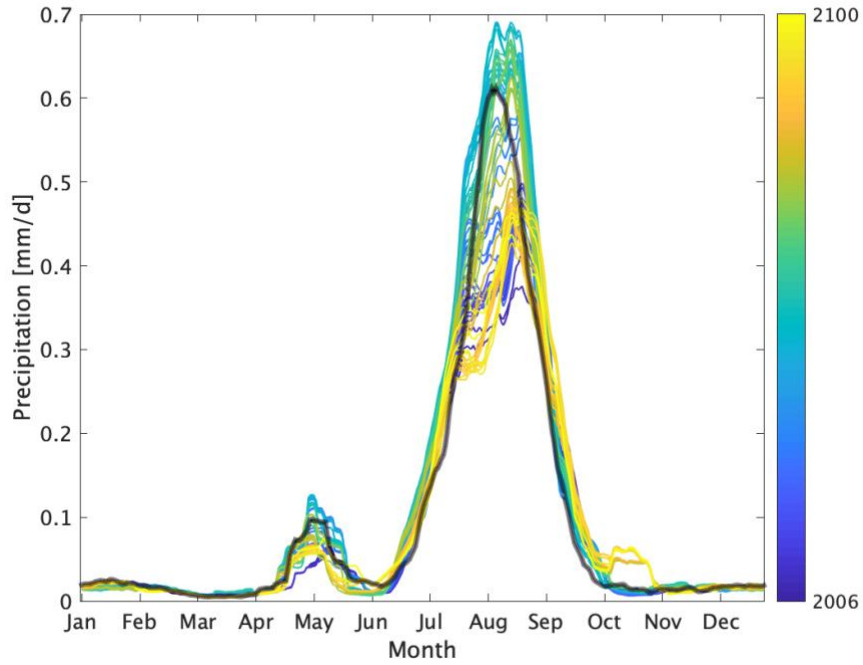


Figure 10 – MASH plot for precipitation in the Main Nile sub-basin for RCP 4.5. The black shaded line represents the mean over the CP (bias-adjusted).

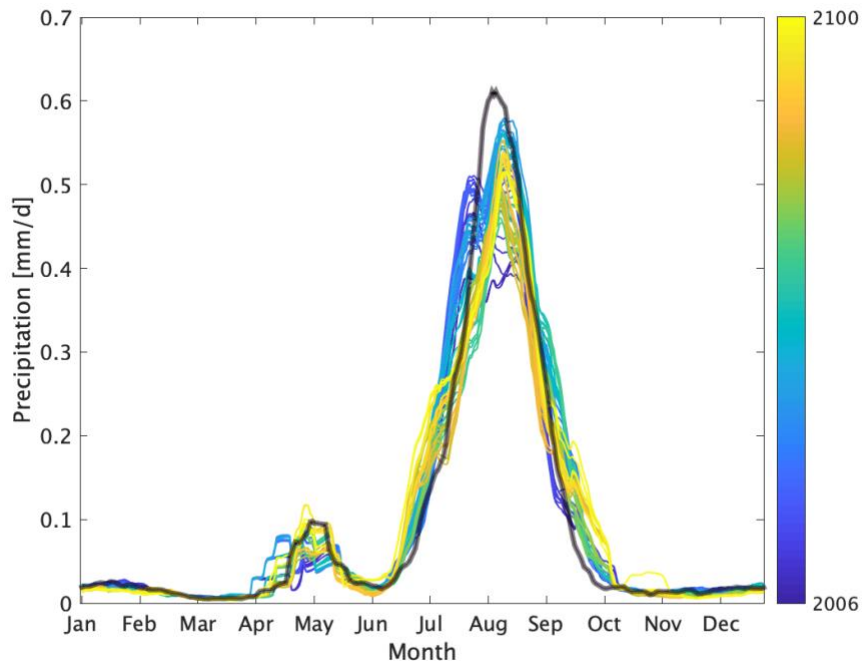


Figure 11 – MASH plot for precipitation in the Main Nile sub-basin for RCP 8.5. The black shaded line represents the mean over the CP (bias-adjusted).

Figures 12, 13 and 14 report the MASH plots of the temperatures, respectively for RCP 2.6, 4.5, 8.5. The temperatures in the Main Nile show a less complex behaviour, compared to the precipitations, with a similar course as the CP, and the peaks occurring in July-August (around 31 °C in the CP, 33 °C in RCP 2.6, 34°C in RCP 4.5, and 36-7 °C in RCP 8.5). The minimum temperatures are in December and January and range around 14 °C in CP, while 15°C in RCP 2.6, 16 °C in RCP 4.5, and 18 °C in RCP 8.5. The temperature increases progressively in all RCPs through time, except for RCP 2.6, which shows higher temperatures around the mid of the century and slightly lower ones towards 2100, with lower variability from one year to another. Also, it can be observed a widening of the warmer period, compared to the past. Especially in RCP 8.5 from March to June the increase is quite relevant, with temperatures reaching values of approx. 30 °C already in April towards 2100.

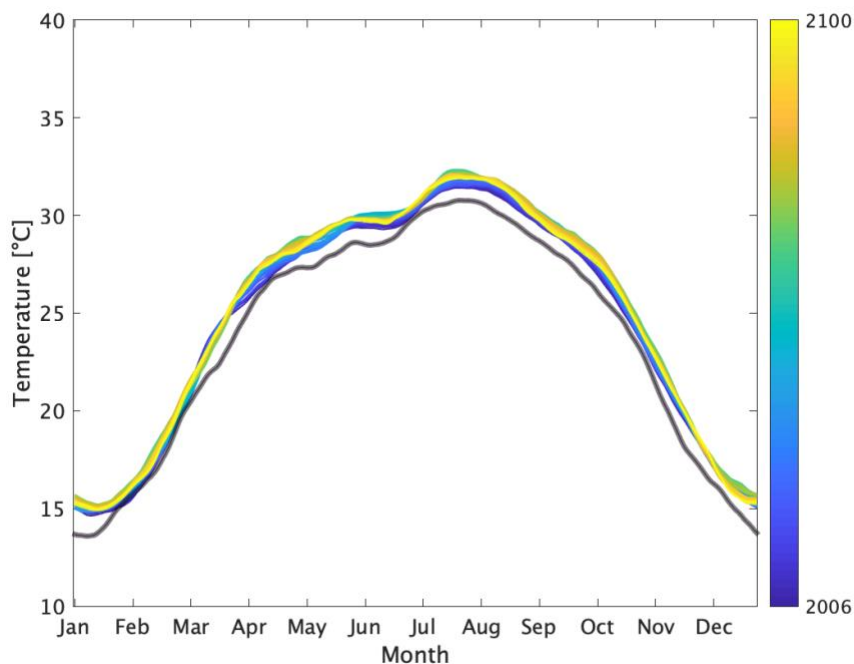


Figure 12– MASH plot for temperature in the Main Nile sub-basin for RCP 2.6. The black shaded line represents the mean over the CP (bias-adjusted).

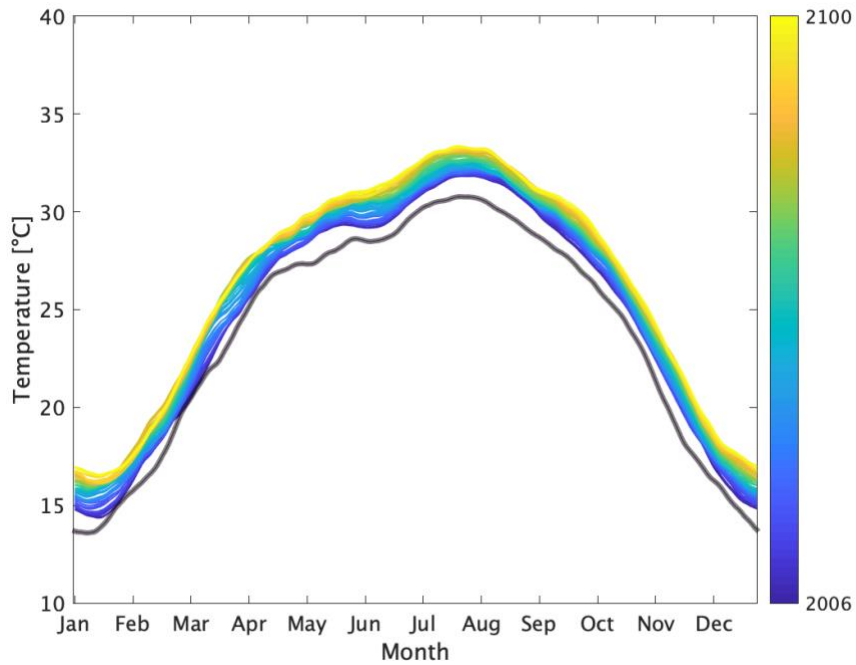


Figure 13 – MASH plot for temperature in the Main Nile sub-basin for RCP 4.5. The black shaded line represents the mean over the CP (bias-adjusted).

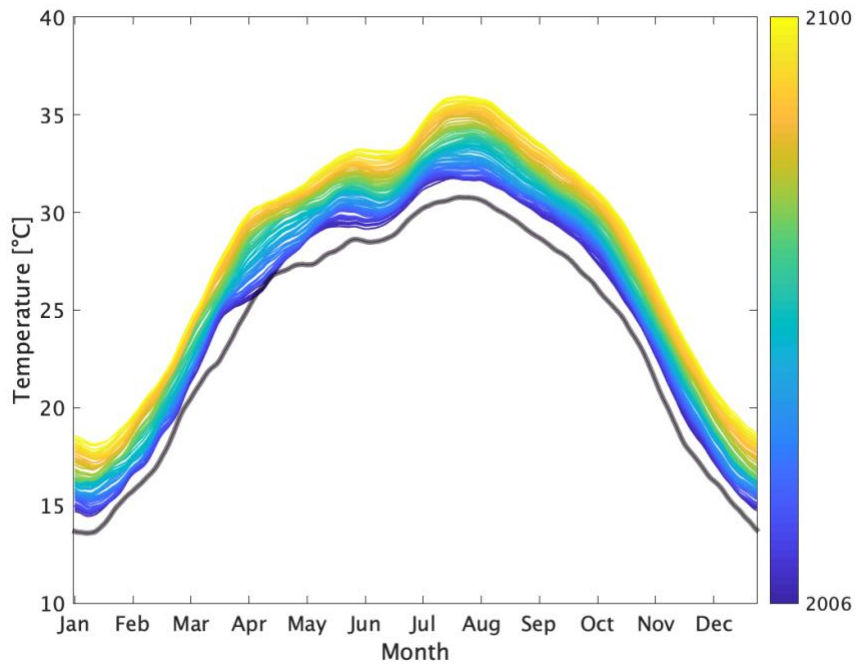


Figure 14 – MASH plot for temperature in the Main Nile sub-basin for RCP 8.5. The black shaded line represents the mean over the CP (bias-adjusted).

4.1.2 Blue Nile sub-basin

Figures 15, 16, 17 represent the MASH plots of the mean precipitation over the Blue Nile sub-basin, respectively for RCP 2.6, 4.5, 8.5. In the Blue Nile, precipitation ranges between zero and approx. 9.5 mm/d in the CP, where two main peaks can be observed, the first between April and May (approx. 4.5 mm/d) and the second in July and August (highest values up to 9,5 mm/d). In the future projections, precipitation looks like decreasing in time during the two main peak periods. RCP 2.6 reaches around 4 mm/d in the first one, while about 8-9 mm/d in summer, with a decrease of almost 1 mm/d as 2100 is approached. On the other hand, RCP 2.6 shows increasing rainfall values in October (1-2 mm/d). RCP 4.5 presents a similar behaviour to some extent, though predicting higher interannual variability, especially in summer (in which precipitation decreases in time down to 8 mm/d). In the months October-December, precipitation slightly increases in time up to 2 mm/d. Finally, RCP 8.5 shows a similar values range of the CP at the beginning of the century and progressively lower in time, with higher annual variability and lower (and shifted) peaks as time runs. At the end of the century, the first peak reaches about 3.5 mm/d, while the second one 8 mm/d.

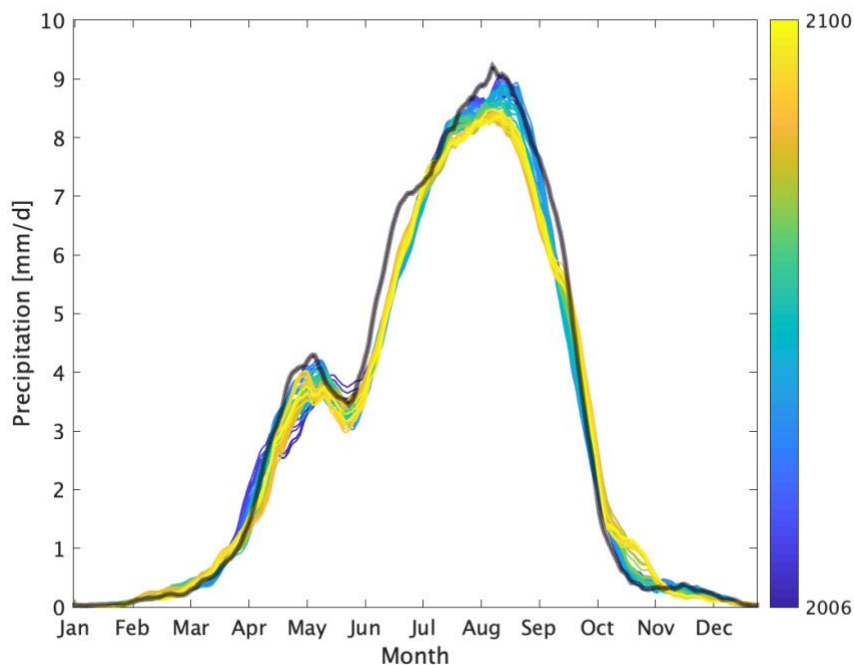


Figure 15 – MASH plot for precipitation in the Blue Nile sub-basin for RCP 2.6. The black shaded line represents the mean over the CP (bias-adjusted).

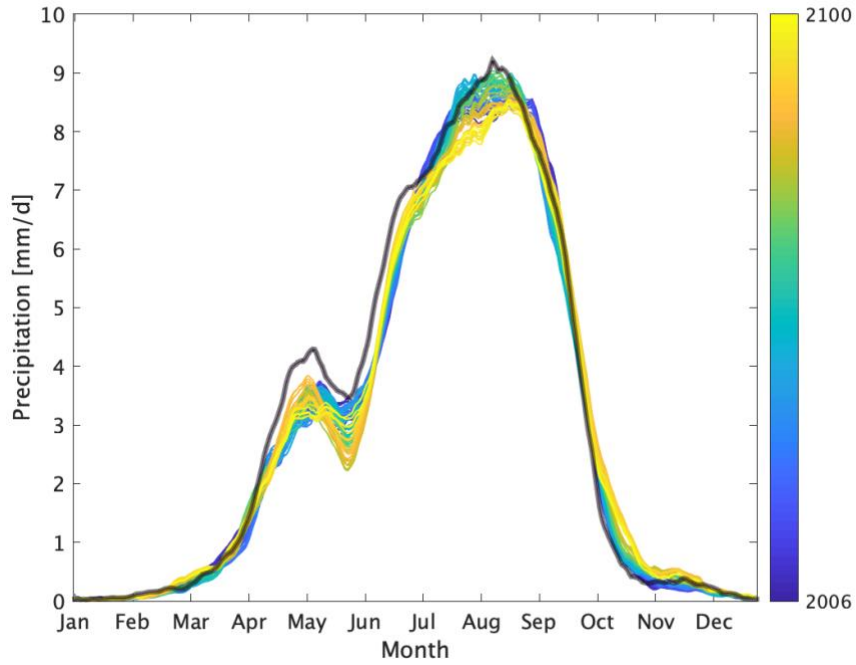


Figure 16 – MASH plot for precipitation in the Blue Nile sub-basin for RCP 4.5. The black shaded line represents the mean over the CP (bias-adjusted).

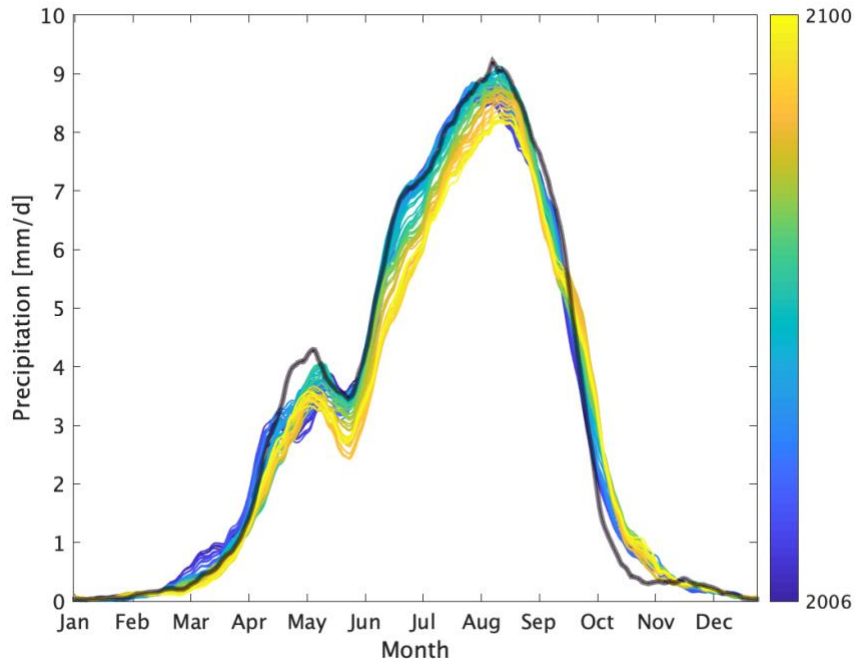


Figure 17 – MASH plot for precipitation in the Blue Nile sub-basin for RCP 8.5. The black shaded line represents the mean over the CP (bias-adjusted).

Figures 18, 19 and 20 report the MASH plots of the temperatures, respectively for RCP 2.6, 4.5, 8.5. In the Blue Nile sub-basin, the CP presents a temperature range between minimum values of 19 °C (around the mid of August and the December-January) and maximum values of 24.5 °C (in late March – beginning of April) and 23 °C (end of October-November). Another evident peak occurs around the end of May (22.5 °C). The different peak periods detected in CP are smoothed in the future projections, while the values reached are significantly higher. For RCP 2.6, the temperature growth in time is reported to be about 1-2 °C, while in RCP 4.5 between 2-3 °C. Also, the increase detected in RCP 2.6 is higher in the first mid of the century compared to the years closer to 2100, while the temperature increase is more evident as the end of the century is approached for the other two scenarios. In particular, RCP 8.5 shows the highest temperature range (e.g., the highest peak in spring was about 24-25 °C in the CP and for RCP 8.5 increases to more than 29 °C in 2100).

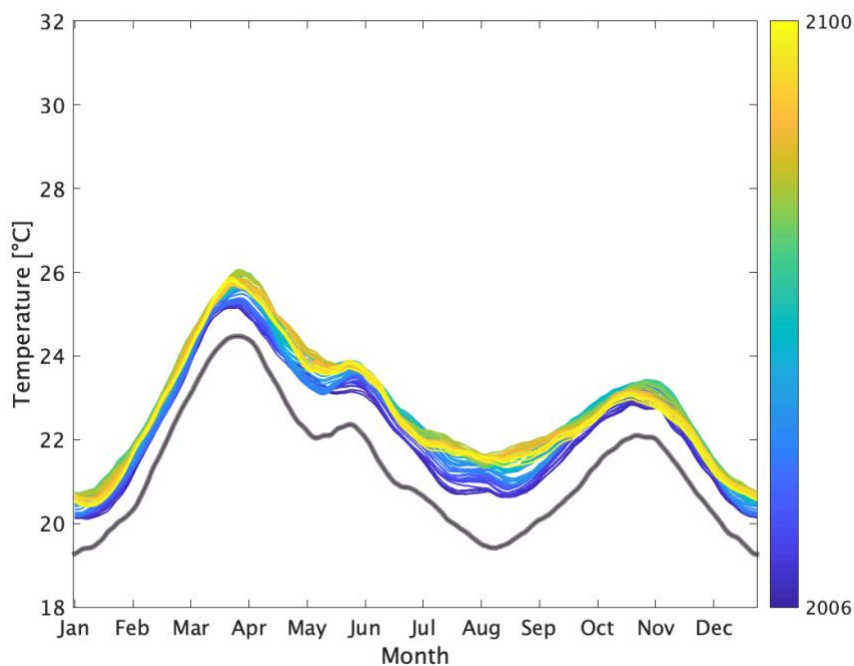


Figure 18– MASH plot for temperature in the Blue Nile sub-basin for RCP 2.6. The black shaded line represents the mean over the CP (bias-adjusted).

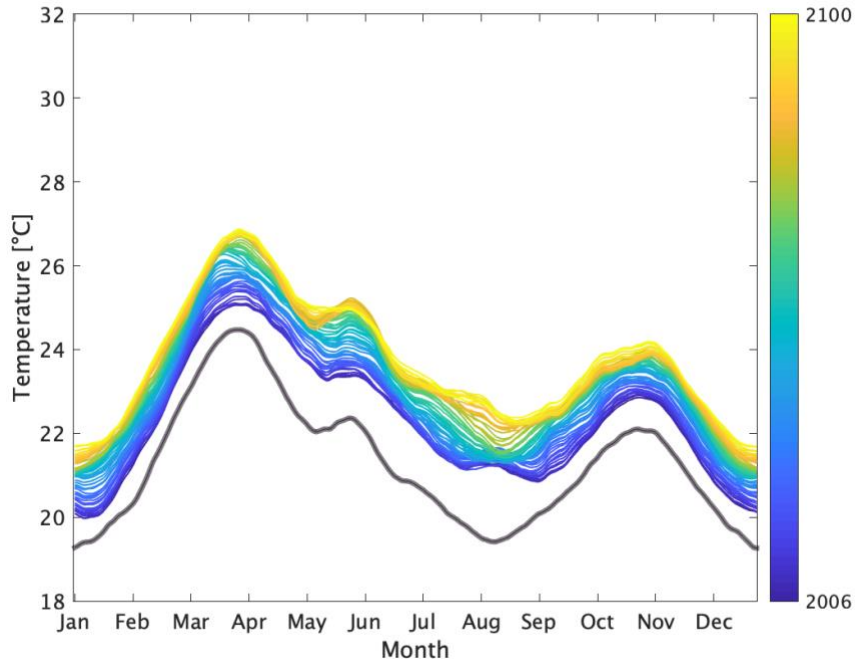


Figure 19 – MASH plot for temperature in the Blue Nile sub-basin for RCP 4.5. The black shaded line represents the mean over the CP (bias-adjusted).

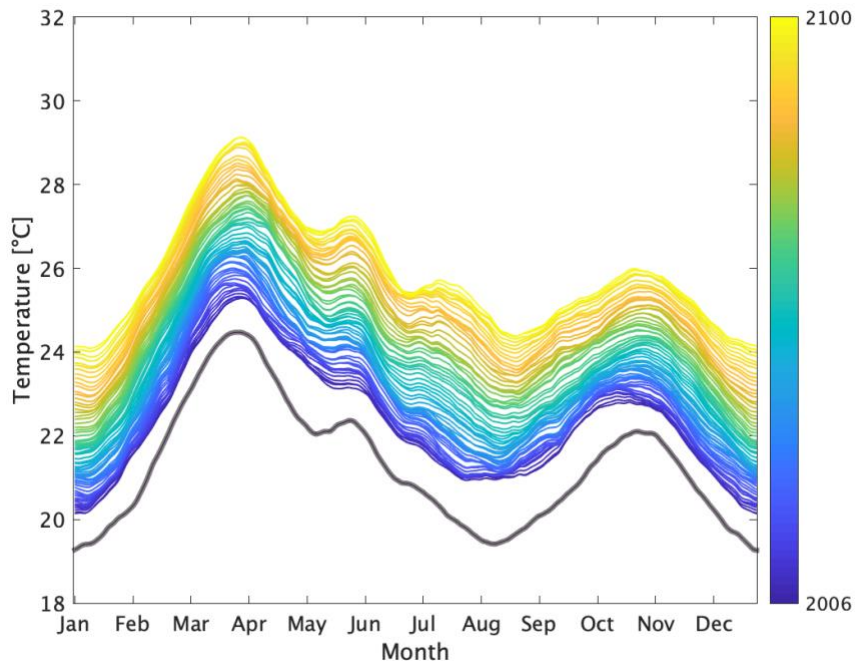


Figure 20 – MASH plot for temperature in the Blue Nile sub-basin for RCP 8.5. The black shaded line represents the mean over the CP (bias-adjusted).

4.1.3 White Nile sub-basin

Figures 21, 22 and 23 report the MASH plots of the mean precipitation over the White Nile sub-basin, respectively for RCP 2.6, 4.5, 8.5. In the White Nile sub-basin, the rainfall can occur from April to October. The CP and RCPs show a similar behaviour of the one observed in the Blue Nile, where in the CP, the first peak reaches 4 mm/d around end of April-May and the second 7 mm/d at the beginning of August. In RCP 2.6, the peak in May maintains values of about 4 mm/d in the first decades of the century (blue lines), when in June the values decrease in all years compared to the CP. The highest peak is delayed to the end of August and decreases to 6 mm/d by 2100. In general, precipitation decreases by about 1 mm/d both in late spring and in late summer. Higher variability and a decreasing trend are noticeable in RCP 4.5 and 8.5. In the first scenario, rainfall increases during summer by the mid of the century and then decreases towards the end of it down to 6 mm/d, while the values are similar in the spring period (shifted peaks). RCP 8.5 shows more interannual variability, especially anticipating the spring peaks and the summer ones before 2050 with much lower values, while delaying the summer one in the second half of the century, when rainfall diminishes to more than 1 mm/d. All future projections report higher precipitation (around 1-4 mm/d) in autumn (from the mid of September to the end of October).

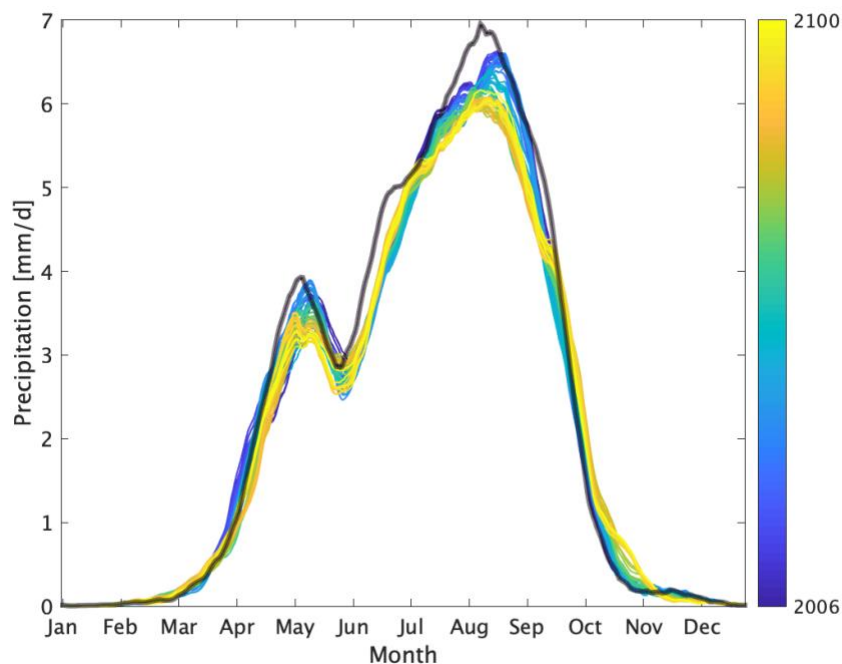


Figure 21 – MASH plot for precipitation in the White Nile sub-basin for RCP 2.6. The black shaded line represents the mean over the CP (bias-adjusted).

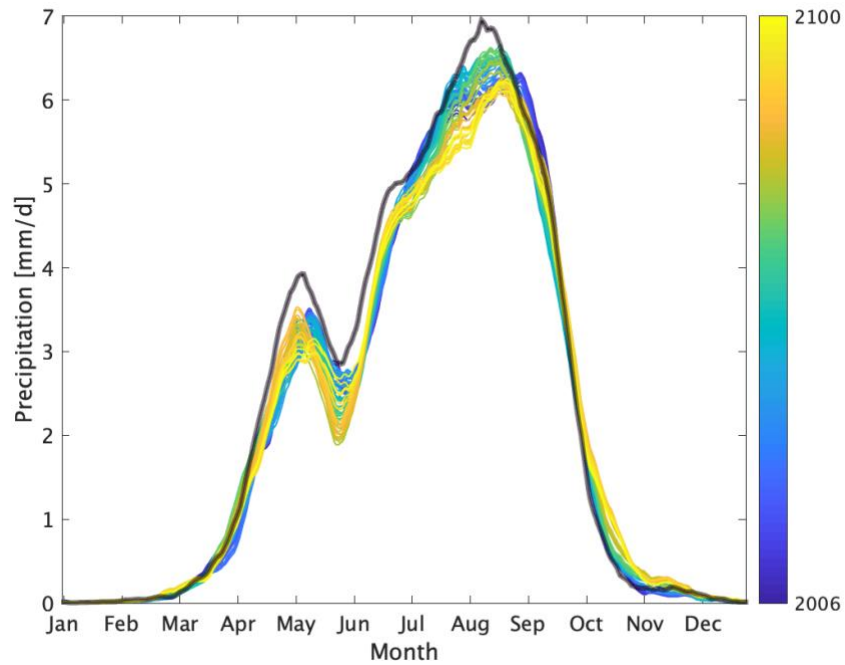


Figure 22 – MASH plot for precipitation in the White Nile sub-basin for RCP 4.5. The black shaded line represents the mean over the CP (bias-adjusted).

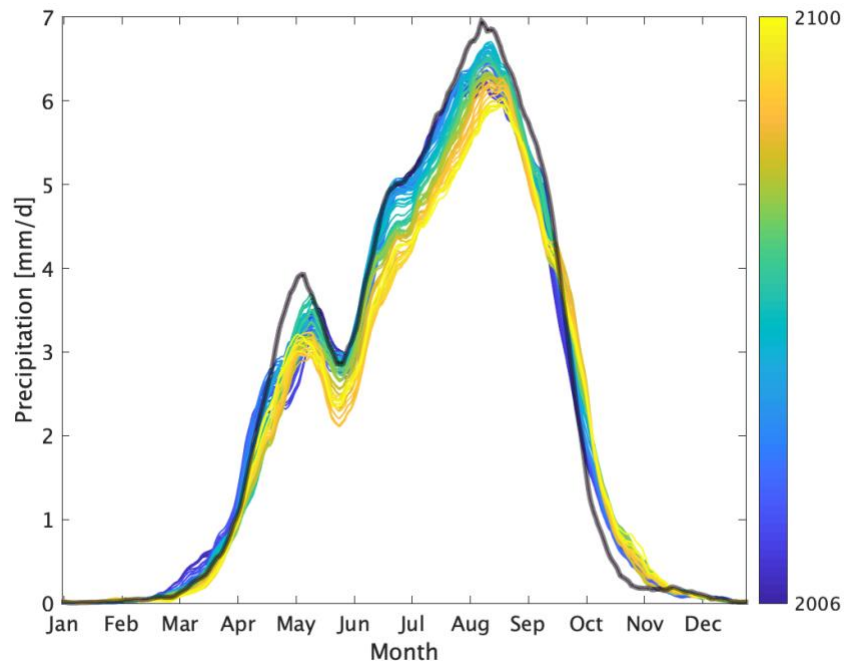


Figure 23 – MASH plot for precipitation in the White Nile sub-basin for RCP 8.5. The black shaded line represents the mean over the CP (bias-adjusted).

Figures 24, 25 and 26 report the MASH plots of the mean temperatures over the White Nile sub-basin. Looking at the CP, the peak periods are comparable with the ones observed in the Blue Nile sub-basin. In the White Nile, the lowest ones in January and December reach about 21 °C and about 22 °C in August, while the highest occur in late March (27 °C), late May (24.5 °C), late October (25 °C). For RCP 2.6, the temperatures show an increase of about 1 °C comparing 2060 to 2006, to then decrease of approx. 0.5 °C between 2060 and 2100 in late spring and in autumn. RCP 4.5 show a more progressive and larger increase in time (approx. 1-2 °C for highest temperatures, 2-3 °C for the lowest ones, comparing the beginning to the end of the century). The most evident and significant growth of temperatures is registered by RCP 8.5, in which the variation looks rather consistent over the years with a difference of approx. 4 °C between 2006 and 2100, even higher when compared with the CP values.

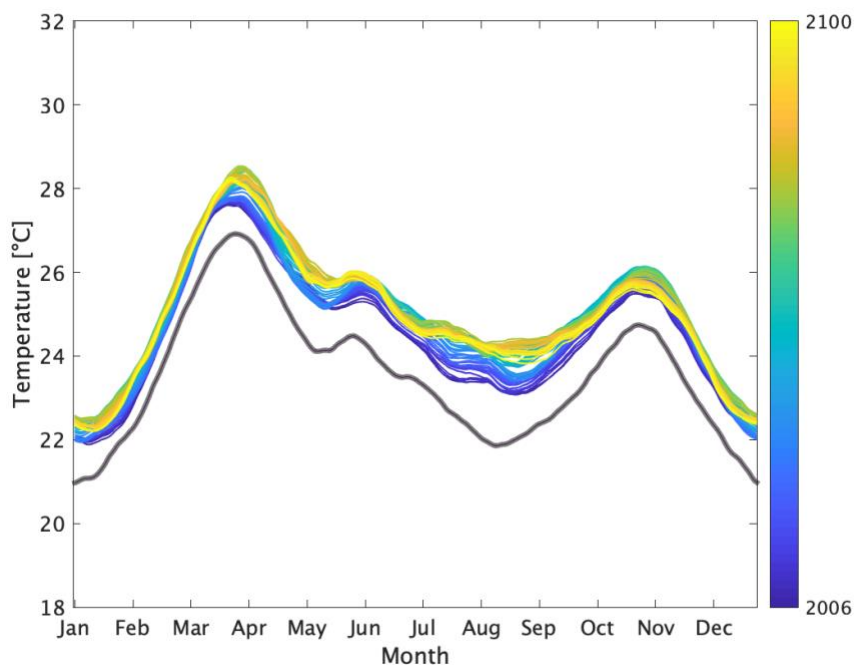


Figure 24– MASH plot for temperature in the White Nile sub-basin for RCP 2.6. The black shaded line represents the mean over the CP (bias-adjusted).

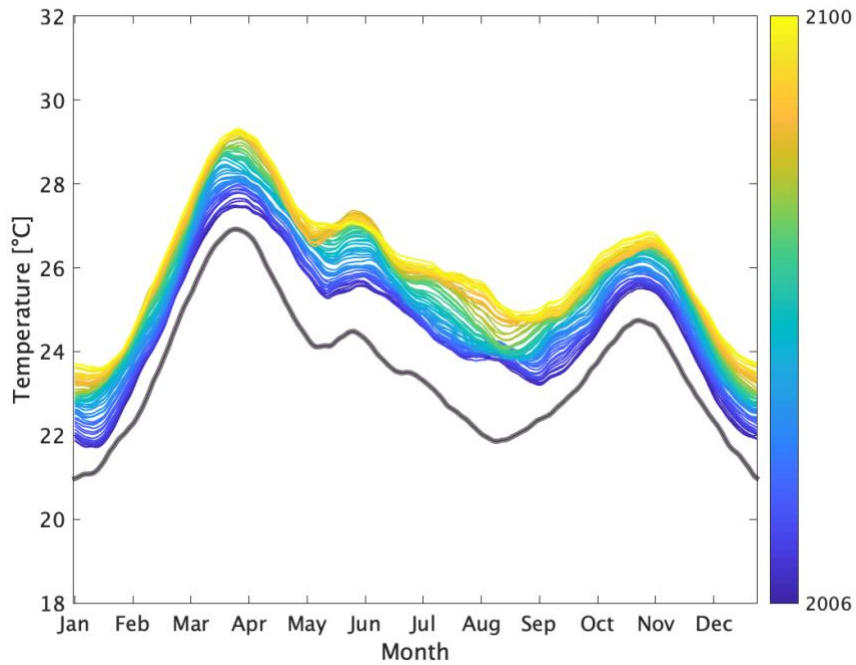


Figure 25 – MASH plot for temperature in the White Nile sub-basin for RCP 4.5. The black shaded line represents the mean over the CP (bias-adjusted).

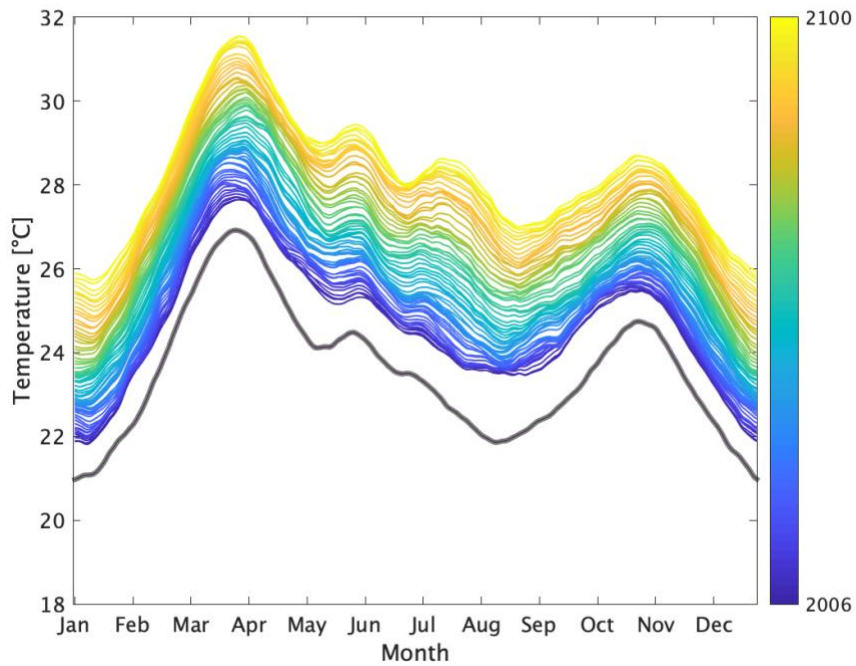


Figure 26 – MASH plot for temperature in the White Nile sub-basin for RCP 8.5. The black shaded line represents the mean over the CP (bias-adjusted).

The MASH plots of the remaining Nile sub-basins (Bahr el Jebel, Bahr el Ghazal, Baro Akobbo Sobat, Tekeze Atbara, Victoria Nile, Lake Victoria, and Lake Albert) are reported in Annex I.

4.2 CLIMATE INDICATORS

In the previous sections, it is observed how climate is changing in time and the different sub-basins of the Nile. Any change in frequency and severity of extreme events has profound impacts on nature and society. A fundamental tool to assess climate impacts and to analyse extreme events at the local level is the calculation of climate change indicators (CCI). CCI consist of a (usually linear) transformation of the historical daily precipitation and temperature series at the annual scale, considering the extremes of the probability distribution of these variables. Some examples are the annual cumulative intense rainfall, which considers only the values of precipitation above a certain percentile; or the drought duration, which considers only the period of maximum annual duration in which no rainfall events occur.

Table 2 – Description of the climate indices analysed in this study for the ten Nile sub-basins.

| Indices | Descriptive name | Definition | Units |
|---------|------------------------------------|---|-------|
| PRCPTOT | Annual total wet day precipitation | Annual total PRCP in wet days (RR \geq 1 mm) | mm |
| R95P | Very wet days | Annual total PRCP when RR $>$ 95 th percentile | mm |
| CDD | Consecutive dry days | Maximum number of consecutive days with RR $<$ 1 mm | Days |
| TX90 | Warm days | Percentage of days when TX $>$ 90 th percentile | % |
| TR | Tropical nights | Annual count when TN (daily minimum) $>$ 20 °C | Days |
| WSDI | Warm spell duration indicator | Annual count of days with at least 6 consecutive days when TX $>$ 90 th percentile | Days |

To create a common framework for the CCI, the ETCCDI (Expert Team on Climate Change Detection and Indices) has drawn up a list of 27 indicators³⁵. Among these, Table 2 reports the ones computed in this study, as considered more relevant to assess climate change with the local climate conditions. The mathematical formulation of each of these indicators is available here³⁶. The tool used for the calculation is RCLimDex, based on R and freely available on GitHub at this link: <https://github.com/ECCC-CDAS/RCLimDex>. The downscaled climate data of each Nile sub-basin are

examined after QC criteria testing for the presence of possible outliers, inhomogeneity, or missing data. Using the RCLimDex software, this assessment allows for the identification and documentation of potential non-systematic errors and ensures that the data series are free of gross errors.

4.2.1 Main Nile sub-basin

Figure 27 reports the climate indicators computed statistically downscaling the *mean* climate data on the Main Nile sub-basin under the forcing pathway RCP 2.6, where the solid line shows the trend computed by linear least squares and the dashed line is calculated through a locally weighted linear regression using a less smooth function (more information here³⁷). Statistics of the linear trend fitting are displayed on the plots. This will be the same for all subsequent plots.

The cumulated total precipitation in wet days (PRCPTOT, top-left) shows a decreasing trend and lower extremes in time, with the highest value of approx. 170 mm/d in 2030 (the peak is also depictable in the R95P plot, top-right). Very wet days occur rarely and mostly in the first half of the century, while they tend to decrease and happen seldom in the second half. The CDD indicator (mid-left) shows high variability and high values of consecutive dry days (when rainfall falls lower than 1 mm/d), meaning that the Main Nile sub-basin is almost always dry. Also, CDD shows almost no change in the trend between 2006 and 2100.

Regarding temperatures, TR20 (mid-right), TX90 (bottom-left) and WSDI (bottom-right) increase relevantly around mid of century to then decrease after a peak in 2050-2060, as dictated by the emission pathway RCP 2.6. In fact, the growth in the frequency of heatwaves is dependent on the increase in emissions. Nevertheless, the trend of the three indicators is slightly increasing across the entire century. The indicator of the tropical nights (TR) reports the annual count of the days in which the minimum daily temperature (TN) is higher than 20 °C and they occur at least for 1/3 of the year, as the range calculated is between 120 and 160 days. The warm day's indicator (TX90) reaches its maximum of almost 25 days around the year 2060, while at the same time the WSDI present a higher intensity and extremes in the years 2060-2080.

Figure 28 reports the six climate indicators for the RCP 4.5, while Figure 29 the ones for RCP 8.5. In both cases, the annual total precipitation (top-left) reaches a maximum of approx. 100 mm/d in the mid of century for RCP 4.5 and different years after 2030 in RCP 8.5. Looking at R95P, extreme events will be rarer in RCP 4.5 but with high peaks in 2040-2050 and 2080 (40-50 mm/d), while their intensity and interannual variability will be more consistent in RCP 8.5, especially in the second half of the century. Consequently, the trend of CDD is hardly defined in both pathways, although its values remain very high. This confirms the high unpredictability of rainfall in the Main Nile sub-basin. The temperature indicators reflect the RCP 4.5 and 8.5 emission pathways, as they present a progressive growth during the entire century, higher for RCP 8.5. In both cases (but with different

magnitudes) TX90 and WSDI (bottom-left and bottom-right, respectively) also show an increase in the variability, after 2040 in RCP 4.5, while more evident in the last two decades in RCP 8.5. E.g., WSDI was lower than 20 days before the mid of the century and arrives until ranges of 80-130 days closer to 2100, when almost 50% of the time extreme temperatures will be reached (TX90).

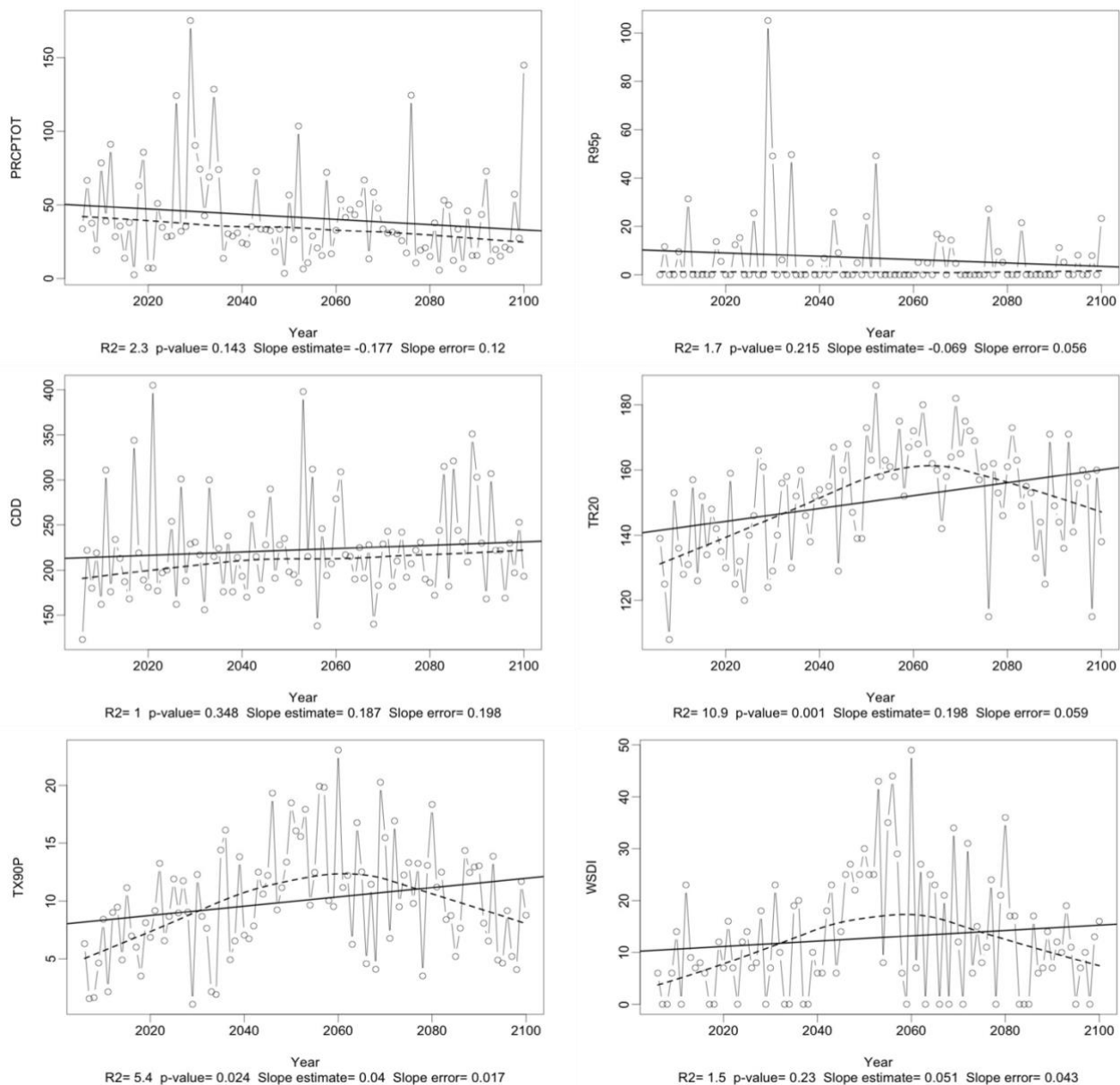


Figure 27 – Climate indices PRCPTOT (top-left), R95P (top-right), CDD (mid-left), TR20 (mid-right), TX90P (bottom-left), WSDI (bottom-right) in the Main Nile sub-basin for RCP 2.6. The solid line shows the trend computed by linear least squares and the dashed line is calculated through a locally weighted linear regression using a loess smoother function. Statistics of the linear trend fitting are displayed on the plots. This will be the same for all subsequent plots.

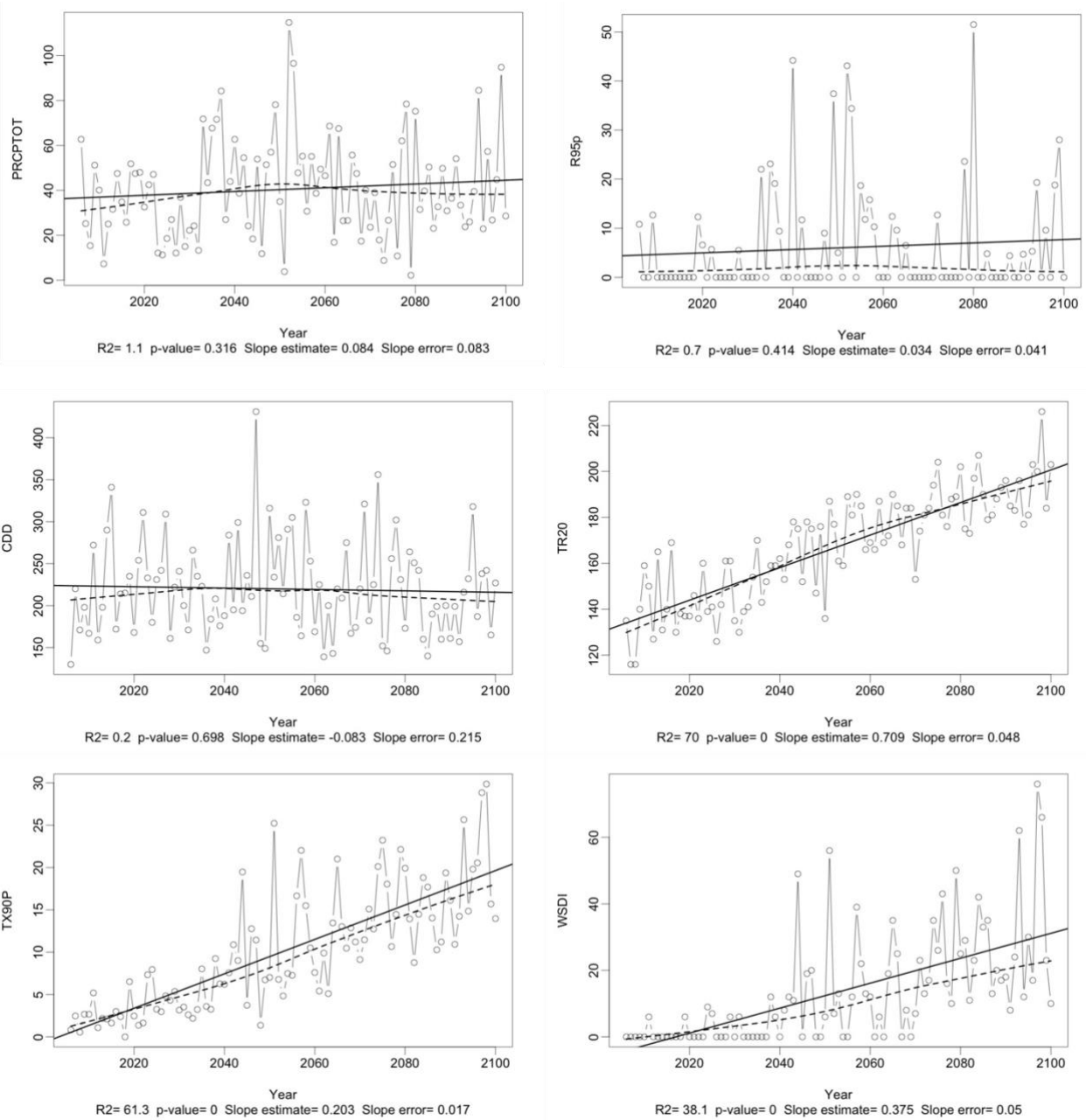


Figure 28 – Climate indices PRCPTOT (top-left), R95P (top-right), CDD (mid-left), TR20 (mid-right), TX90P (bottom-left), WSDI (bottom-right) in the Main Nile sub-basin for RCP 4.5.

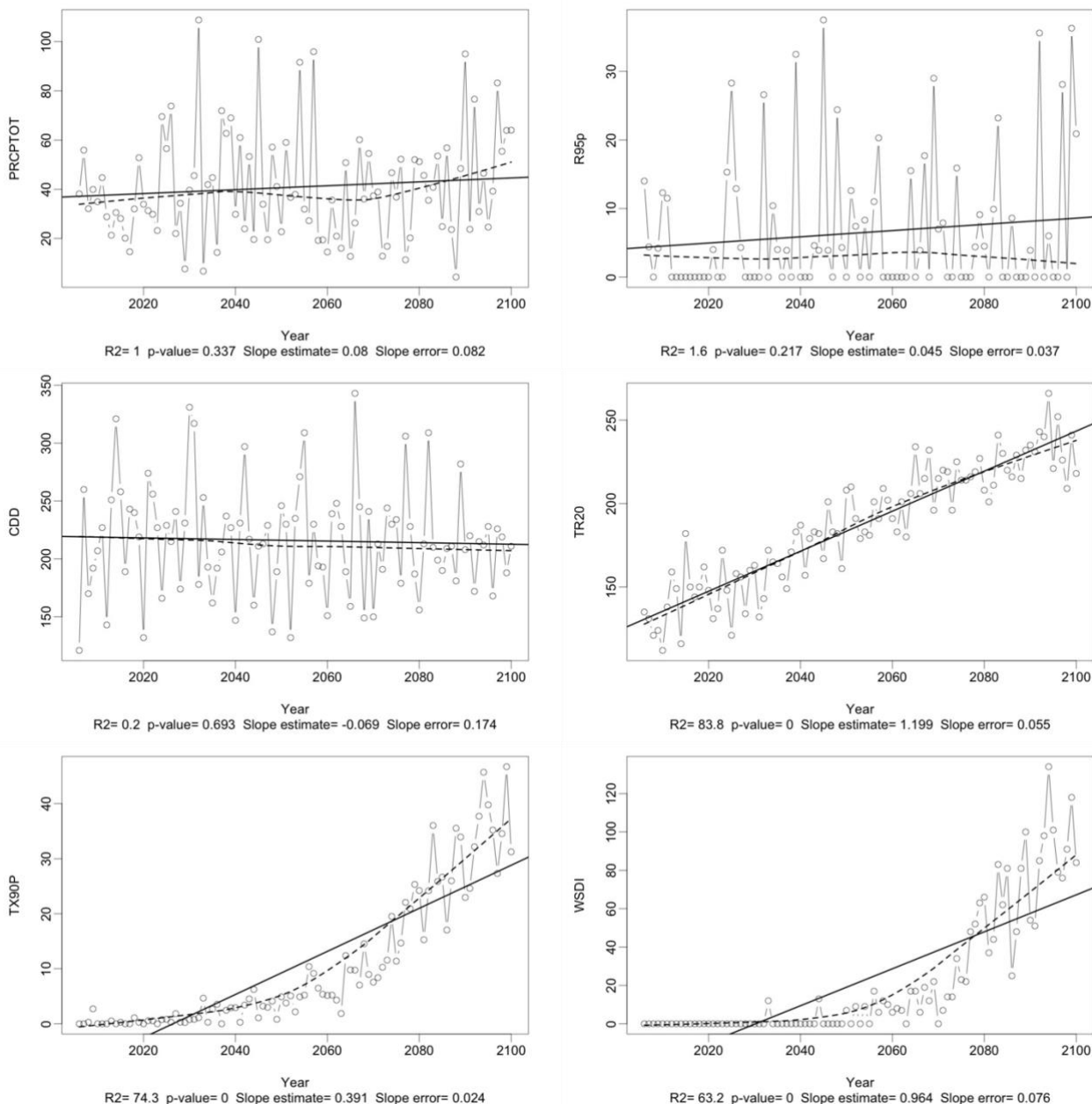


Figure 29 – Climate indices PRCPTOT (top-left), R95P (top-right), CDD (mid-left), TR20 (mid-right), TX90P (bottom-left), WSDI (bottom-right) in the Main Nile sub-basin for RCP 8.5.

4.2.2 Blue Nile sub-basin

Figures 30, 31 and 32 report the climate indicators PRCPTOT (top-left), R95P (top-right), CDD (mid-left), TR20 (mid-right), TX90P (bottom-left), WSDI (bottom-right), computed from the *mean* climate

data statistically downscaled on the Blue Nile sub-basin for the three forcing pathways RCP 2.6, 4.5, 8.5, respectively.

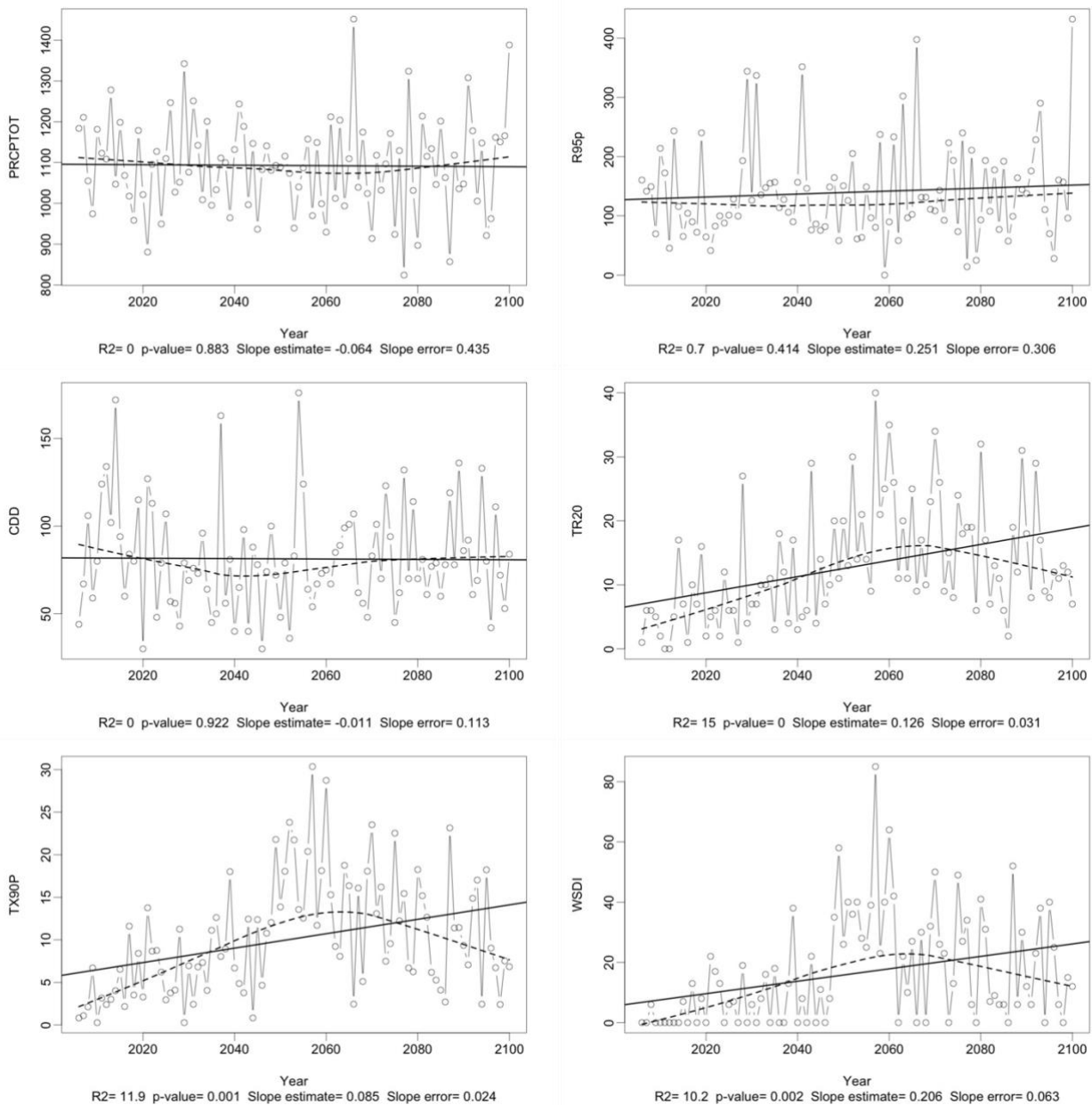


Figure 30 – Climate indices PRCPTOT (top-left), R95P (top-right), CDD (mid-left), TR20 (mid-right), TX90P (bottom-left), WSDI (bottom-right) in the Blue Nile sub-basin for RCP 2.6.

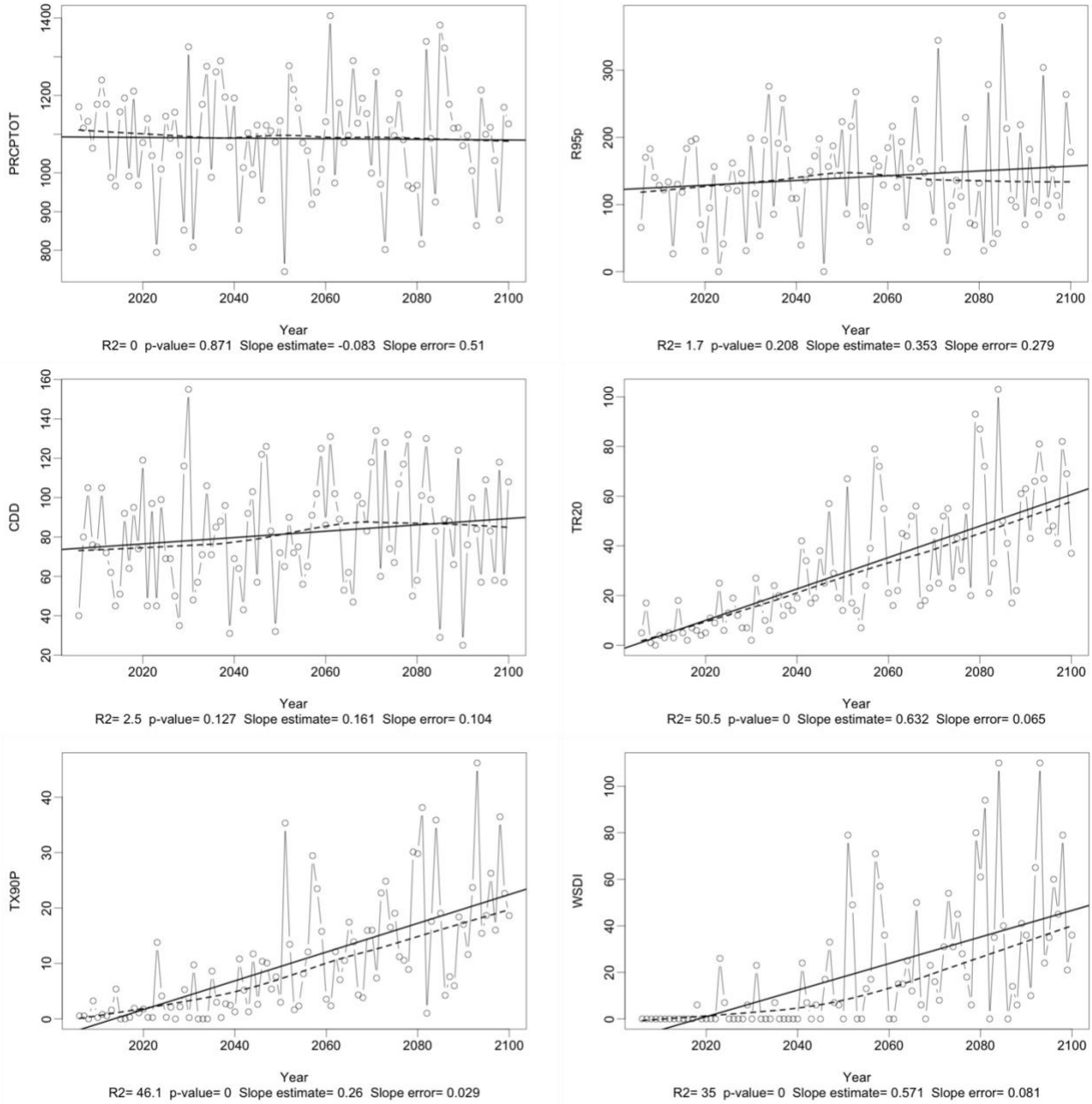


Figure 31 – Climate indices PRCPTOT (top-left), R95P (top-right), CDD (mid-left), TR20 (mid-right), TX90P (bottom-left), WSDI (bottom-right) in the Blue Nile sub-basin for RCP 4.5.

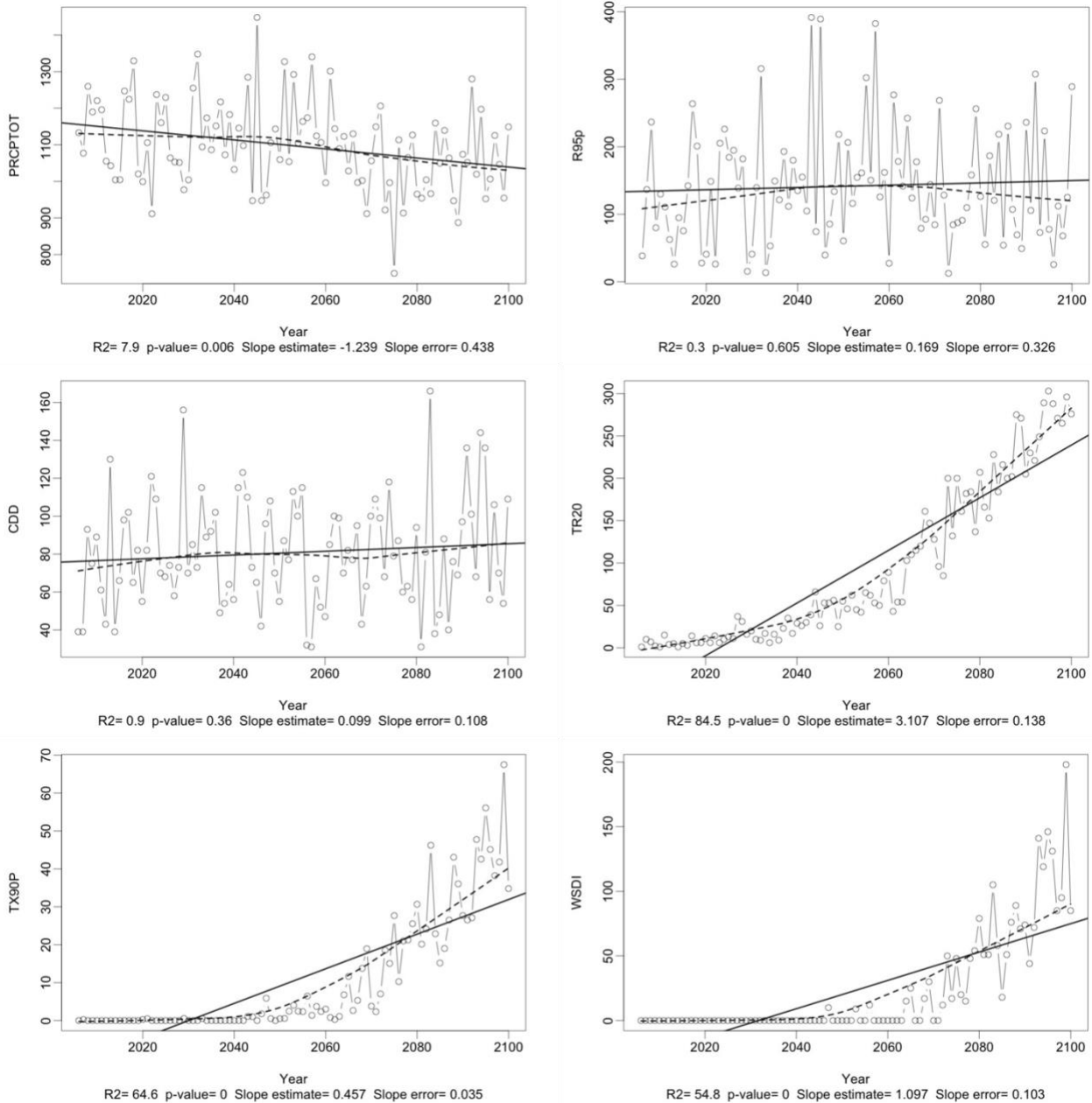


Figure 32 – Climate indices PRCPTOT (top-left), R95P (top-right), CDD (mid-left), TR20 (mid-right), TX90P (bottom-left), WSDI (bottom-right) in the Blue Nile sub-basin for RCP 8.5.

For all scenarios, the first thing to notice is that the precipitation amount is much more consistent than in the Main Nile. The annual cumulated rainfall (PRCPTOT) ranges between 800 and 1400 mm/d and the extreme rainfall (R95P) can reach values of 400 mm/d. The precipitation indices analysed show no clear trend in time for the three different pathways, although PRCPTOT seems to decrease

especially in the second half of the century in RCP 8.5 (Figure 32, top-left). R95P (top-right) present a complex behaviour, where in RCP 2.6 (Figure 30) frequency and intensity are higher around 2060 while lower peaks but still frequent can be noticed towards 2100. In RCP 4.5 (Figure 31) the extreme events will occur more often and with progressively higher values in time (mostly between 50 mm/d and 200-300 mm/d), while much interannual higher variability is observed for RCP 8.5, with the highest peaks of 300-400 mm/d and the lowest of zero (Figure 32, top-right). Also looking at the maximum drought duration index CDD, no clear trend can be depicted. CDD values range between more than 20-30 and 160 days, lower for RCP 2.6, while higher for RCP 4.5 with similar intensity in time, and with higher variability for RCP 8.5.

Regarding temperatures, similar behaviour as the one of the Main Nile can be observed. For RCP 2.6, the three temperature-related indices present a relevant increase until the mid of the century and a decrease afterwards, while remaining higher than the ones at the beginning. In the same year 2057, TR20 reaches a peak of 40 days, TX90 of 30% and WSDI of 85 days. RCP 4.5 and 8.5 scenarios show a different behaviour from RCP 2.6, as they experience both a progressive increase of temperatures in time. The occurrence of the tropical nights (TR20) and long-lasting temperature extremes (TX90 and WSDI) clearly grows in intensity and interannual variability across the century, more intensively in the second half for RCP 8.5, compared to the first (TR20 equal to 250-300 days in the last two decades, while up to maximum 100 days in RCP 4.5).

4.2.3 White Nile sub-basin

Figures 33, 34 and 35 report the climate indicators PRCPTOT (top-left), R95P (top-right), CDD (mid-left), TR20 (mid-right), TX90P (bottom-left), WSDI (bottom-right) computed by statistically downscaling the *mean* climate data on the White Nile sub-basin for the three forcing pathways RCP 2.6, 4.5, 8.5, respectively.

Looking first at the three rainfall-related indicators, the trends are hardly detected. The annual precipitation range (PRCPTOT) lies between 600 mm/d and 1100 mm/d in any of the three scenarios considered, where RCP 2.6 present a decrease of the extremes in the mid of the century and again higher variability towards the last decades. This high variability across the century is even more evident in RCP 4.5 and in RCP 8.5, which also shows a decreasing trend. RCP 2.6 will experience less intense events (R95P) between 2035 and before 2060, and even lower after 2080, except for the years 2091-2093, and 2100 (350 mm/d). Extreme precipitation will occur more frequently in RCP 4.5 and its occurrence is projected to change relevantly from one year to another (e.g., from zero in 2084 to 300 mm/d in 2085). In comparison, RCP 8.5 presents higher values of R95P between 2040 and 2060, while the lower occurrence of such high values in the second half of the century. The consecutive dry day's index (CDD) seems to slightly decrease in the first two-three decades in RCP

2.6 but shows a very high interannual variability. This is more evident in RCP 4.5, where the CDD reaches higher values more frequently during the century, as well as in RCP 8.5, which also reports a slight increase of the indicator.

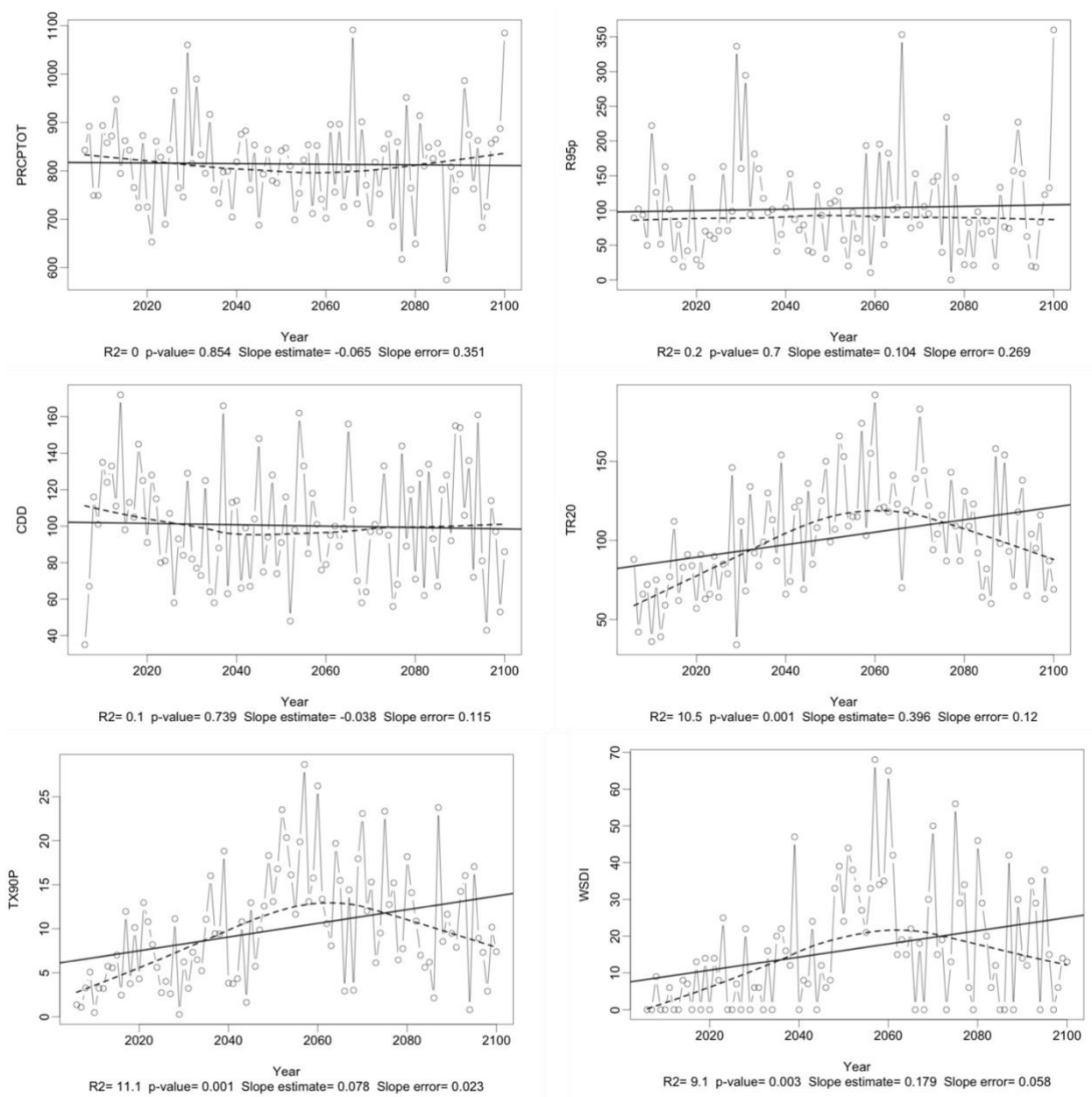


Figure 33 – Climate indices PRCPTOT (top-left), R95P (top-right), CDD (mid-left), TR20 (mid-right), TX90P (bottom-left), WSDI (bottom-right) in the White Nile sub-basin for RCP 2.6.

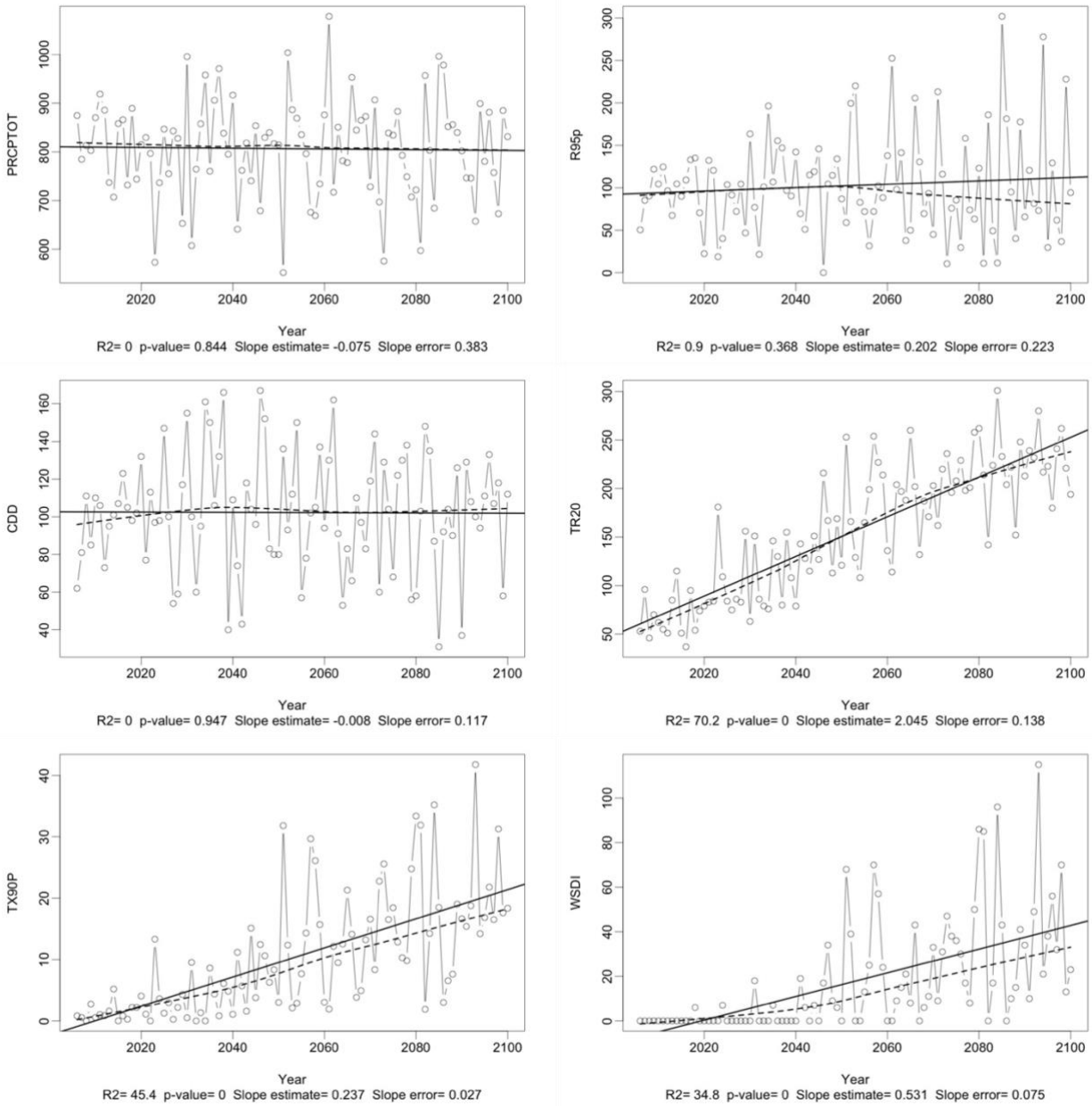


Figure 34 – Climate indices PRCPTOT (top-left), R95P (top-right), CDD (mid-left), TR20 (mid-right), TX90P (bottom-left), WSDI (bottom-right) in the White Nile sub-basin for RCP 4.5.

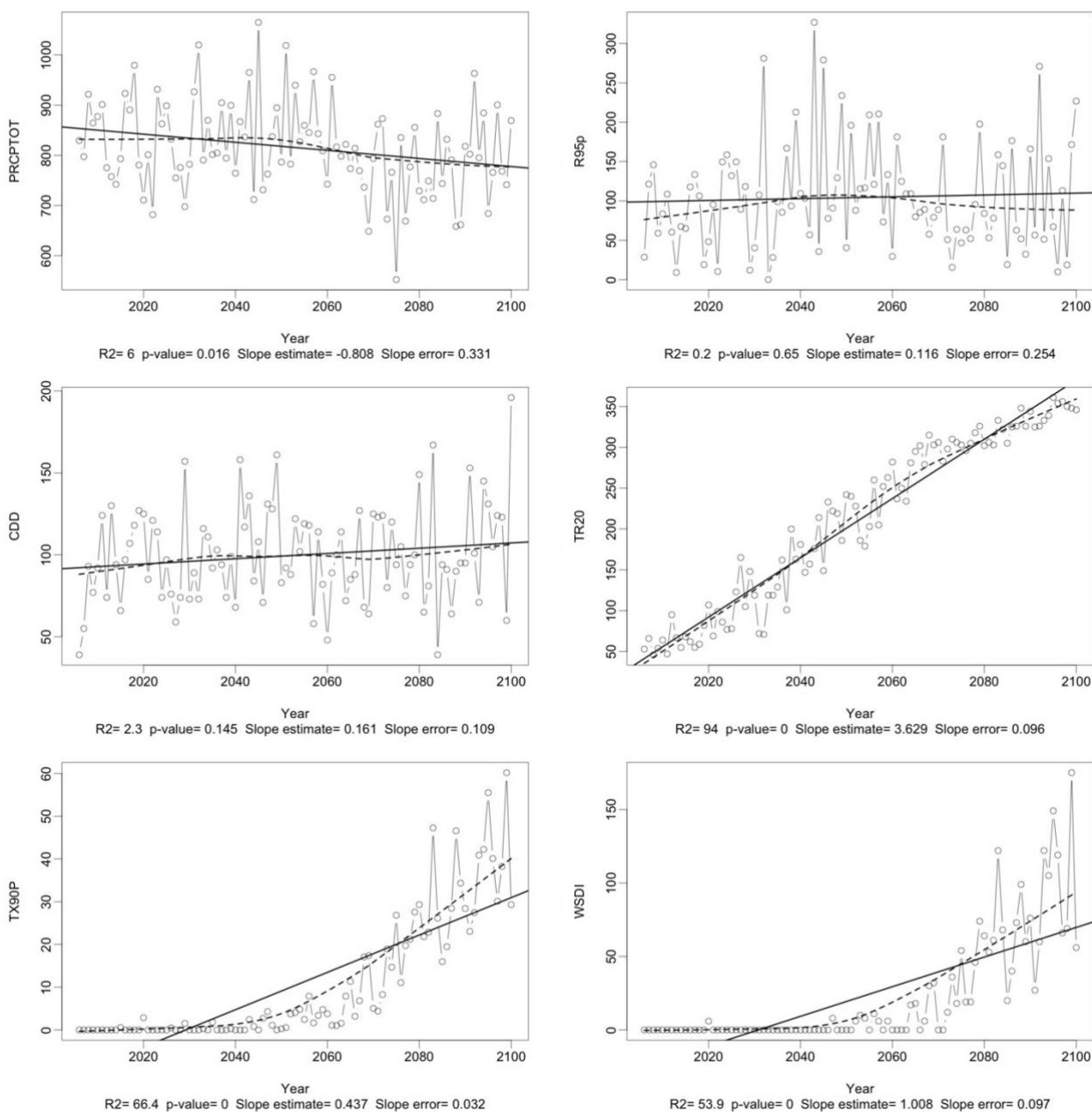


Figure 35 – Climate indices PRCPTOT (top-left), R95P (top-right), CDD (mid-left), TR20 (mid-right), TX90P (bottom-left), WSDI (bottom-right) in the White Nile sub-basin for RCP 8.5.

The tropical nights, warm days and warm spell duration indicators report the usual behaviour observed in the previous cases. In the RCP 2.6 scenario, they relevantly increase until 2050-2060, to

then decrease to lower values, similar or slightly higher than the initial ones, although the occurrence of the higher values in time produces an increasing linear trend across the entire century. A more evident and progressive growing trend can be observed in RCP 4.5 and RCP 8.5, e.g., TR20 ranges between 150 and 300 days in the last two decades of the century in the first scenario, while it increases almost linearly in the second one, reaching values around 250 days and higher already after 2060. In RCP 8.5, extreme temperatures will occur 20 to 60% of the year after 2080 varying from one year to another, mostly lasting more than 6 consecutive days more than 50 days per year.

The plots of the climate indicators calculated for the resting Nile sub-basins (Bahr el Jebel, Bahr el Ghazal, Baro Akobbo Sobat, Tekeze Atbara, Victoria Nile, Lake Victoria, and Lake Albert) are reported in Annex II.

4.3 A CLOSER LOOK AT EGYPT

As mentioned at the beginning of this section, some highlights of the analysis lead from the high-resolution (*gridded*) climate data are reported for Egypt, as it is the location of the AWESOME micro-level models of WP5, where the project demo-sites are being implemented.

The maps in the next figures (Figure 36, 37, 38, and 39) show some snapshots of the spatially distributed mean precipitation and maximum temperatures respectively occurring on the wettest and hottest days in the CP and then in the three different future scenarios. The daily rainfall values are represented in a coloured scale progressively ranging from dark blue to green to yellow, as precipitation decreases from the highest values (60 mm/d for the CP, while 150 mm/d for the RCPs) to the lowest (null), while the white area indicates Qattara depression in the north-western desert. The daily temperatures are indicated by the same scale of colours, but the coldest (lower values) are in dark blue, while the hottest are in yellow. The main river stretch and the main canals of the Main Nile are represented in cyan, while the boundary of its hydrological sub-basin in black (thin). As can be noticed both in the plots of the CP and in the ones of the future projections, precipitation shows a significantly high spatial variability in comparison to the temperature. Rainfall increases in some cells and decreases in others, presenting a complex and hard-to-predict behaviour. In general, the amount of rainfall is predicted to be low and occasional. The snapshots taken in the CP report a rather homogeneous precipitation of 20 mm/d, except for the northern strip next to Alexandria (Figure 36, left) and in the Sinai region (Figure 36, right) where the highest peaks reach 60 mm/d. Looking at the wettest days in the different RCPs (Figure 38), the spatial variability is higher and precipitation is predicted to be zero in large areas of the country (RCP 2.6 and RCP 8.5) while it occurs in a high amount up to 150 mm/d in some other regions, different from scenario to scenario.

RCP 4.5 foresees a wider distributed precipitation in the central-eastern part of Egypt, in the range of 50-100 mm/d.

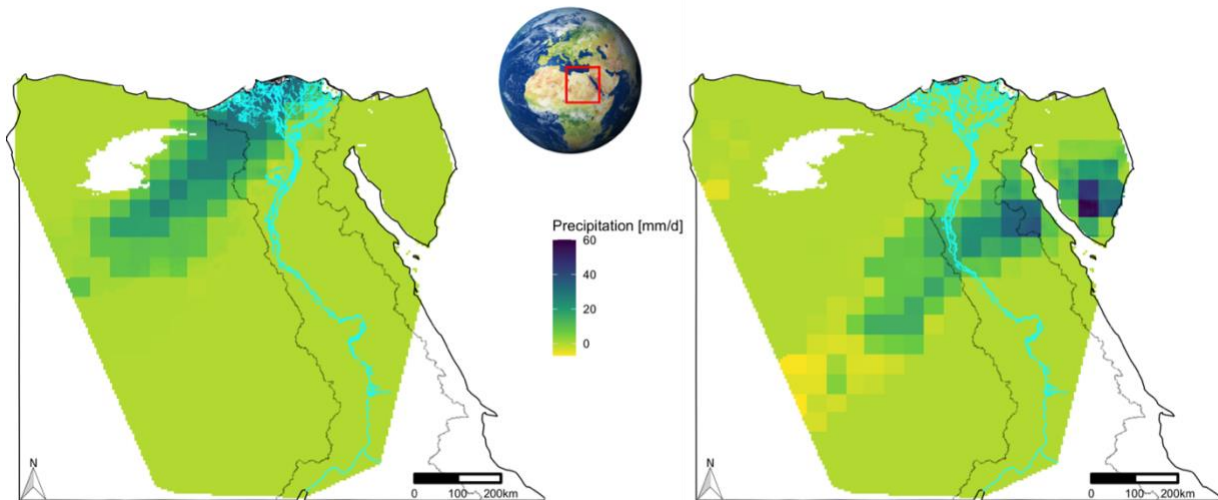


Figure 36 – Snapshots of the spatially distributed mean precipitation [mm/d] (*gridded* data) in Egypt on the two wettest days in the CP: 11th of March 1984 (left) and 1st of May 1997 (right). The white area indicates the Qattara depression in the Egyptian north-western desert.

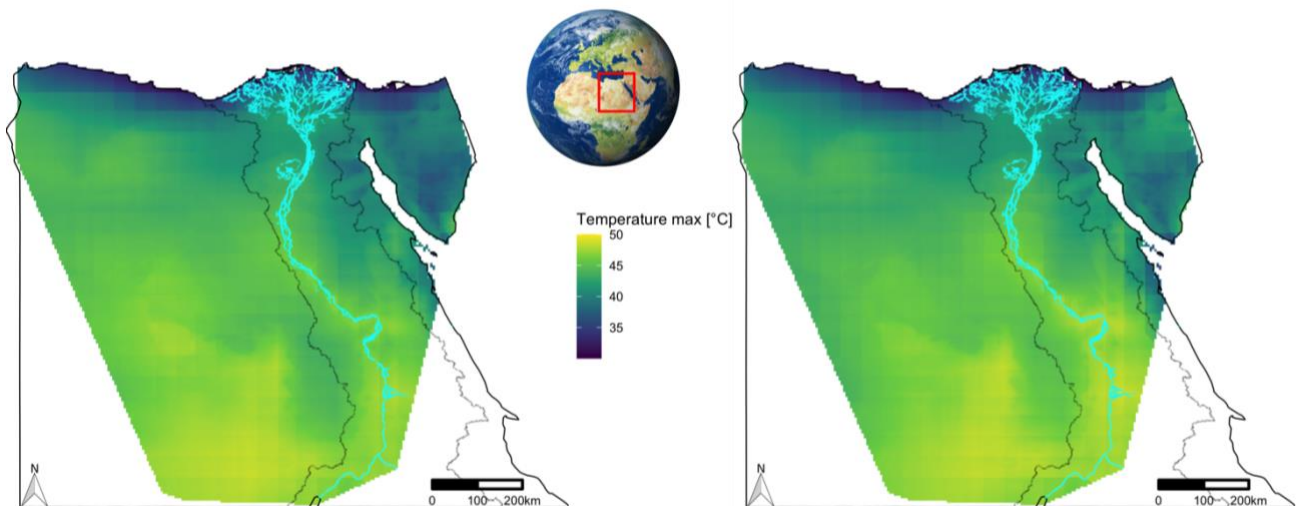


Figure 37 – Snapshots of the spatially distributed maximum surface temperature [°C] (*gridded* data) in Egypt on the two hottest days in the CP: 11th of July 1997 (left) and 10th of July 1997 (right).

Regarding the maximum temperatures in Egypt, these seem to be distributed very similarly in the past (Figure 37) and in the three future projections (Figure 39), presenting a colder climate along the northern coast to the Mediterranean Sea, in the Suez Gulf and the eastern Sinai mountainous region (down to 30 °C in the CP), while the hottest values are occurring in the southern desertic

areas, along with some eastern and western parts (up to 53 °C for RCP 8.5). Despite a similar spatial distribution, the maximum temperatures are predicted to increase considerably in the entire country for all RCP, the least for RCP 2.6 (Figure 39, left), which shows slight colder values in the north-western strip and the hottest one in the north-western desert. RCP 8.5 presents the most evident increase in maximum temperatures along the northern coast and the southern desertic region (higher than 50 °C), while the coldest in the east coast next to the Red Sea. RCP 4.5 reports colder values along the north-western coast of the delta (down to 35 °C) and the highest in the central western desert.

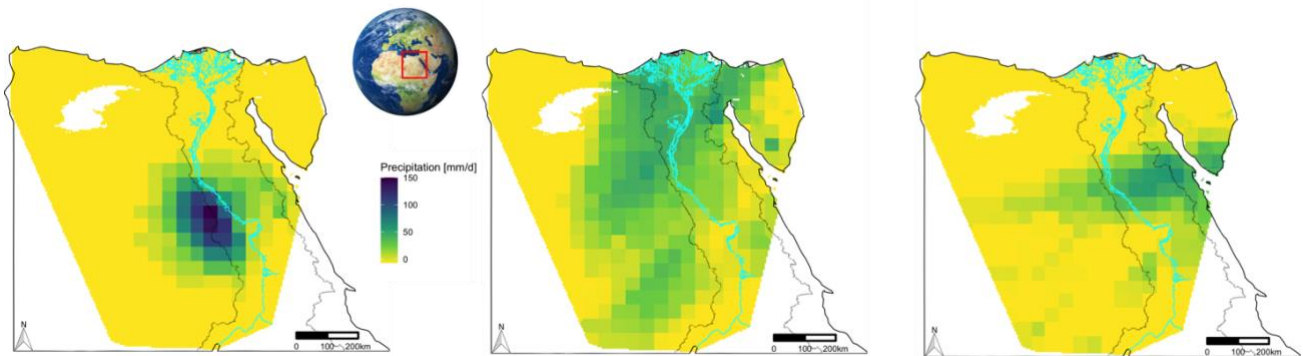


Figure 38 – Snapshots of the spatially distributed precipitation [mm] (*gridded* data) in Egypt on the wettest days for RCP 2.6 (left), RCP 4.5 (middle), and RCP 8.5 (right): respectively the 16th of October 2065, the 12th of May 2049, and the 8th of May 2092. The white area indicates the Qattara depression in the Egyptian north-western desert.

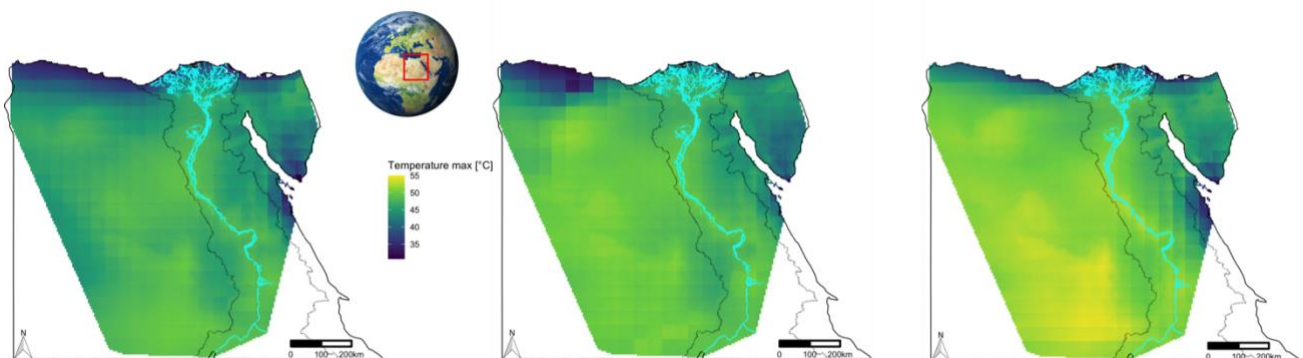


Figure 39 – Snapshots of the spatially distributed maximum temperature [°C] (*gridded* data) in Egypt on the hottest days for RCP 2.6 (left), RCP 4.5 (middle), and RCP 8.5 (right): respectively the 25th of July 2044, the 9th of June 2066, and the 11th of July 2090.

To analyse the climate trends in Egypt, as done in section 4.1 for the Nile sub-basins, the MASH plots of the mean precipitation, the maximum and minimum temperatures (*gridded* data) are reported for Egypt, considering the three RCP 2.6, 4.5, and 8.5 in Figures 40 and 41, respectively. As explained at the beginning of section 3.1, the MASH plots are showing the trajectories of the moving average

over 20 consecutive days computed on a shifting horizon of 30 consecutive years, where each line of the plot represents the moving average indicated by shaded colours as time runs from 2006 (blue) to 2050 (green) until the end of the century (yellow). The black shaded line identifies the mean of the analysed variable in the CP (1981-2005).

Figure 40 reports the mean precipitation in Egypt, which is predicted to remain very low for all RCPs. In the CP, the highest peak in spring is lower than 0.3 mm/d, while the future scenarios report values in the range 0.2-0.4 mm/d (the highest at the beginning of the century). The future MASH plots present three peak periods (all lower than 0.4 mm/d): in late spring (around May), in late summer (August-September) and in October. RCP 2.6 shows the highest values in the first one (up to 0.4 mm/d), while lower in the rest of the year (the second peak is shifted to September). The trend for RCP 4.5 reports the first two peak periods up to max. 0.3 mm/d, while RCP 8.5 the highest precipitation up to 0.37 mm/d in April-May, while almost zero in the other months (lower than 0.1 mm/d).

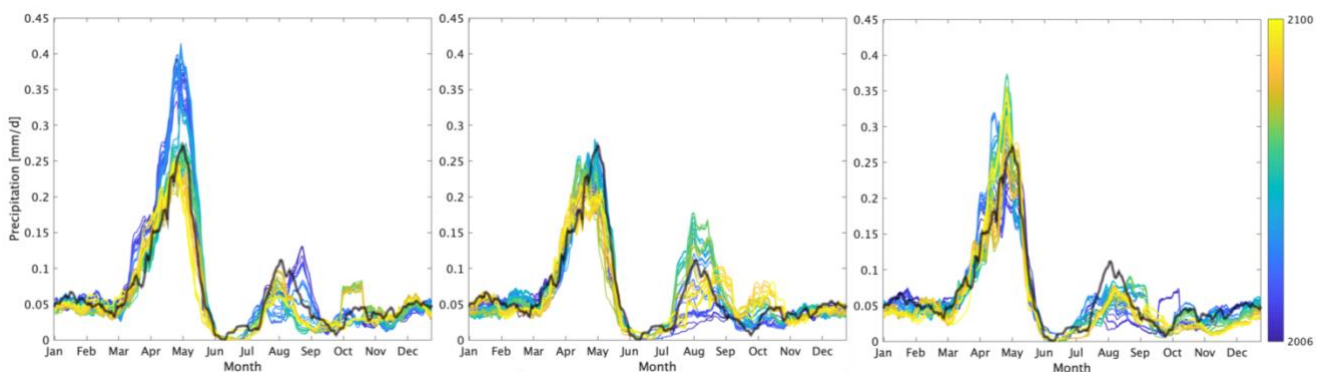


Figure 40 - MASH plots of mean precipitation in Egypt considering RCP 2.6 (left), RCP 4.5 (middle), and RCP 8.5 (right). The black shaded line represents the mean over the CP (bias-adjusted).

The predicted minimum and maximum temperatures (TN, TX, respectively) in Egypt follow the same course (when compared to each other) during the century, while the values are obviously changing, comparing the different scenarios (Figure 41). Looking at the peaks, they occur in July-August in all cases, and they are equal to approx. 38 °C and 23 °C during the control period, respectively. In the RCP 2.6 case, the temperatures trend shows an increase of about 1-1.5 °C around the mid of the century, to then decrease of about 0.5 °C by the end of it (+ 1 °C compared to CP), when in RCP 4.5 TX increases to approx. 40 °C and TN to 25 °C. The highest variation is observed in RCP 8.5, since temperatures increase by about 5 °C, comparing TX and TN to the CP.

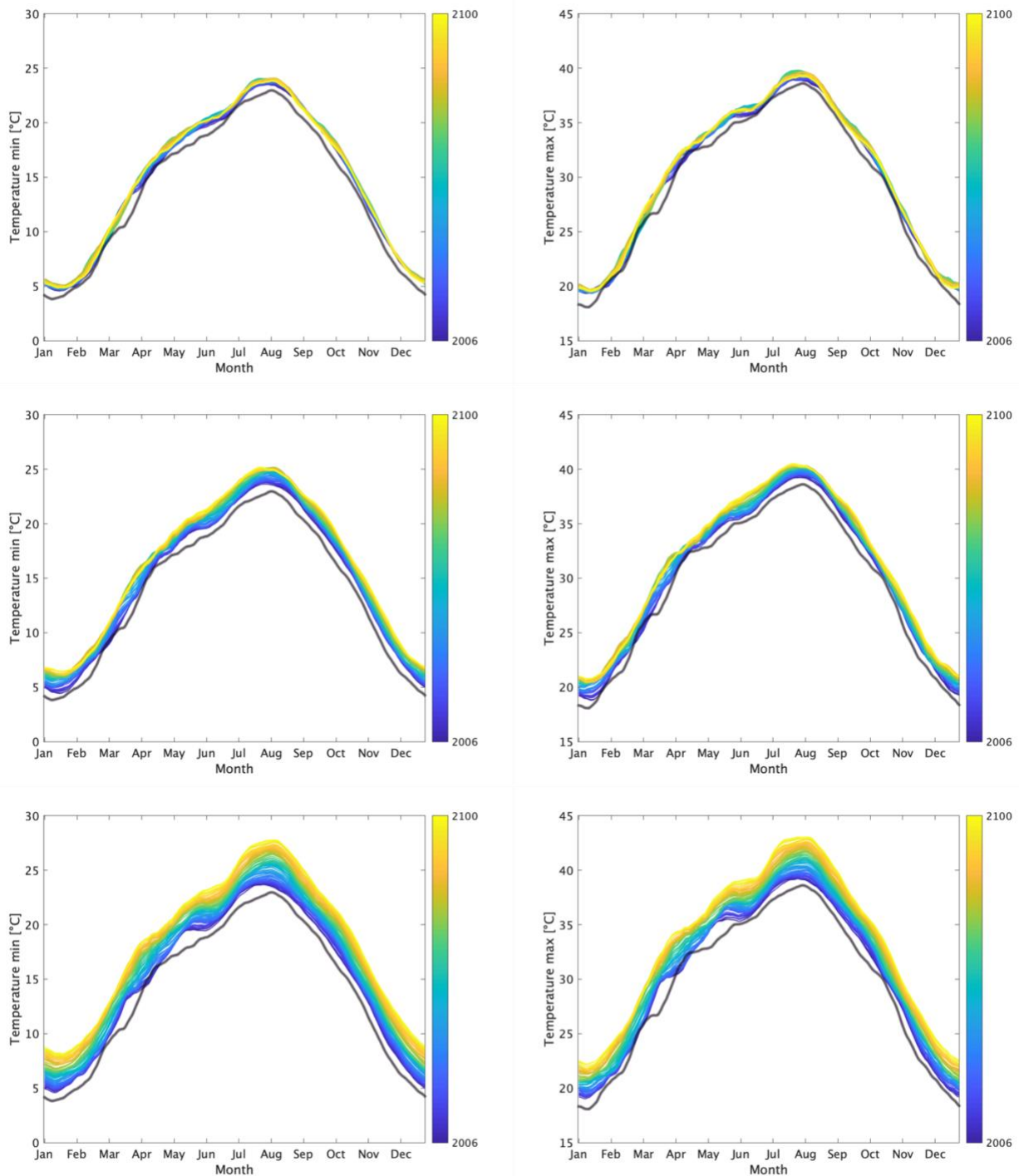


Figure 41 - MASH plots for minimum (left) and maximum (right) temperatures in Egypt considering RCP 2.6 (top), RCP 4.5 (middle), and RCP 8.5 (bottom). The black shaded line represents the mean over the CP (bias-adjusted).

To further investigate the climate change effects on precipitations and on the extreme temperatures in Egypt, some climate indicators calculated for the three forcing scenarios (RCP 2.6, 4.5 and 8.5, respectively) are reported in Figures 42, 43, and 44. PRCPTOT (top-left) and R95P (top-right) are very low in all cases. For RCP 2.6 a decreasing trend can be observed, where the annual cumulated precipitation ranges between 0 and 80 mm/d, but the values are mostly lower than 30 mm/d. Extreme rainfalls are predicted to occur with less frequency during the century and to reach lower peaks. Scarce precipitation is foreseen also in RCP 4.5 and 8.5 (both lower than 2.6), along with increased interannual variability of extreme rainfall (max 30 mm/d). TR20 and TX90 follow the usual trend observed previously for the Nile sub-basins in the RCP 2.6 scenario (peak and decline), while a clear progressive increase is predicted for RCP 4.5 and RCP 8.5. In the first case, TR20 and TX90 reach peaks of 160 days and 25%, respectively, while 220 days and almost 35% in the second case.

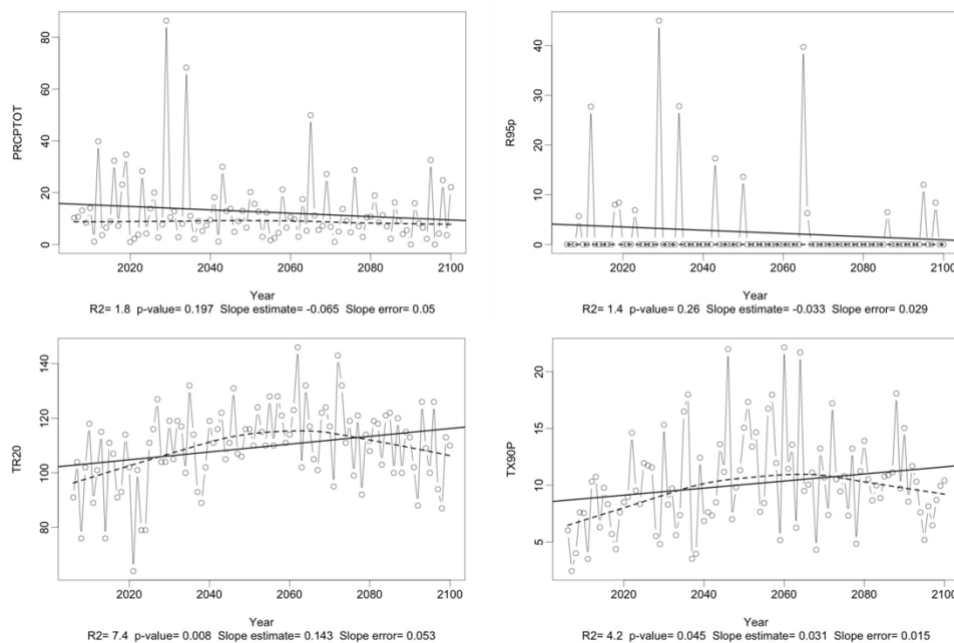


Figure 42– Climate indices PRCPTOT (top-left), R95P (top-right), TR20 (bottom-left), TX90P (bottom-right) in Egypt for RCP 2.6.

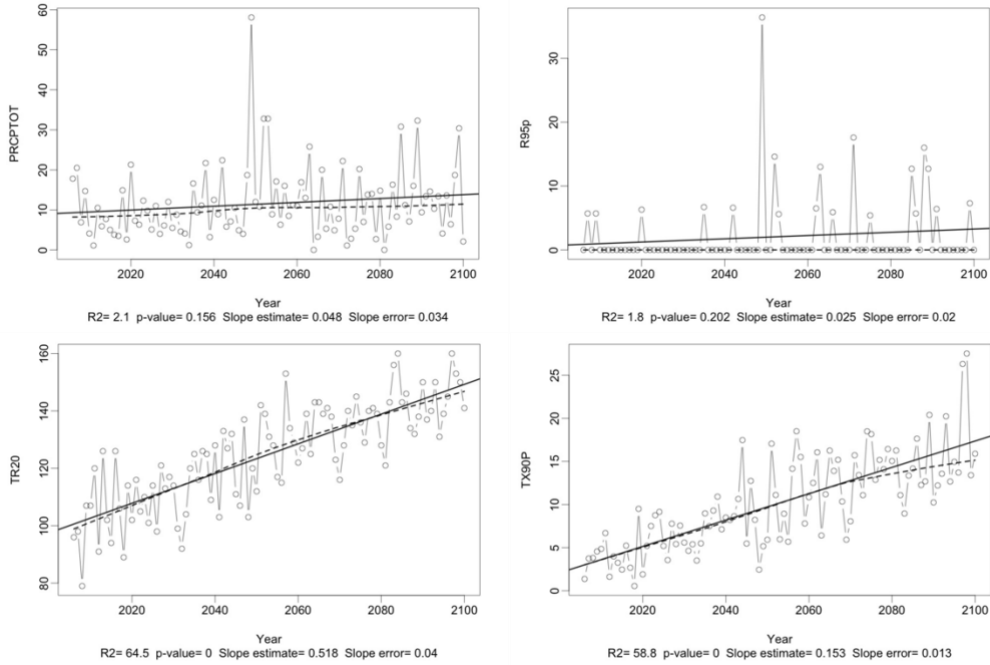


Figure 43 – Climate indices PRCPTOT (top-left), R95P (top-right), TR20 (bottom-left), TX90P (bottom-right) in Egypt for RCP 4.5.

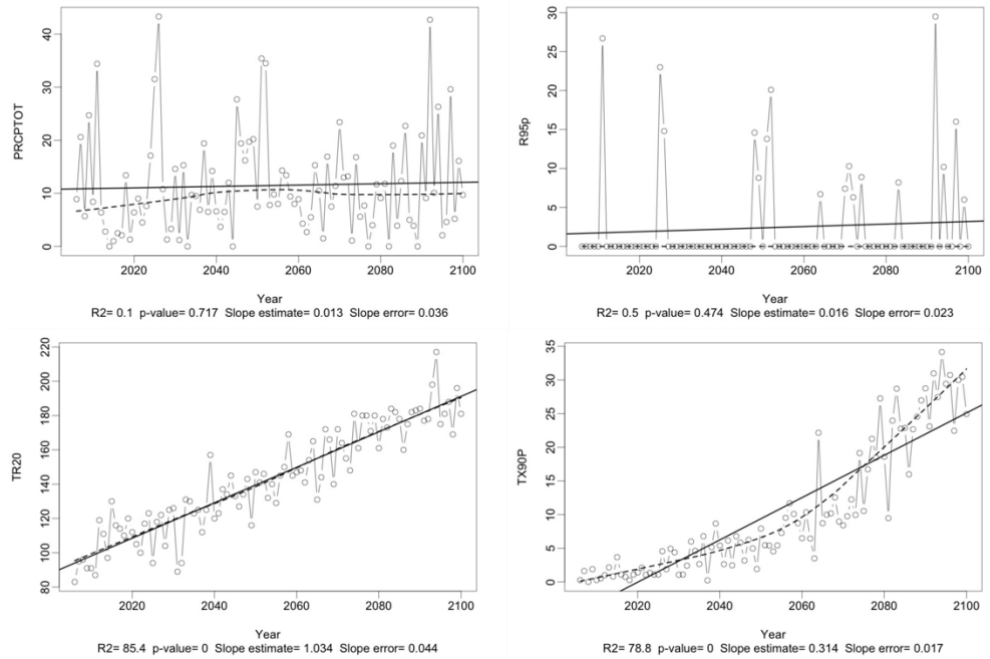


Figure 44 – Climate indices PRCPTOT (top-left), R95P (top-right), TR20 (bottom-left), TX90P (bottom-right) in Egypt for RCP 8.5.

4.3.1 Comparing different futures

To enable a direct comparison among the three scenarios investigated (RCP 2.6, 4.5, and 8.5) and explore in such a way the different possible futures for Egypt, further analyses have been conducted, as reported in the following plots.

Figure 45 represents the variation of the precipitations (x-axis) and the maximum temperatures (y-axis) in Egypt in the period 2040-2100, compared to the control period 1981-2005. Observing the plot, it is possible to compare how the three scenarios analysed (RCP 2.6, 4.5, 8.5) predict a considerable increase of temperature, i.e., less than 1 °C in the case of RCP 2.6 (green circle), approx. 1.7 °C for RCP 4.5, while it reaches more than 3 °C for RCP 8.5. In the case of precipitation, all scenarios foresee a slight increase in the second mid of century, probably due to the occurrence of extreme events, although the variations are very low and can be neglected. Therefore, Egypt’s climate is predicted to be very dry, with occasional precipitation events, the amount of which is hard to predict.

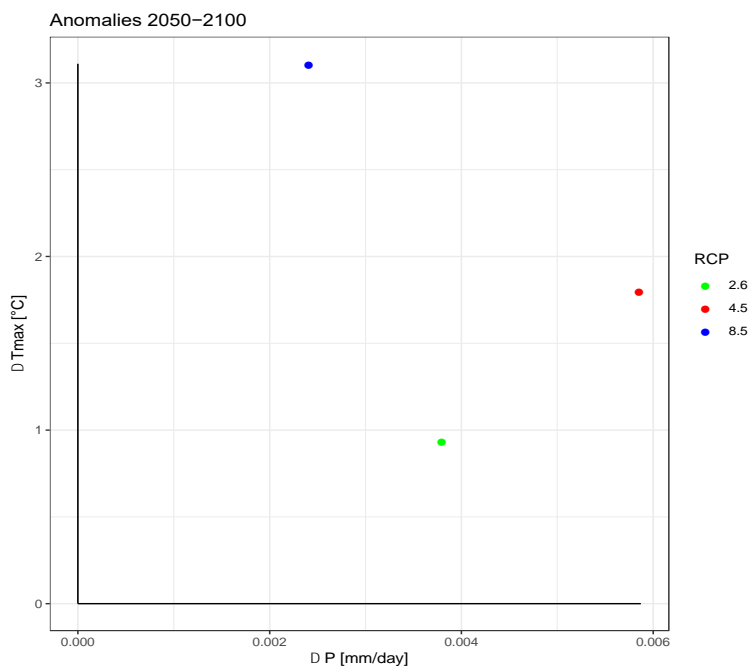


Figure 45 – Variations in precipitation and maximum temperature in the period 2040-2100 compared to the period 1983-2005 in Egypt for the three scenarios RCP 2.6 (green circle), RCP 4.5 (red circle), and RCP 8.5 (blue circle).

The warmer, drier, and more unpredictable future foreseen for Egypt, can be further assessed looking at Figures 46 and 47, in which the climate indices CDD and WSDI are plotted for the three different RCPs.

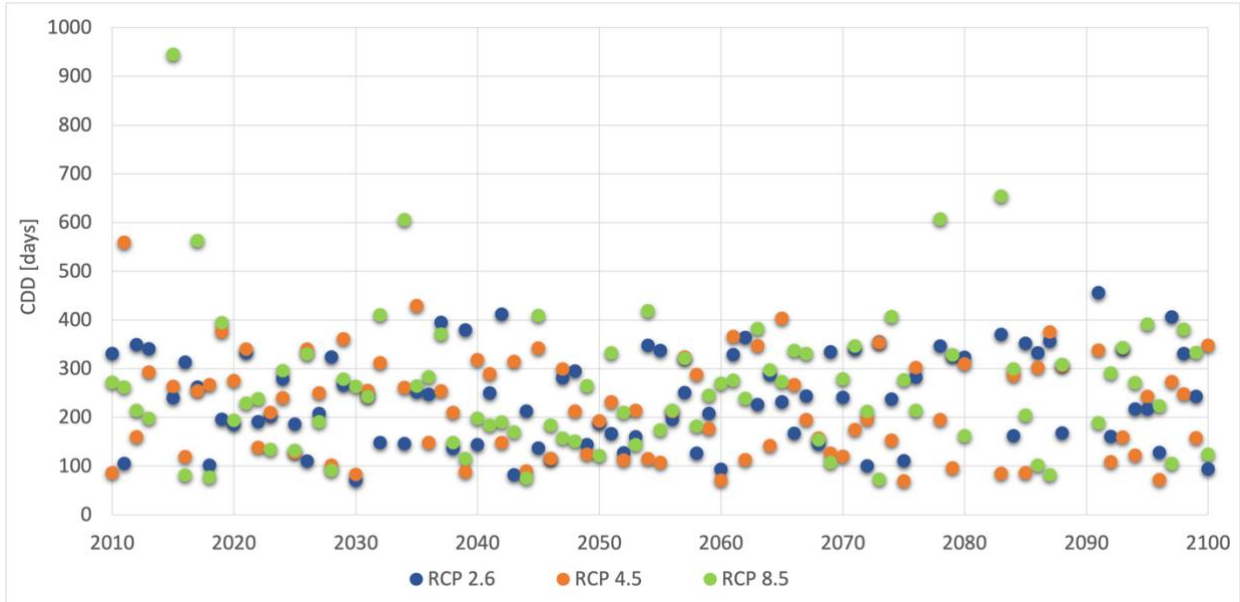


Figure 46- Consecutive Dry Days (CDD) for RCP 2.6 (blue), RCP 4.5 (red), and RCP 8.5 (green).

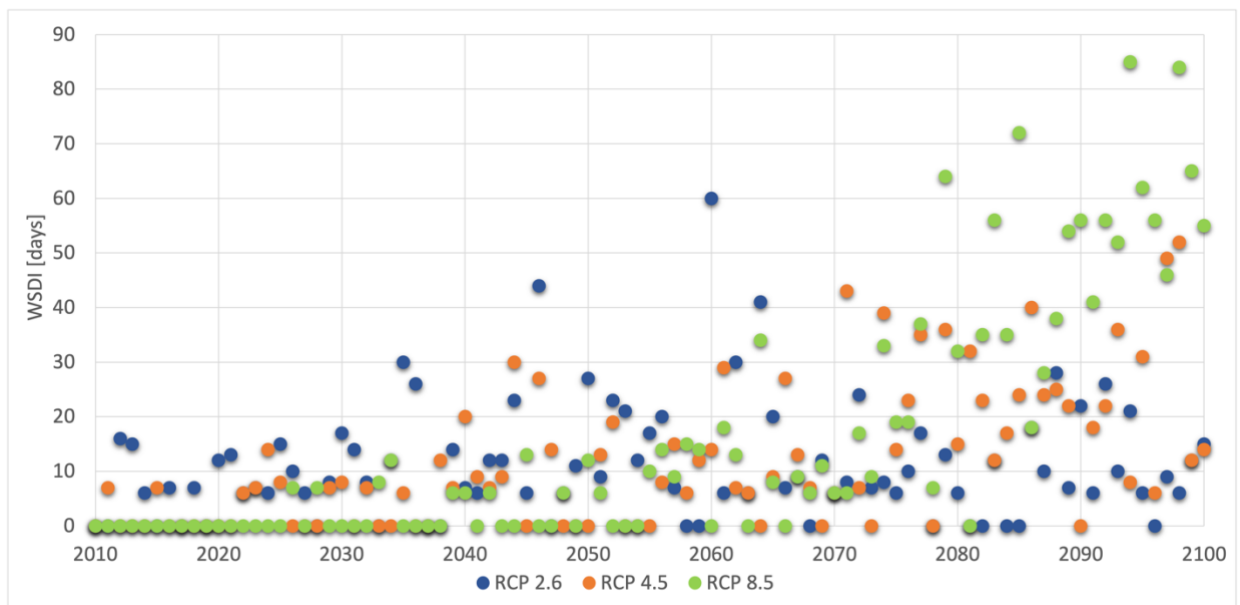


Figure 47- Warm Spell Duration Indicator (WSDI) for RCP 2.6 (blue), RCP 4.5 (red), and RCP 8.5 (green).

The CDD plot in Figure 46 shows how dry will be the country in the current century, as the indicator is varying among values higher than 50 days in all scenarios, while especially for RCP 8.5 it occurs more frequently that no rainfall is registered for more than 1 consecutive year. Also, the interannual variability is different from scenario to scenario. Regarding temperature extremes, WSDI behaviour in Figure 47 shows some interannual variability as well. While in the first three decades of the century the heat waves do last longer than 6 consecutive days for less than 20 days a year, a relevant increase is observable from approx. 2035 in all scenarios. RCP 2.6 shows higher peaks compared to the other until 2060 (up to 60 days) to then decrease to peaks of about 30 days. RCP 4.5 increases around 2045 to then stabilize between 0 and maximum values of about 50 days. RCP 8.5 shows a progressive increase, starting from the lowest values (in the first 25 years WSDI is zero), to then reach the highest values towards the end of the century (40-85 days/ year of long-lasting extreme temperatures). Further comparison among the other climate indicators (R95P and TX90) is reported in Annex III.

5. FINAL REMARKS

Deliverable D2.2 of WP2 is a comprehensive report that presents the downscaled climate scenarios developed for the AWESOME project.

The CORDEX-Africa daily data of precipitation and temperature are collected for the model ensemble ICHEC EC-EARTH (GCM) and SMHI-RCA4 (RCM) and three forcing scenarios RCP 2.6, 4.5, and 8.5 for a complete analysis. Observation data are retrieved from CHC global datasets to downscale the regional climate data at higher resolution, over the entire Nile River Basin.

While a relevant temperature increase is evident in all considered scenarios, especially for RCP 4.5 and 8.5, the interpretation of the precipitation future projections is more complex to assess. Especially in very dry areas, such as the Main Nile sub-basin (and Egypt), precipitation is almost always lower than 1 mm/d, which leads to higher modelling uncertainty. Nevertheless, the analysis outcomes are reported for the principal Nile sub-basins and Egypt (location of the project's demo-sites), along with some consideration on climate trends and indices.

It can be concluded that the concomitance of the predicted warming, the longer-lasting high temperatures, the increasing occurrence of tropical nights, and the high interannual variability of precipitation (very low in some areas) are expected to significantly challenge the agricultural fields and crop productivity in the Nile River Basin.

REFERENCES

1. IPCC. *Climate Change 2014: Synthesis Report. Contribution of Working Groups I, II and III to the Fifth Assessment Report of the Intergovernmental Panel on Climate Change. Core Writing Team, R.K. Pachauri and L.A. Meyer (eds.)* <http://www.ipcc.ch>. (2014).
2. Moss, R. H. *et al.* The next generation of scenarios for climate change research and assessment. *Nature* vol. 463 747–756 (2010).
3. Diallo, I., Giorgi, F., Sukumaran, S., Stordal, F. & Giuliani, G. Evaluation of RegCM4 driven by CAM4 over Southern Africa: mean climatology, interannual variability and daily extremes of wet season temperature and precipitation. *Theor. Appl. Climatol.* **121**, 749–766 (2015).
4. Nikulin, G. *et al.* The effects of 1.5 and 2 degrees of global warming on Africa in the CORDEX ensemble. *Environ. Res. Lett.* **13**, 065003 (2018).
5. Liersch, S., Koch, H. & Hattermann, F. F. Management Scenarios of the Grand Ethiopian Renaissance Dam and Their Impacts under Recent and Future Climates. *Water* **9**, 728 (2017).
6. Jeuland, M. & Whittington, D. Water resources planning under climate change: Assessing the robustness of real options for the Blue Nile. *Water Resour. Res.* **50**, 2086–2107 (2014).
7. Parkes, B., Cronin, J., Dessens, O. & Sultan, B. Climate change in Africa: costs of mitigating heat stress. *Clim. Change* **154**, 461–476 (2019).
8. Gebrechorkos, S. H., Hülsmann, S. & Bernhofer, C. Long-term trends in rainfall and temperature using high-resolution climate datasets in East Africa. *Sci. Rep.* **9**, 1–9 (2019).
9. Endris, H. S. *et al.* Assessment of the performance of CORDEX regional climate models in simulating East African rainfall. *J. Clim.* **26**, 8453–8475 (2013).
10. Endris, H. S. *et al.* Future changes in rainfall associated with ENSO, IOD and changes in the mean state over Eastern Africa. *Clim. Dyn.* **52**, 2029–2053 (2019).
11. Intergovernmental Panel on Climate Change (IPCC). Archive-reports. https://archive.ipcc.ch/pdf/assessment-report/ar5/syr/SYR_AR5_FINAL_full_wcover.pdf.
12. Lennard, C. J., Nikulin, G., Dosio, A. & Moufouma-Okia, W. On the need for regional climate information over Africa under varying levels of global warming. *Environ. Res. Lett.* **13**, 060401 (2018).
13. Dosio, A. Projection of temperature and heat waves for Africa with an ensemble of CORDEX Regional Climate Models. *Clim. Dyn.* **49**, 493–519 (2017).
14. Ahmadalipour, A., Moradkhani, H., Castelletti, A. & Magliocca, N. Future drought risk in Africa: Integrating vulnerability, climate change, and population growth. *Sci. Total Environ.* **662**, 672–686 (2019).
15. FAO. AQUASTAT - FAO's Global Information System on Water and Agriculture. <http://www.fao.org/aquastat/en/>.
16. NWRP/MWRI. *National Water Resources Plan/Ministry of Water Resources and Irrigation, Egypt. Final Report: The National Water Resources Plan for Egypt – 2017.* (2005).
17. Moussa, A. M. A., El, M. & Omar, D. M. Impacts of Climate Change on Water Balances at the

- Governorates Level in Egypt. *Nile Water Sci. Eng. J.* **9**, (2016).
18. USAID. *Climate Change Information Fact Sheet EGYPT*.
[https://www.climatelinks.org/sites/default/files/asset/document/Egypt Climate Info Fact Sheet_FINAL.pdf](https://www.climatelinks.org/sites/default/files/asset/document/Egypt%20Climate%20Info%20Fact%20Sheet_FINAL.pdf) (2015).
 19. Climate forcing | Copernicus. <https://atmosphere.copernicus.eu/climate-forcing>.
 20. Boé, J., Terray, L., Habets, F. & Martin, E. Statistical and dynamical downscaling of the Seine basin climate for hydro-meteorological studies. *Int. J. Climatol.* **27**, 1643–1655 (2007).
 21. Wilby, R. L. & Dessai, S. Robust adaptation to climate change. *Weather* **65**, 180–185 (2010).
 22. Maps | Nile Basin Initiative (NBI). <https://nilebasin.org/media-center/maps>.
 23. Wheeler, K. G. *et al.* Exploring Cooperative Transboundary River Management Strategies for the Eastern Nile Basin. *Water Resour. Res.* **54**, 9224–9254 (2018).
 24. Dinku, T. *et al.* Validation of the CHIRPS satellite rainfall estimates over eastern Africa. *Q. J. R. Meteorol. Soc.* **144**, 292–312 (2018).
 25. Hersbach, H. *et al.* The ERA5 global reanalysis. *Q. J. R. Meteorol. Soc.* **146**, 1999–2049 (2020).
 26. Harris, I., Osborn, T. J., Jones, P. & Lister, D. Version 4 of the CRU TS monthly high-resolution gridded multivariate climate dataset. *Sci. Data* **7**, 1–18 (2020).
 27. Berg, P., Almén, F. & Bozhinova, D. HydroGFD3.0: a 25 km global near real-time updated precipitation and temperature data set. *Earth Syst. Sci. Data in review*, (2020).
 28. Funk, C. *et al.* The climate hazards infrared precipitation with stations - A new environmental record for monitoring extremes. *Sci. Data* **2**, 1–21 (2015).
 29. Funk, C. *et al.* A high-resolution 1983–2016 TMAX climate data record based on infrared temperatures and stations by the climate hazard center. *J. Clim.* **32**, 5639–5658 (2019).
 30. CHIRTSdaily | Climate Hazards Center - UC Santa Barbara.
<https://www.chc.ucsb.edu/data/chirtsdaily>.
 31. Cordex – Coordinated Regional Climate Downscaling Experiment. <https://cordex.org/>.
 32. Dosio, A. *et al.* What can we know about future precipitation in Africa? Robustness, significance and added value of projections from a large ensemble of regional climate models. *Clim. Dyn.* **53**, 5833–5858 (2019).
 33. Anghileri, D., Pianosi, F. & Soncini-Sessa, R. Trend detection in seasonal data: From hydrology to water resources. *J. Hydrol.* **511**, 171–179 (2014).
 34. Giuliani, M., Li, Y., Castelletti, A. & Gandolfi, C. A coupled human-natural systems analysis of irrigated agriculture under changing climate. *Water Resour. Res.* **52**, 6928–6947 (2016).
 35. Zhang, X. *et al.* Indices for monitoring changes in extremes based on daily temperature and precipitation data. *Wiley Interdisciplinary Reviews: Climate Change* vol. 2 851–870 (2011).
 36. ETCCDI. ETCCDI Climate Indices. http://etccdi.pacificclimate.org/list_27_indices.shtml.
 37. Powell, E. J. & Keim, B. D. Trends in daily temperature and precipitation extremes for the southeastern United States: 1948-2012. *J. Clim.* **28**, 1592–1612 (2015).

ANNEX I

I. MASH PLOTS OF THE OTHER NILE SUB-BASINS

The MASH plots (s. section 4.1) for precipitation and temperature of the other Nile sub-basins are reported in the following figures (Figure I.1 to I.14), considering RCP 4.5. All MASH plots generated also for the other RCP (2.6 and 8.5) are accessible to all partners and stored in the project repository at *AWESOME_project/Work_packages/WP2/Climate/Data*. The black shaded line represents the mean over the CP (bias-adjusted).

Tekeze-Atbara sub-basin

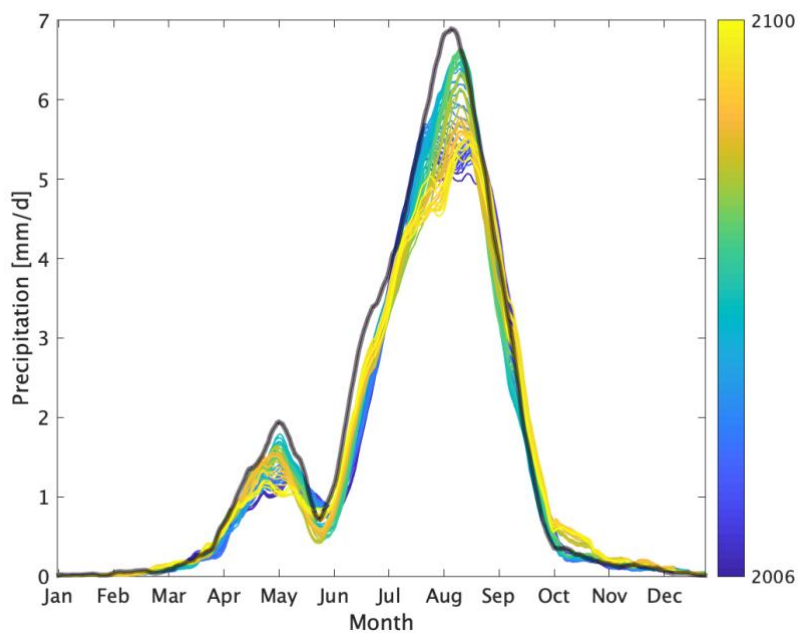


Figure I.1 – MASH plot for precipitation in Tekeze-Atbara sub-basin (RCP 4.5).

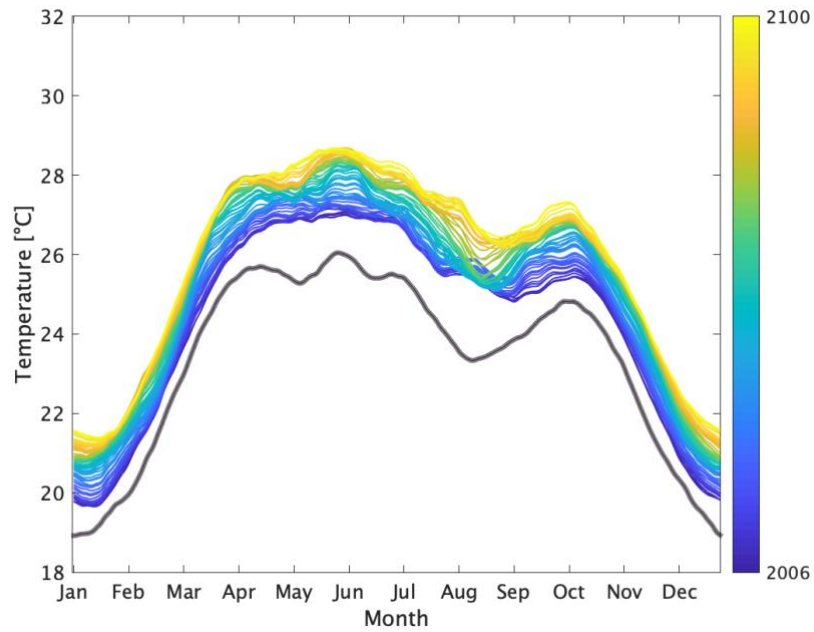


Figure I.2 – MASH plot for temperature in Tekeze-Atbara sub-basin (RCP 4.5)

Baro Akobbo Sobat sub-basin

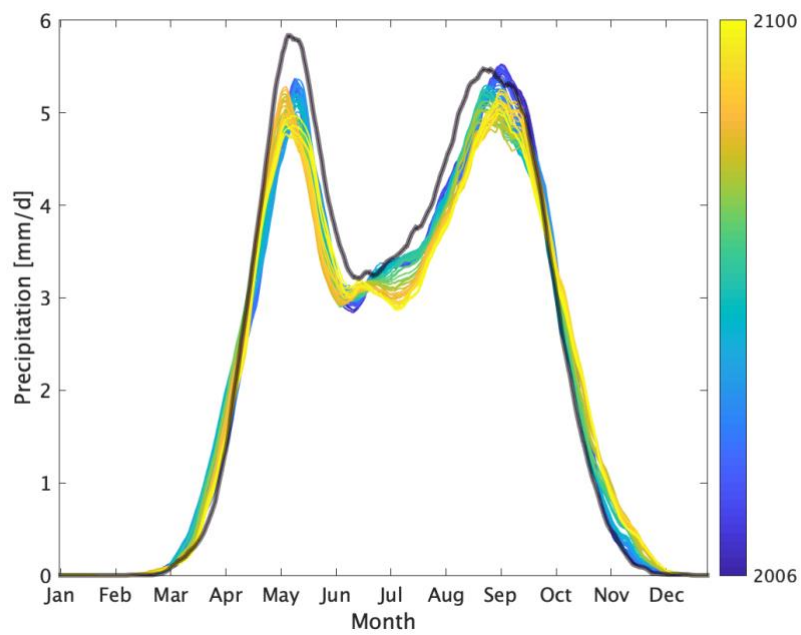


Figure I.3 – MASH plot for precipitation in Baro Akobbo Sobat sub-basin (RCP 4.5)

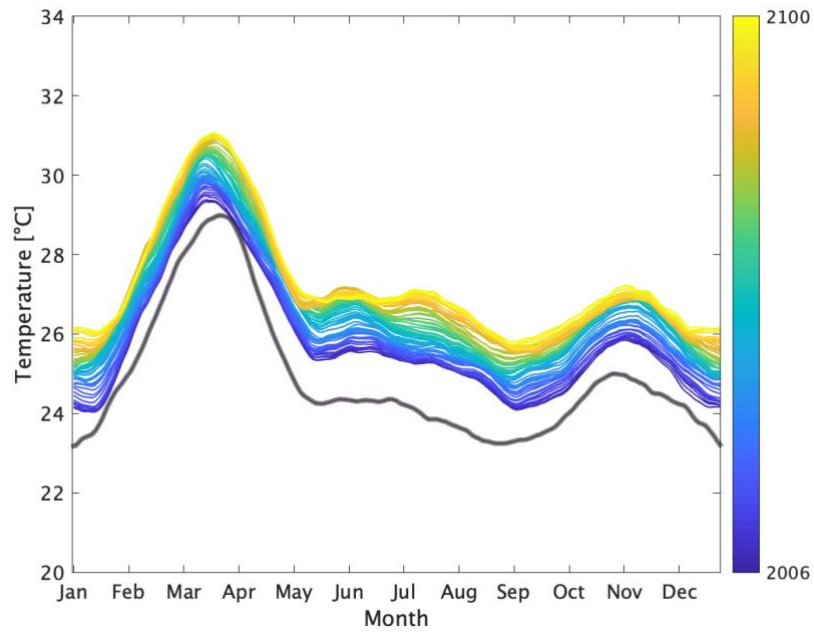


Figure I.4 – MASH plot for temperature in Baro Akobbo Sobat sub-basin (RCP 4.5)

Bahr El Jebel sub-basin

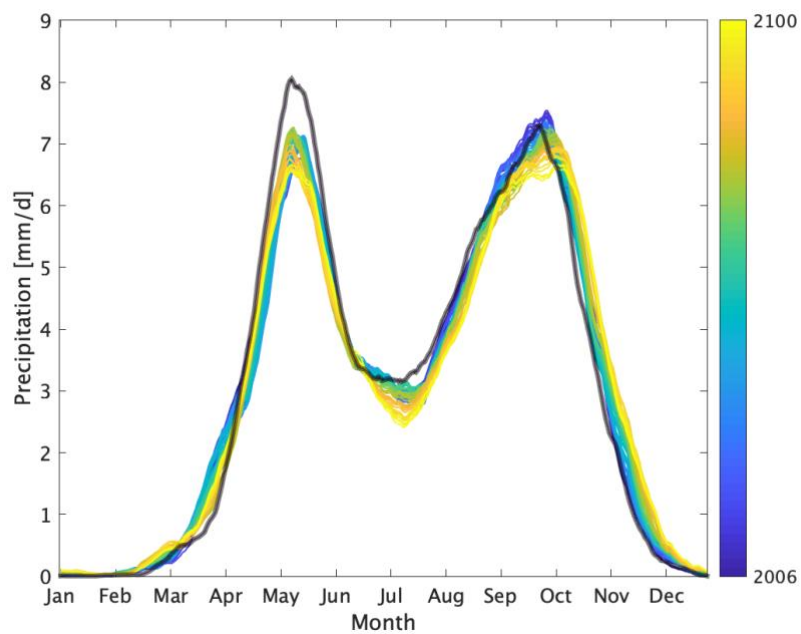


Figure I.5 – MASH plot for precipitation in Bahr El Jebel sub-basin (RCP 4.5)

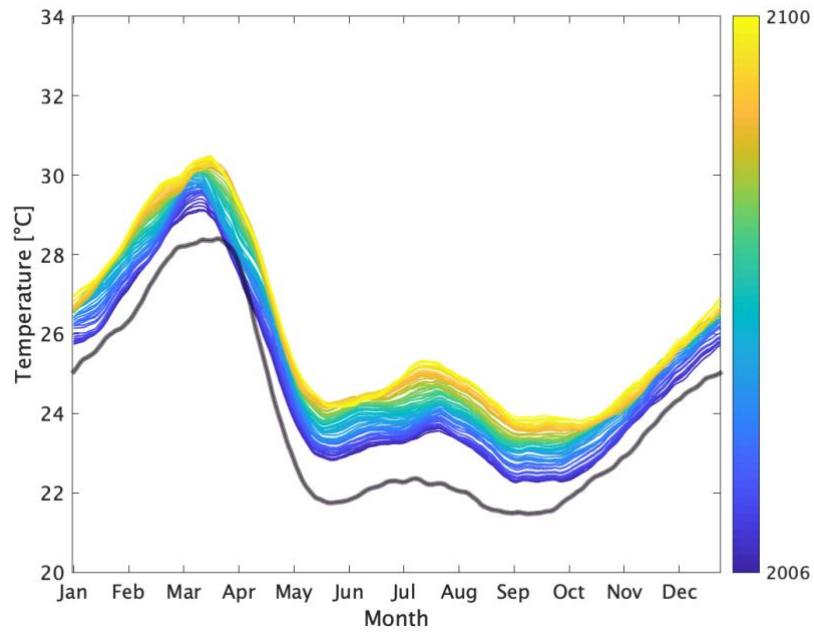


Figure I.6 – MASH plot for temperature in Bahr El Jebel sub-basin (RCP 4.5)

Bahr El Ghazal sub-basin

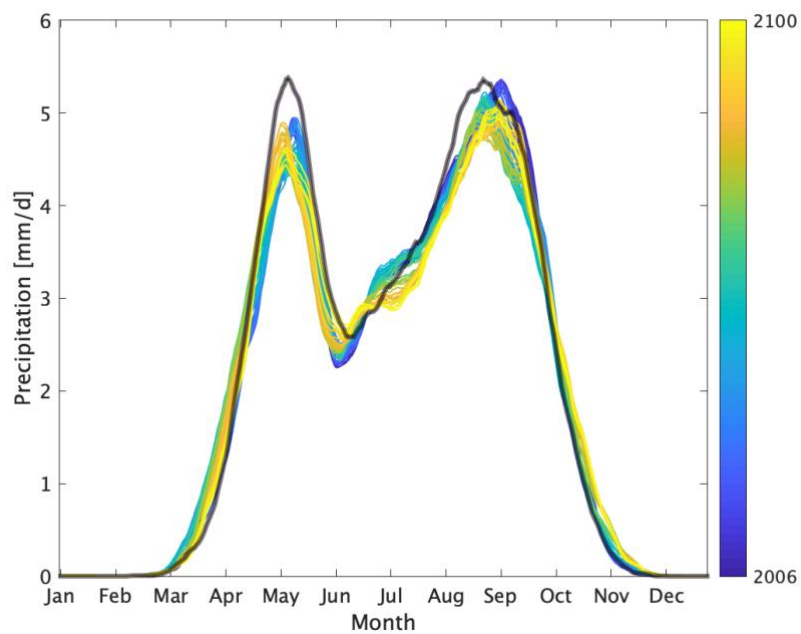


Figure I.7 – MASH plot for precipitation in Bahr El Ghazal sub-basin (RCP 4.5)

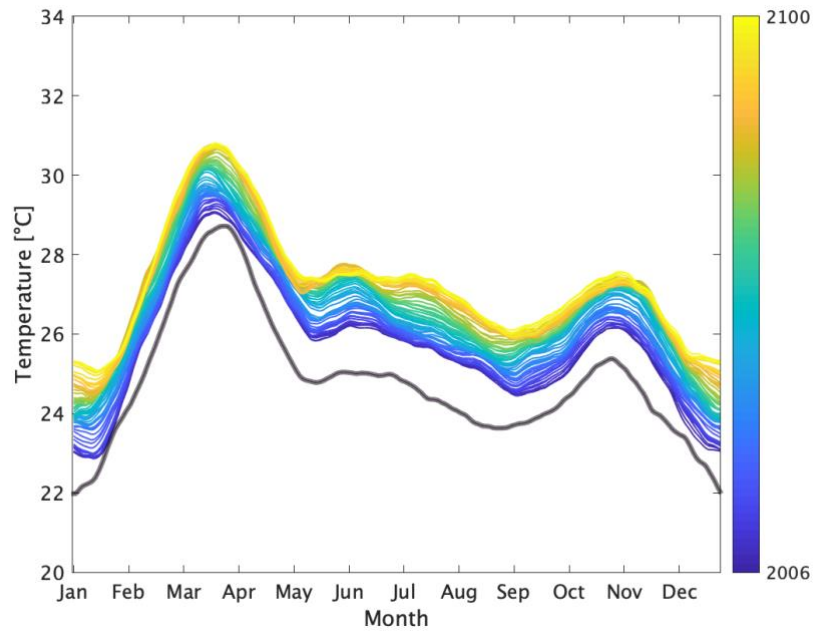


Figure I.8 – MASH plot for temperature in Bahr El Ghazal sub-basin (RCP 4.5)

Victoria Nile sub-basin

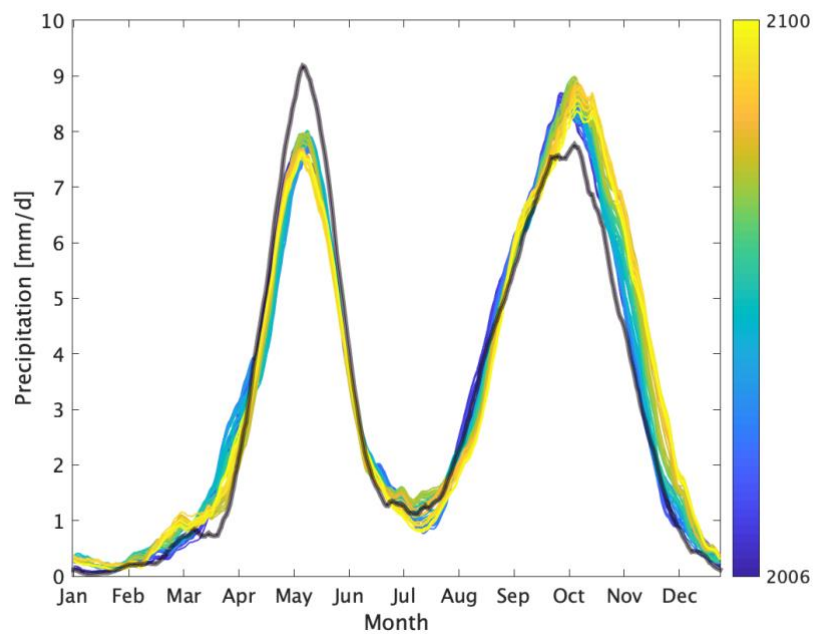


Figure I.9 – MASH plot for precipitation in Victoria Nile sub-basin (RCP 4.5)

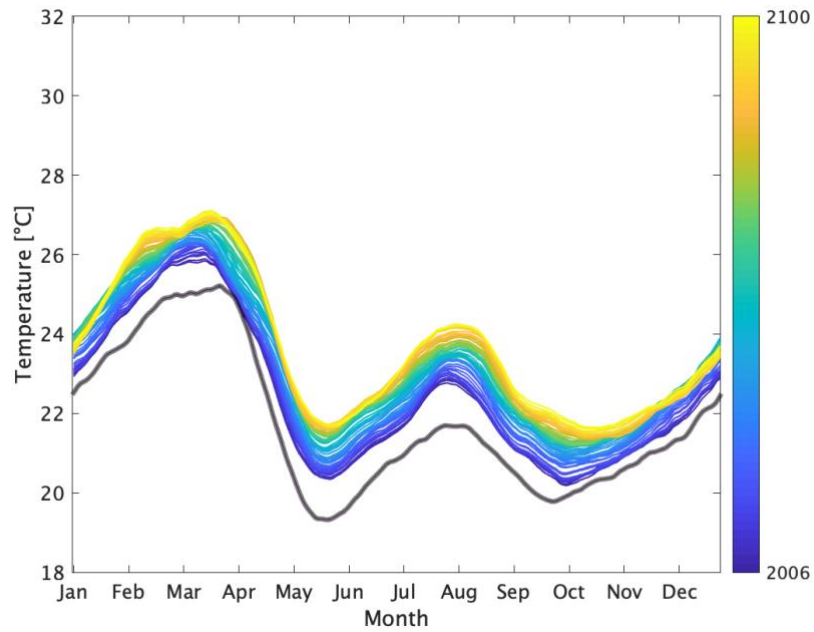


Figure I.10 – MASH plot for temperature in Victoria Nile sub-basin (RCP 4.5)

Lake Victoria sub-basin

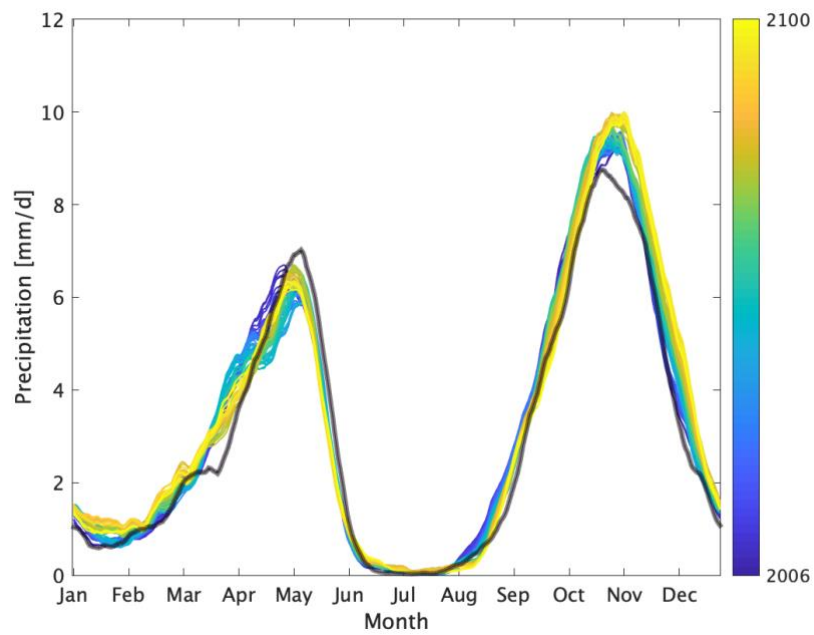


Figure I.11 – MASH plot for precipitation in Lake Victoria sub-basin (RCP 4.5)

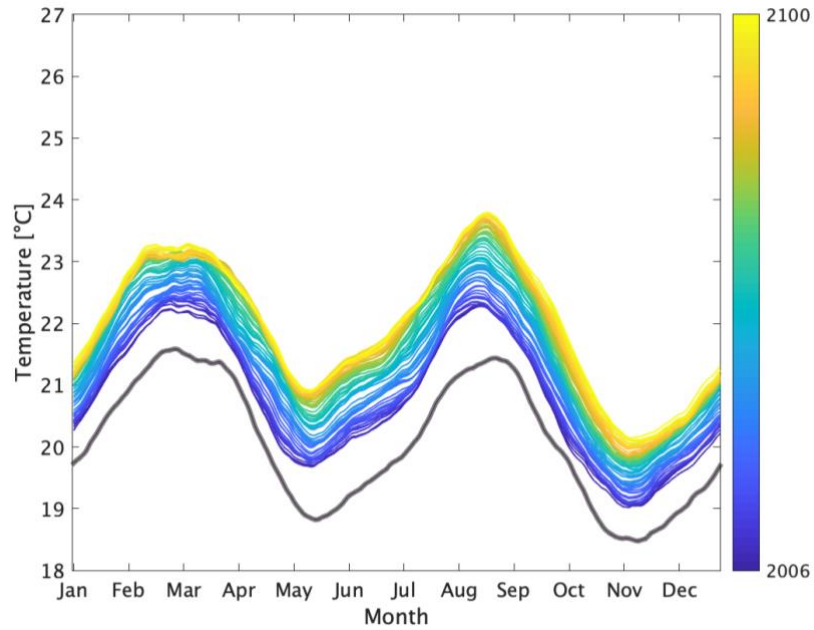


Figure I.12 – MASH plot for temperature in Lake Victoria sub-basin (RCP 4.5)

Lake Albert sub-basin

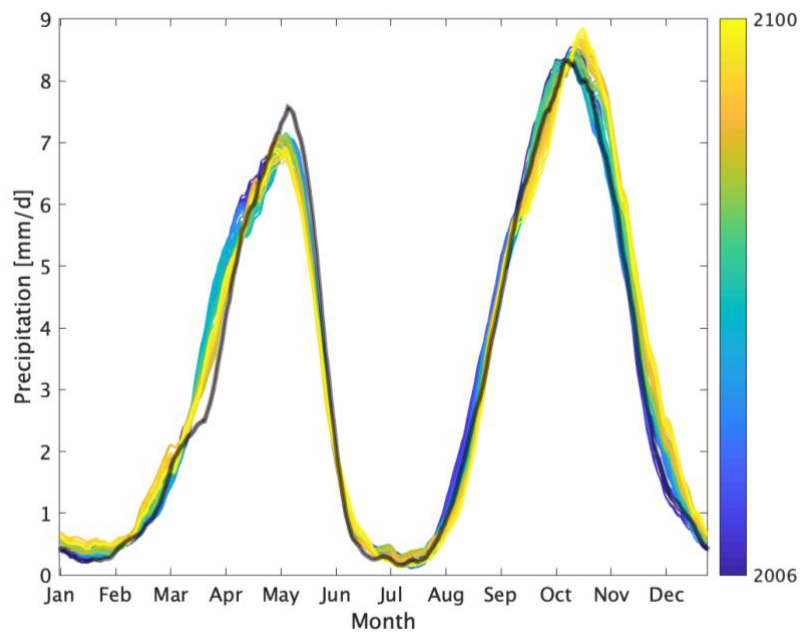


Figure I.13 – MASH plot for precipitation in Lake Albert sub-basin (RCP 4.5)

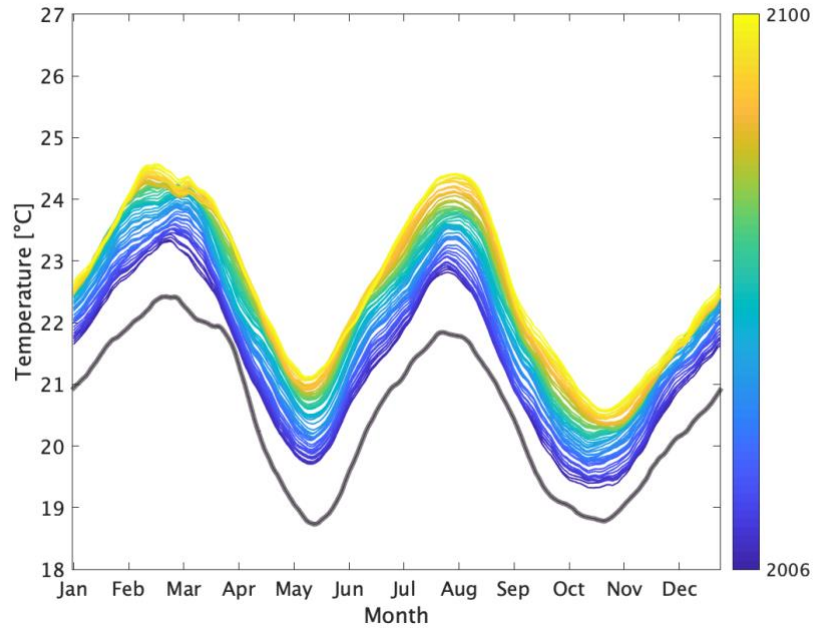


Figure I.14 – MASH plot for temperature in Lake Albert sub-basin (RCP 4.5)

ANNEX II

II. CLIMATE INDICATORS OF THE OTHER NILE SUB-BASINS

The climate indicators PRCPTOT, R95P, CDD, TR20, TX90P, and WSDI (s. section 4.2) of the other Nile sub-basins are reported in the following figures (Figure II.1 to II.7), considering RCP 4.5. All climate indices and related plots generated also for the other RCP (2.6 and 8.5) are accessible to all partners and stored in the project repository at *AWESOME_project/Work_packages/WP2/Climate/Data*.

Tekeze-Atbara sub-basin

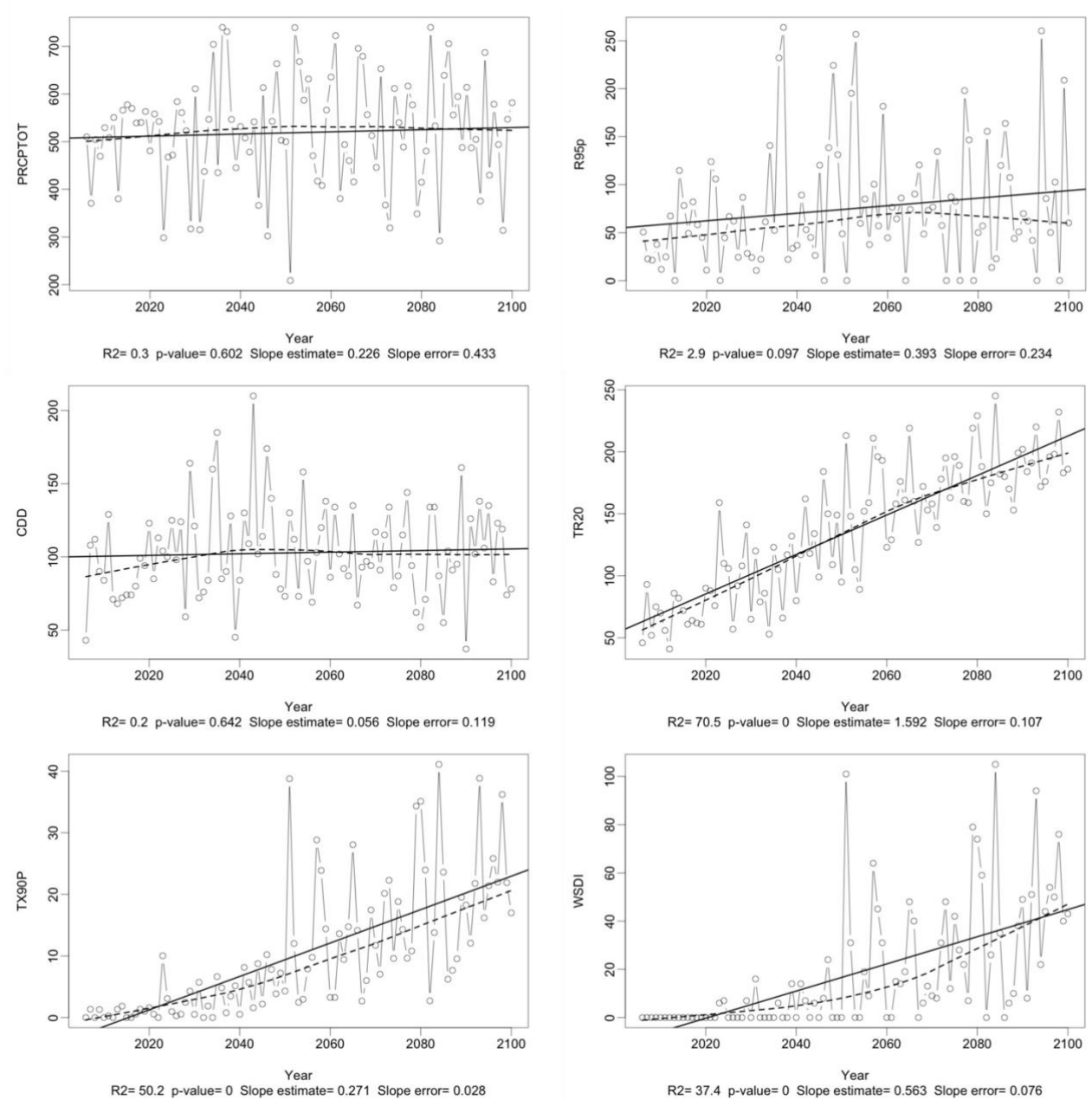


Figure II.1 – Climate indices PRCPTOT (top-left), R95P (top-right), CDD (mid-left), TR20 (mid-right), TX90P (bottom-left), WSDI (bottom-right) in Tekeze-Atbara sub-basin for RCP 4.5. The solid line shows the trend computed by linear least squares and the dashed line is calculated through a locally weighted linear regression using a loess smoother function. Statistics of the linear trend fitting are displayed on the plots. This will be the same for all subsequent plots.

Baro Akobbo Sobat sub-basin

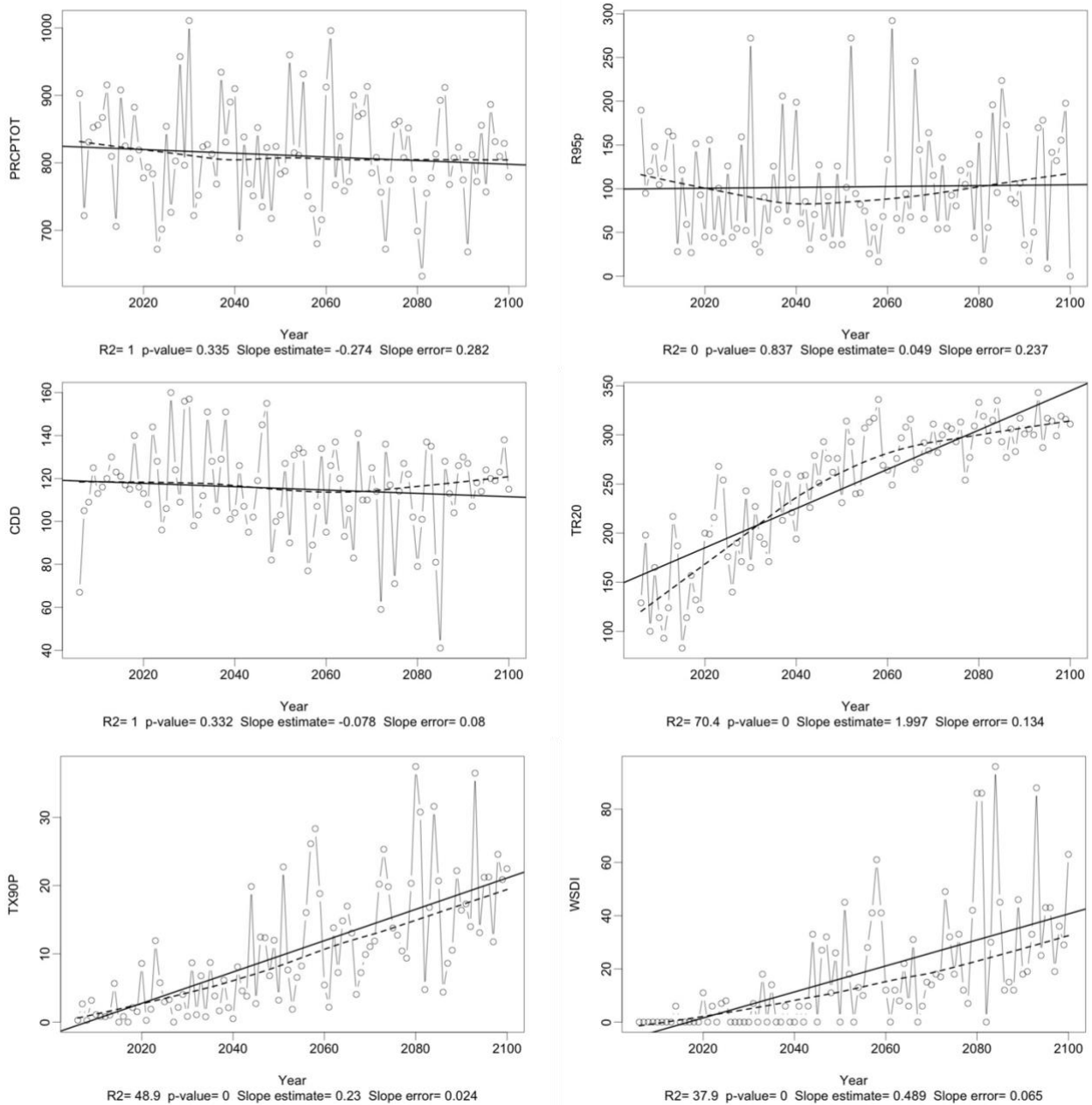


Figure II.2 – Climate indices PRCPTOT (top-left), R95P (top-right), CDD (mid-left), TR20 (mid-right), TX90P (bottom-left), WSDI (bottom-right) in Baro Akobbo Sobat sub-basin for RCP 4.5.

Bahr El Jebel sub-basin

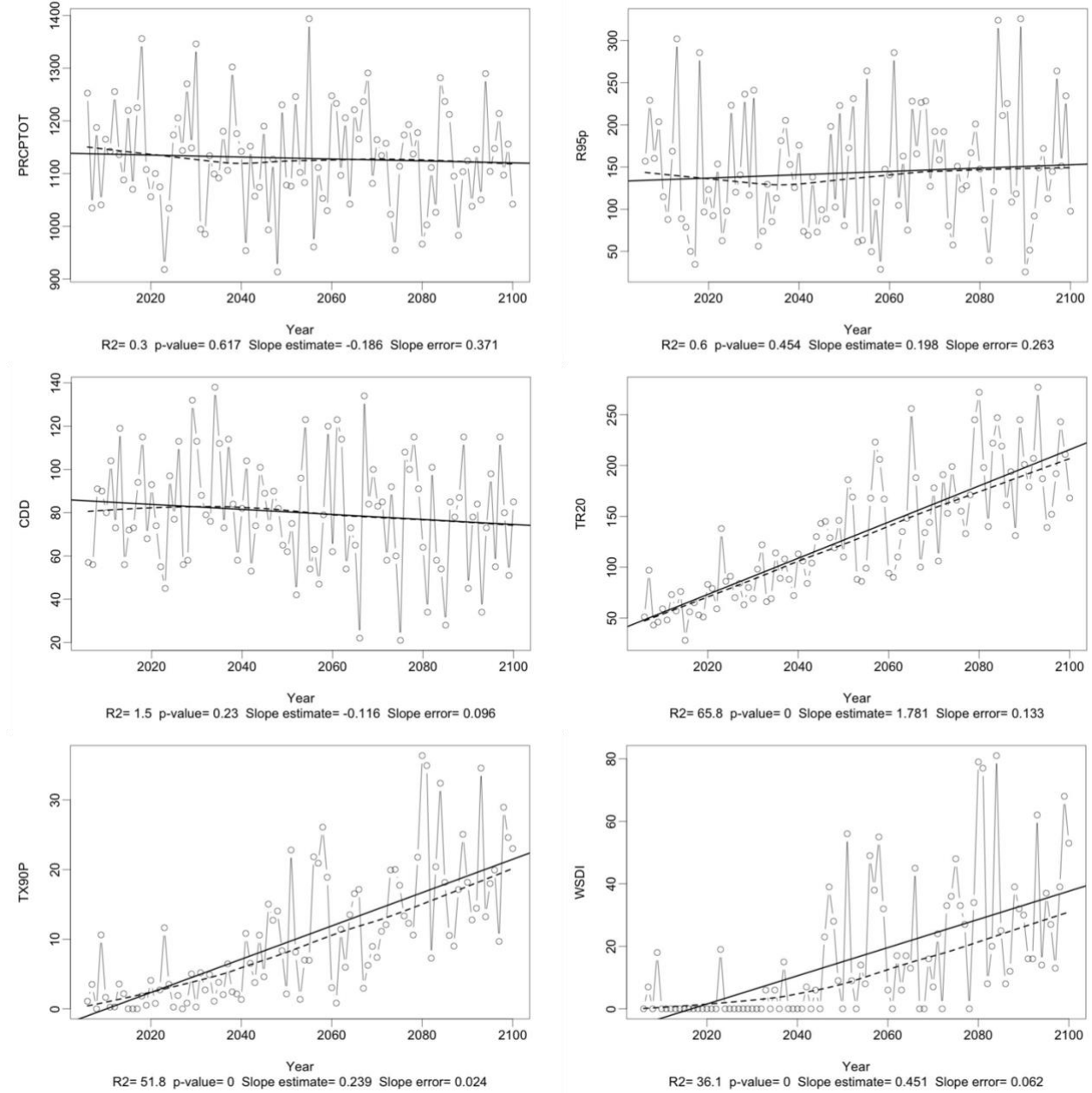


Figure II.3 – Climate indices PRCPTOT (top-left), R95p (top-right), CDD (mid-left), TR20 (mid-right), TX90P (bottom-left), WSDI (bottom-right) in Bahr El Jebel sub-basin for RCP 4.5.

Bahr El Ghazal sub-basin

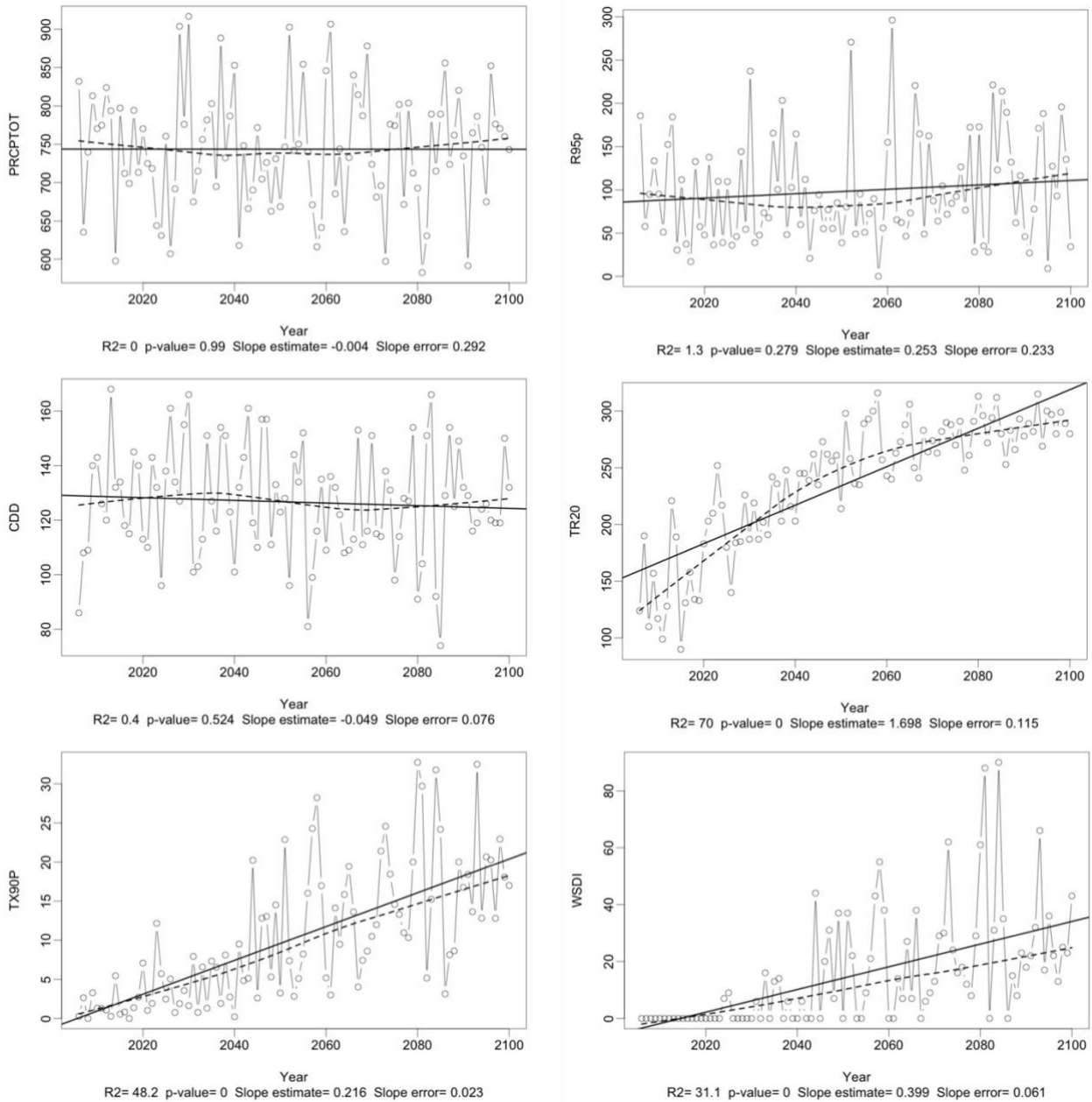


Figure II.4 – Climate indices PRCPTOT (top-left), R95P (top-right), CDD (mid-left), TR20 (mid-right), TX90P (bottom-left), WSDI (bottom-right) in Bahr El Ghazal sub-basin for RCP 4.5.

Victoria Nile sub-basin

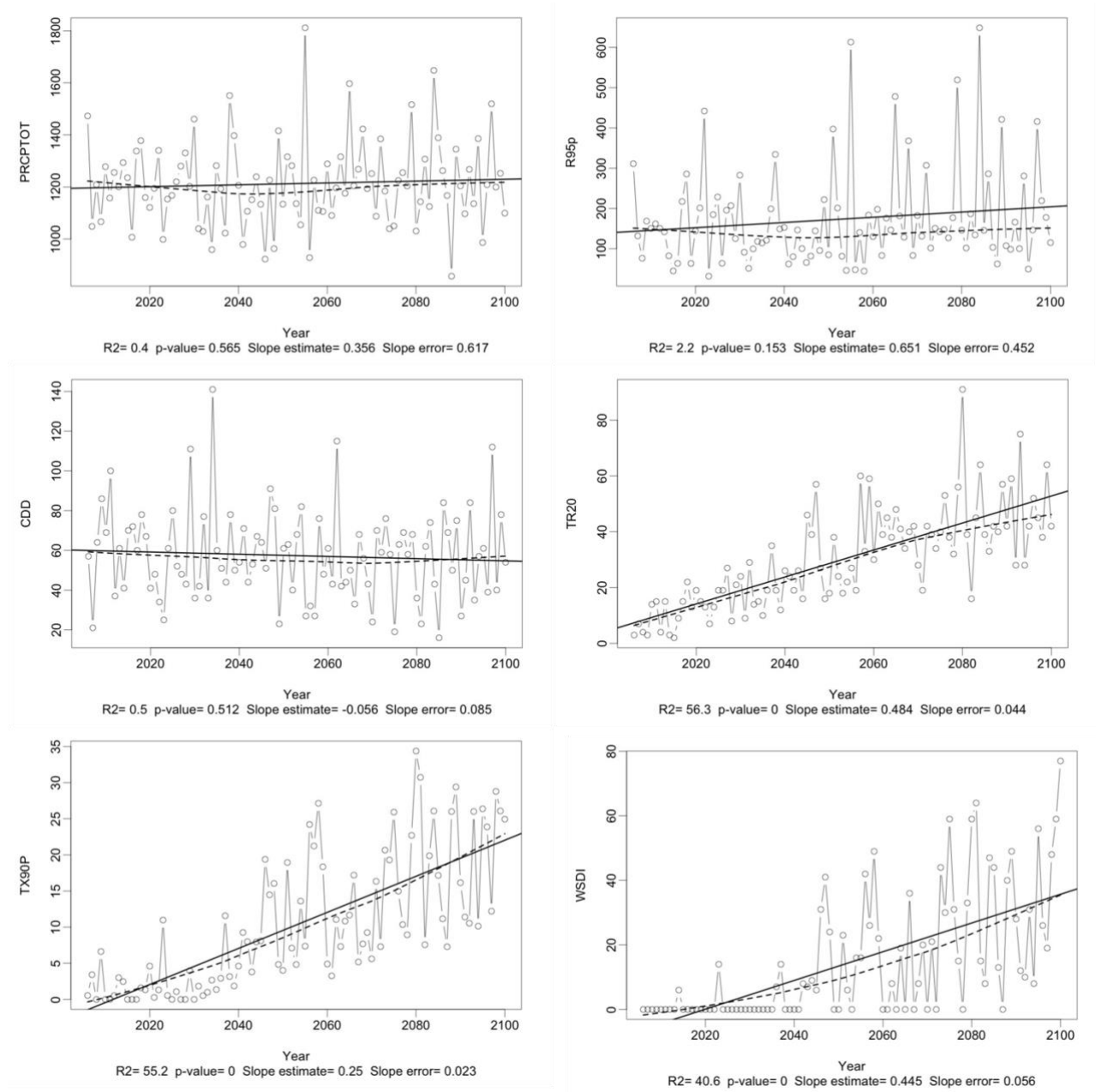


Figure II.5 – Climate indices PRCPTOT (top-left), R95P (top-right), CDD (mid-left), TR20 (mid-right), TX90P (bottom-left), WSDI (bottom-right) in Victoria Nile sub-basin for RCP 4.5.

Lake Victoria sub-basin

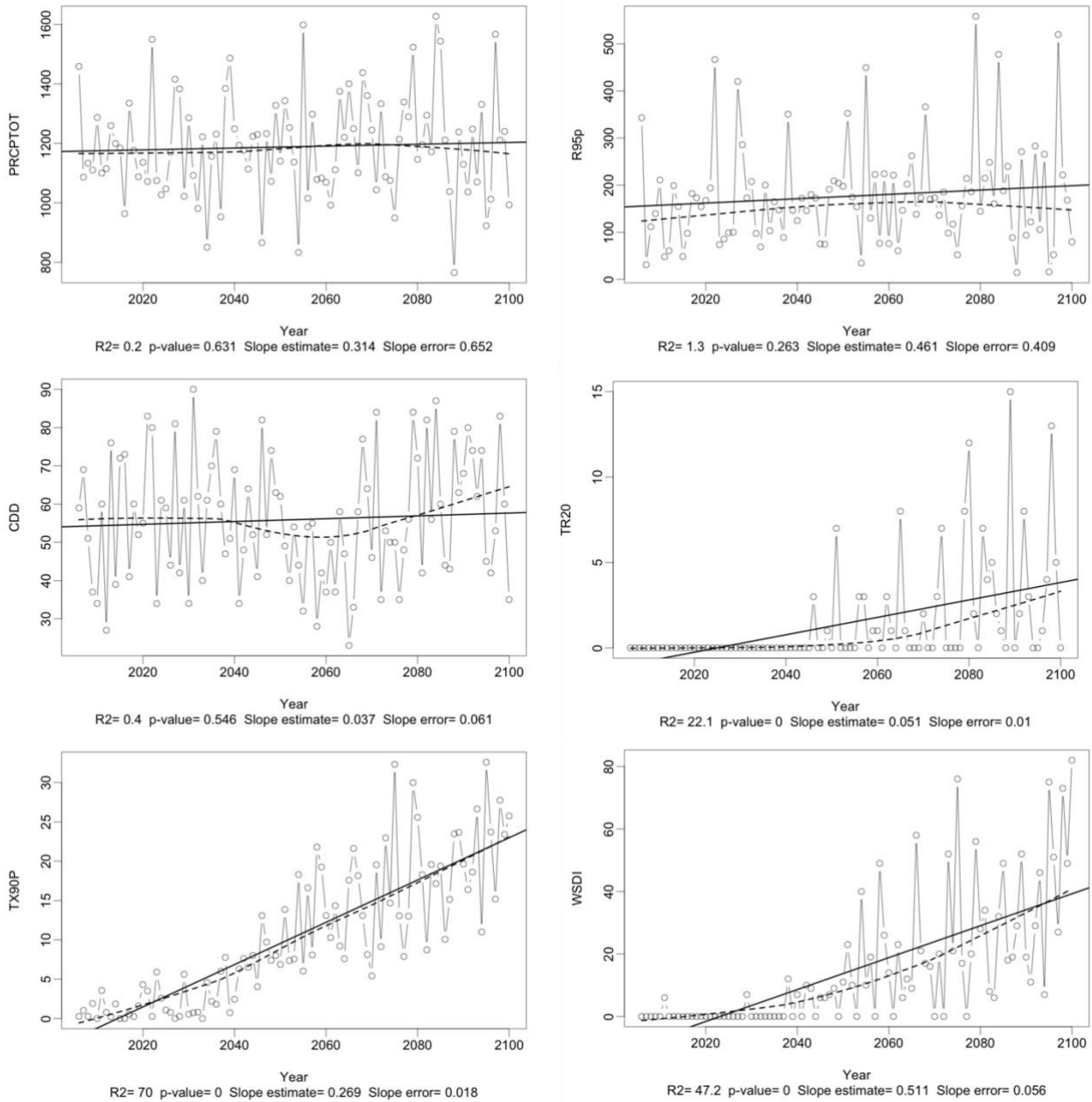


Figure II.6 – Climate indices PRCPTOT (top-left), R95P (top-right), CDD (mid-left), TR20 (mid-right), TX90P (bottom-left), WSDI (bottom-right) in Lake Victoria sub-basin for RCP 4.5.

Lake Albert sub-basin

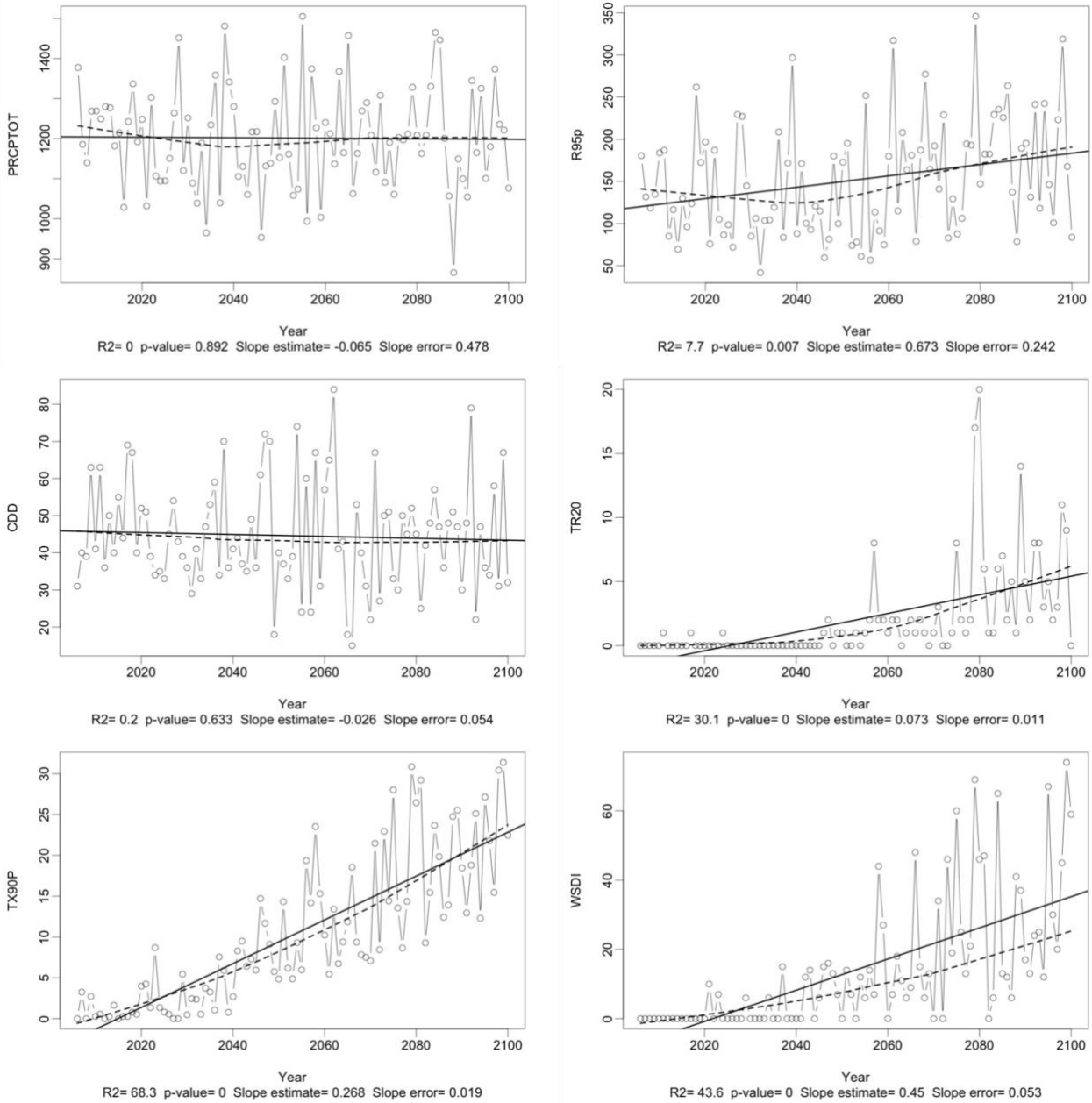


Figure II.7 – Climate indices PRCPTOT (top-left), R95P (top-right), CDD (mid-left), TR20 (mid-right), TX90P (bottom-left), WSDI (bottom-right) in Lake Albert sub-basin for RCP 4.5.

ANNEX III

III. Egypt

Further comparison among the extreme precipitation and temperatures climate indicators (R95P and TX90) is reported in Figures III.1 and III.2, respectively.

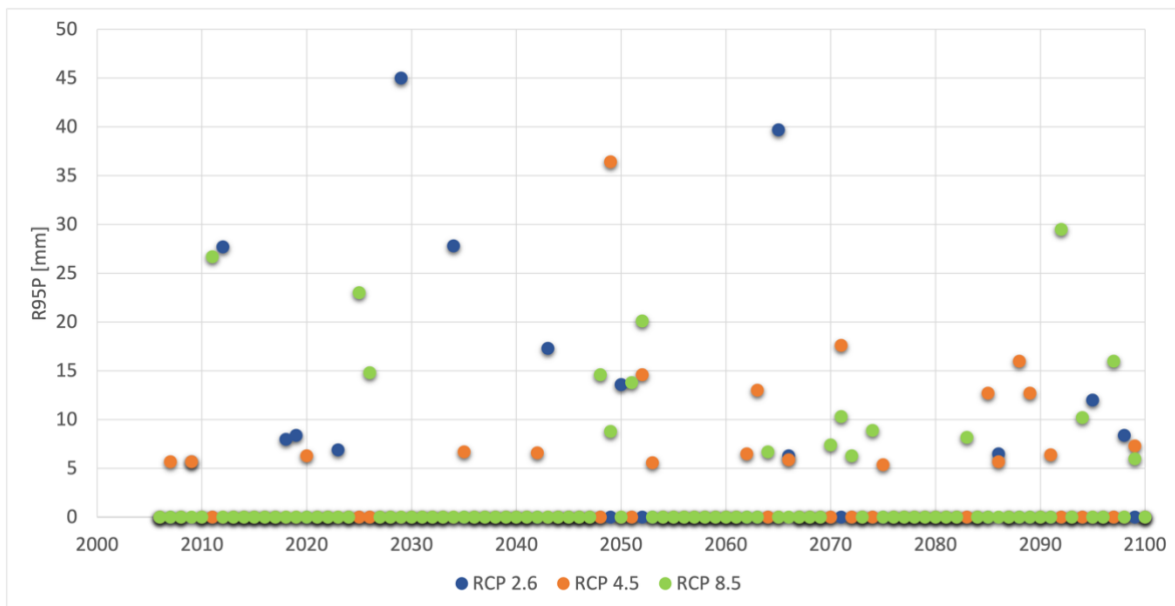


Figure III.1 - Extreme precipitation (R95P) for RCP 2.6 (blue), RCP 4.5 (red), and RCP 8.5 (green).

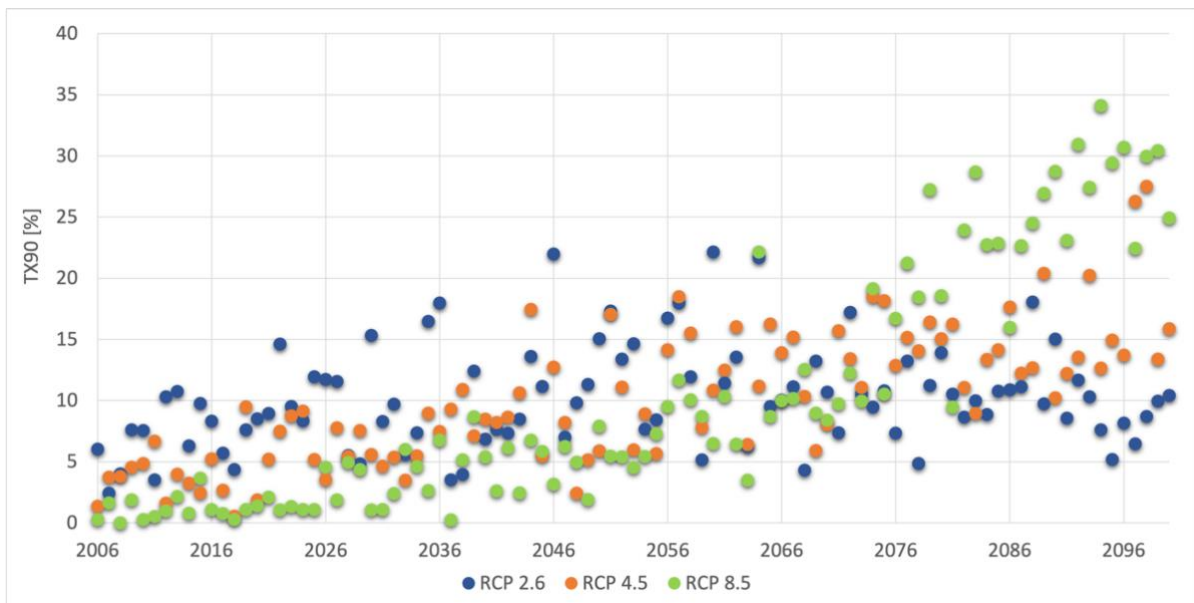


Figure III.2- Warm days (TX90) for RCP 2.6 (blue), RCP 4.5 (red), and RCP 8.5 (green).